Diss. ETH No. 18641

Collective Interaction Between a Bose-Einstein Condensate and a Coherent Few-Photon Field

A dissertation submitted to the
Swiss Federal Institute of Technology
Zurich

for the degree of
Doctor of Sciences

presented by

Claudius Ferdinand Brennecke

Dipl.-Phys., University of Hamburg, Germany
born 23.03.1979 in Starnberg, Germany
citizen of Germany

accepted on the recommendation of
Prof. Dr. Tilman Esslinger, examiner
Prof. Dr. Atac Imamoglu, co-examiner

2009

Zusammenfassung

Im Rahmen dieser Doktorarbeit wurde die kollektive Wechselwirkung zwischen einem Bose-Einstein Kondensat und dem Feld eines optischen Resonators mit kleinem Modenvolumen und exzellenter Güte experimentell realisiert und erforscht. Dieses System eröffnet ein neues Forschungsgebiet innerhalb der Resonator-Quantenelektrodynamik, in welchem eine makroskopische Materiewelle eine starke Wechselwirkung mit wenigen Photonen eingeht. Kernstück des experimentellen Aufbaus bildet ein optischer Transportmechanismus, der es erlaubt, mehrere hunderttausend ultrakalte Atome in einen optische Resonator zu transferieren, welcher bereits für einzelne Atome im stark-koppelnden Regime operiert. Erstmals können damit unter Beteiligung weniger Photonen in der Resonatormode kollektive Phänomene in den internen und externen Freiheitsgraden eines Bose-Einstein Kondensates experimentell untersucht werden. Wie unsere Messungen und theoretischen Überlegungen belegen, lassen sich damit zwei zentrale Modellsysteme im Bereich der Quantenoptik und der Resonator-Optomechanik realisieren.

Im Bereich der Resonator-Quantenelektrodynamik stellt unser System eine ideale Realisierung des Tavis-Cummings Modells dar, welches die kollektive Wechselwirkung zwischen N gleichartig gekoppelten zwei-Niveau Systemen und einem harmonischen Oszillator beschreibt. Einzelne atomare Anregungen des gekoppelten Systems verteilen sich in Form einer kohärenten Quantenüberlagerung auf alle Atome, und wechselwirken deshalb, im Gegensatz zum einzelnen Atom, mit der $\sqrt{N}$-fachen Kopplungsstärke mit dem Resonatorfeld. Zur Charakterisierung des gekoppelten Systems messen wir das Energiespektrum aus, und weisen das vorhergesagte Skalierungsverhalten der kollektiven Kopplungsstärke nach. Die Messungen befinden sich in sehr guter Übereinstimmung mit unserer theoretischen Modellbeschreibung, welche die nicht-resonante Kopplung an höhere Resonatormoden mit einbezieht.

Im dispersiven Limes erfährt die kohärente Materiewelle ein optisches Gitterpotential, welches durch Resonator-Lichtkräfte hervorgerufen wird und

bereits in der Anwesenheit einzelner Photonen einen signifikanten Einfluss auf die atomare Bewegung hat. Im Gegensatz zu klassischen optische Gitterpotentialen hängt die Tiefe dieses Gitterpotentials aufgrund der dispersiven Rückkopplung der Atome auf das Resonatorfeld entscheidend davon ab, wie sich die Atome innerhalb der Modenstruktur des Resonators anordnen. Dies bewirkt eine hochgradig nichtlineare Kopplung zwischen kollektiver atomarer Bewegung und dem Resonatorfeld. Wie in der vorliegenden Doktorarbeit erstmals erkannt wurde, lässt sich dieses System im Rahmen der Resonator-Optomechanik beschreiben, wobei kollektive Oszillationen der Kondensatsdichte die Rolle des mechanischen Freiheitsgrades spielen. Die außerordentliche Kontrolle über die atomaren Bewegungsfreiheitsgrade ultrakalter Gase ermöglicht es prinzipiell, mit diesem System in das Quantenregime der Resonator-Optomechanik vorzustossen. Wir beobachten eine ausgeprägte optische Bistabilität in Anwesenheit einzelner Photonen, hervorgerufen durch die kollektive Verschiebung der Atome innerhalb der Modenstruktur des Resonators. Anhand des Lichtfeldes welches den Resonator verlässt, sind wir erstmals in der Lage, kohärente Dichteoszillationen kleiner Amplitude innerhalb eines Bose-Einstein Kondensates in Echtzeit zu beobachten. Ferner untersuchen wir den Einfluss eines zusätzlichen statischen Gitterpotentials auf die kollektive atomare Bewegung, und demonstrieren eine weitere mögliche Realisierung eines optomechanischen Systems mit stark lokalisierten ultrakalten Atomen. Unsere Beobachtungen lassen sich quantitativ im Rahmen einer Mean-Field-Theorie erklären.

Abstract

Collective coupling between a Bose-Einstein condensate and the field of a small-volume ultrahigh-finesse optical cavity is experimentally achieved and investigated for the first time. This system opens access to a conceptually new regime of cavity quantum electrodynamics where a macroscopic matter wave strongly couples to few optical photons. The core of the experimental setup is given by an optical-transport scheme, that allows to transfer several hundred thousands of ultracold atoms into an optical resonator, which operates in the single-atom strong coupling regime. With few photons occupying the cavity mode, we explore collective phenomena both in the internal and motional degrees of freedom of a Bose-Einstein condensate. Our measurements and theoretical investigations confirm that our system realizes two fundamental model systems in quantum optics as well as cavity optomechanics.

In the context of cavity quantum electrodynamics, our system constitutes an ideal realization of the Tavis-Cummings model, which describes the coherent interaction between a single harmonic oscillator and N two-level systems, all coupling identically. Single excitations are coherently shared among all atoms, and exchanged with the cavity field at a rate which is enhanced by a factor of $\sqrt{N}$, compared to the single atom case. To characterize the coupled system, we map out its eigenenergy spectrum, and confirm the predicted scaling behavior of the collective coupling strength. These measurements are in very good agreement with our theoretical model description which additionally takes into account the off-resonant coupling to higher-order cavity modes.

In the dispersive regime, the cavity-induced dipole forces provide an optical lattice potential which is collectively sensed by the coherent matter-wave. Furthermore, due to dispersive retroaction on the cavity field, the lattice depth dynamically depends on the atomic density distribution within the cavity mode. This causes highly nonlinear dynamics of the collective atomic motion and the cavity field intensity. Within the scope of this thesis, it

was established for the first time that the system can be described within the framework of cavity optomechanics, where the role of the mechanical oscillator is played by a collective density excitation of the condensate. The tremendous control over the external degrees of freedom of ultracold gases provides – in principle – a direct access to the quantum regime of cavity optomechanics. Here, we report on the observation of optical bistability at the single photon level, caused by the collective displacement of the atoms within the cavity mode structure. By detecting the light which leaks out of the optical resonator, we are able to *in-situ* observe coherent small-amplitude density oscillations in a Bose-Einstein condensate. We investigate the influence of an additional static lattice potential on the collective atomic motion, and demonstrate yet another realization of cavity optomechanics with tightly confined ultracold atoms. Our measurements are in very good agreement with a quantitative mean-field model.

Contents

1 Introduction **1**

2 The experimental setup **9**

2.1 Overview of the experimental setup 10
2.2 The optical high-finesse cavity 10
2.2.1 General properties and characteristics 11
2.2.2 Probing the cavity resonance 14
2.2.3 Cavity QED parameters 15
2.2.4 Photon detection efficiency 16
2.3 Preparing a Bose-Einstein condensate inside the optical cavity 17
2.3.1 The optical transport 17
2.3.2 The crossed-beam dipole trap 19
2.3.3 The cavity dipole trap 19

3 Cavity QED with a Bose-Einstein condensate **21**

3.1 Introduction 23
3.2 Collective cavity QED 23
3.2.1 Eigenspectrum for a single excitation 24
3.2.2 Nonlinearity and the second excitation manifold . . . 26
3.3 Coupling a BEC to a single cavity mode: Tavis-Cummings model 26
3.4 Dissipation 29
3.5 Multilevel atoms coupled to a multi-mode cavity 30
3.5.1 Two atomic ground states 30
3.5.2 Two orthogonally polarized cavity modes 33
3.5.3 Higher-order transverse cavity modes 34
3.6 Measurements 35
3.6.1 Excitation spectrum in the weak-probe limit 35
3.6.2 Scaling with atom number 38
3.7 Quantitative modelling of the excitation spectrum 38

3.8 Summary 41

4 Cavity optomechanics with a Bose-Einstein condensate 43
4.1 A short introduction to cavity optomechanics 44
4.2 Dispersive coupling between a BEC and a cavity field 47
4.2.1 Dispersive atom-light interaction 47
4.2.2 The many-body system 49
4.3 Uniform limit and equivalence to cavity optomechanics 49
4.3.1 The two-mode model 50
4.3.2 Mean-field description 51
4.3.3 Equations of motion 52
4.3.4 Cavity quantum optomechanics in the strong coupling regime 53
4.4 Beyond the uniform two-mode model 54
4.4.1 Atom-atom interactions 54
4.4.2 Harmonic confinement along the cavity axis 55
4.4.3 Transverse degrees of freedom 57
4.4.4 Ground state preparation of the mechanical oscillator 58
4.4.5 Atomic multilevel structure 58
4.5 Summary 59

5 Optical bistability at low photon number 61
5.1 Optical Kerr nonlinearity 63
5.1.1 Adiabatic limit 63
5.1.2 Bistability 64
5.1.3 Higher-order Kerr nonlinearity 65
5.2 Experimental observation of optical bistability 67
5.3 Photon number fluctuations and mean-field approximation . . 71
5.4 Summary 72

6 Collective atomic motion in a dynamic optical lattice 73
6.1 Adiabatic elimination of the cavity field dynamics 74
6.2 The optomechanical potential 74
6.3 Energy functional for a dynamic optical lattice 75
6.4 Experimental observation of transient oscillations 78
6.5 Finite cavity lifetime and retardation effects 84
6.6 Summary 88

7 Cavity optomechanics with tightly confined ultracold atoms 89
7.1 Collective motion of tightly confined ultracold atoms 90
7.1.1 Hamiltonian description 90

7.1.2 Characteristic properties of the system 93
7.2 The transition from weak to strong confinement 94
7.2.1 Band structure 94
7.2.2 Interaction with the probe light 95
7.2.3 Measurement of the collective excitation spectrum . . 96
7.2.4 Influence of probe light on the collective motion . . . 98
7.3 *In-situ* observation of collective motion 99
7.4 Summary 101

8 Conclusions and outlook **103**

A Physical constants **107**

Bibliography **108**

List of publications **125**

Credits **127**

1 Introduction

The experimental realization of conceptually simple model systems plays an important role in physics. It promotes continuous development and investigation of experimental techniques, allows to test theoretical model descriptions with increasingly better accuracy, and provides opportunities to realize long standing Gedanken experiments which deepen our understanding of quantum physics. In this spirit, cavity quantum electrodynamics [1, 2] provides a research field which, enabled by technical progress in the fabrication of resonating structures during the last decades, confirmed and refined our understanding of the quantum properties of light, and its interaction with matter at the level of single quanta [3, 4, 5, 6, 7]. Similarly, the field of ultracold quantum gases and Bose-Einstein condensation constitutes a broad playground for the investigation of various macroscopic quantum phenomena [8]. Quantum gases are extremely pure and highly controlled quantum systems, which can be probed [9, 10, 11] and manipulated [12, 13, 14, 15, 16, 17] with light fields in different ways. However, the combination of these two fascinating research fields – cavity quantum electrodynamics and ultracold quantum gases – remained an elusive goal. It would enlarge the experimental possibilities for controlling and sensing the different subsystems with unprecedented accuracy and possibly non-destructively [18, 19, 20, 21], and open the route to realize novel and interesting model systems [22, 23, 24, 25].

Within the scope of this thesis, collective strong coupling between a trapped Bose-Einstein condensate (BEC) and the optical field of a small-volume ultrahigh-finesse Fabry-Perot cavity has been experimentally achieved for the first time (see also [26, 27]). This novel hybrid system opens access to a so far unexplored regime of cavity quantum electrodynamics (QED) where a single light field mode is coherently coupled to a macroscopically occupied matter field mode. We experimentally investigate and theoretically analyze the collective coupling between both electronic and motional degrees of freedom of the coherent atomic ensemble and light fields on the single-photon level. The tremendous control over atomic motion reached in a Bose-Einstein

condensate allows to achieve identical atom-field coupling strengths for all atoms, representing an ideal realization of the Tavis-Cummings model [28]. In the far-dispersive regime, cavity-enhanced light forces and the collective atomic dispersion induce a strong coupling between collective atomic motion and the cavity light intensity. This permits us to explore the field of cavity QED with coherent atomic motion for the first time [29, 30, 31]. In this thesis it was shown both experimentally and theoretically that the dispersively coupled BEC-cavity system can be mapped to the framework of cavity optomechanics [32], with a coherent atomic density excitation acting as a mesoscopic mechanical element.

Cavity QED studies the coherent interaction between matter and the electromagnetic field confined in a resonating structure [1, 2]. In order to overcome the incoherent decay processes of the cavity field and the internal matter excitations, the matter-light coupling strength has to be larger than the associated decay rates. In this strong coupling regime, single excitations are coherently exchanged between matter and field many times before dissipation sets in. Cavity QED systems are therefore considered as ideal key elements for a coherent light-matter interface [33, 34, 35], and for the implementation of quantum information protocols [36, 37].

Experimentally achieving the regime of strong coupling for a single two-level system is a challenging task. So far, it has been reached with Rydberg atoms in microwave resonators [38, 39] and neutral atoms in small-volume optical Fabry-Perot cavities [40]. More recently, systems involving artificial atoms like quantum dots [41] or superconducting Cooper-pair boxes [42] have joint this selected group. In the optical domain the desired system parameters require very high-quality mirrors and a very small cavity mode volume, a constraint which reduces optical access and sets serious limits on the experimental combination with highly controlled quantum systems, like single ions or ultracold quantum gases. Since the atom-light coupling strength spatially varies on a scale given by the optical wavelength, elaborate trapping or cooling techniques [43, 44] are necessary, in order to suppress motional induced decoherence effects in optical cavity QED.

Bose-Einstein condensation of dilute atomic gases allows to routinely prepare a macroscopic number of atoms in a single motional quantum state which is determined by the external trapping potential. Our experimental setup combines this tremendous control over the atomic motional degrees of freedom with the coherent light-matter interaction provided by cavity QED in the strong coupling regime. A key element of our setup is an optical transport mechanism that allows to transfer ultracold atomic samples into the field of a 180 μm-long Fabry-Perot cavity, operating in the single-atom

strong coupling regime. Within the cavity Bose-Einstein condensation is achieved in a harmonic dipole trap by means of evaporative cooling.

In parallel to our experiment, Bose-Einstein condensates have been positioned with high precision inside a fibre-based cavity using atom-chip technology [27], and ultracold non-condensed atomic samples have been tightly confined within the field of a small-volume Fabry-Perot cavity [26, 45]. Previous experiments bringing together BEC physics and cavities concentrated on correlation measurements using single-atom counting [46], and studied collective atomic recoil lasing and cavity enhanced superradiance in a large volume ring cavity [47]. Progress on combining cavity QED with ion-trap technology has been achieved very recently [48] by demonstrating collective strong coupling between an ion Coulomb crystal and the field of an optical cavity.

In general, the coherent coupling of an ensemble of identical two-level systems to a single cavity mode has been a theme of general interest in quantum optics. In his pioneering work in 1954 [49], R.H. Dicke studied the influence of collective behavior on the radiative properties of an atomic ensemble. By treating the entire collection of atoms as a single quantum system, Dicke pointed out that nontrivial interatomic correlations in an excited ensemble give rise to enhancement or suppression of the radiative emission rate. In recent years, the collective interaction between atoms and light has gained renewed interest in the field of quantum information due to its applicability for realizing a quantum memory [34, 50]. This requires a large number of atoms in order to minimize possible information losses due to decoherence, and a large collective atom-light coupling strength for optimal conversion efficiency. The figure of merit for the probability to convert a collective atomic excitation into a cavity photon is given by the collective cooperativity, which in our experiments exceeds 10^6.

Coupling a Bose-Einstein condensate to the field of an optical cavity realizes a collective light-matter interface with unique properties. Since all atoms are prepared in the same motional quantum state, the coupling to the cavity field is identical for all atoms. This situation is described by the Tavis-Cummings model [28] which considers N two-level systems coupled identically to a single resonator mode. Due to collectivity single excitations are coherently shared between all atoms, and exchanged with the cavity field at a rate which is $\sqrt{N}$ times larger as compared to the single atom case. A key characteristic of the Tavis-Cummings model is its eigenenergy spectrum, which we map out with a single excitation present. Furthermore, we demonstrate the predicted scaling behavior of the collective coupling strength as a function of atom number. We perform mean-field calculations of the system

which are in very good agreement with our experimental findings, confirming the high degree of control achieved.

In the dispersive limit of cavity QED, strong coupling between a single macroscopic matter wave and the field of an optical cavity provides an ideal setting to explore cavity-enhanced light forces and atomic collective motion with unprecedented accuracy and – in principle – on the quantum level. Within the scope of this thesis, first experiments have been conducted on a dispersively coupled BEC-cavity system at the single-photon scale, and analyzed in terms of cavity optomechanics.

The fact that light carries momentum and therefore can exert forces on matter always fascinated physicists. Starting with J. Kepler's suggestion that the tail of comets gets deflected by the sun's light, and the first explanation within J.C. Maxwell's theory of electromagnetism, it took until the invention of the laser [51], that light forces could be actually used for manipulating small particles within tightly focused light beams [52, 53]. This development culminated in the invention of atomic laser cooling in 1975 [54], followed by the experimental demonstration in a magneto-optical trap in 1986 [55]. Nowadays, the conservative dipole force exerted by far-detuned laser fields has become a standard tool for trapping and manipulating ultracold atomic gases within tightly focussed laser beams [56] or optical lattices [57].

In general, optical dipole forces are accompanied by the atomic retroaction onto the light field, caused by the atomic index of refraction which shifts the phase of the outgoing light with respect to the incident one. Inside a high-finesse cavity, this effect gets enhanced by the number of roundtrips of light, which can result in a significant change of the cavity resonance frequency, depending on the atomic position. Correspondingly, the cavity light intensity becomes a dynamic degree of freedom which 'optomechanically' couples to the atomic motion. This is in contrast to experiments performed in free space, where the light fields, used to manipulate and trap atoms, can be considered as fixed. Nevertheless, the tiny dispersive shift of the lattice constant caused by cold atoms trapped inside an free-space optical lattice could be observed in [58, 59].

The interplay between radiation pressure forces and mechanical retroaction upon the light field is a general theme of cavity optomechanics. Its core setting is given by a mechanical oscillator which couples to the field of a cavity via radiation pressure [60]. Mechanical retroaction on the light field is mediated by the optical path length of the cavity, which depends on the displacement of the mechanical oscillator. Inspired by early work

of V.B. Braginsky [61] in the context of interferometric gravitational wave experiments, cavity optomechanical systems have found renewed interest through the experimental progress of high-quality optical and microwave cavities and micro- and nanomechanical oscillators. Ongoing research in cavity optomechanics focuses on radiation pressure cooling of mechanical oscillators, heading for ground state preparation [62, 63, 64, 65, 66, 67, 68, 69]. With the preparation of a mechanical oscillator in its motional ground state, the field is expected to enter the quantum regime of cavity optomechanics [70]. This would open new perspectives to address fundamental questions on quantum limits of measurements [61], or to explore the quantum-to-classical boundary.

Coupling a collective motional degree of freedom of an ultracold quantum gas to the optical field of a high-finesse cavity, offers new possibilities for exploring cavity optomechanics in the quantum regime [71]. As was established within the scope of this thesis, a dispersively coupled BEC-cavity system constitutes a cavity optomechanical model system: a collective atomic density excitation matching the cavity mode profile serves as a mechanical oscillator, which retroacts via atomic dispersion onto the cavity field intensity. The control over the atomic motional degrees of freedom provided by Bose-Einstein condensation, places this system well into the quantum regime, where the mechanical oscillator is prepared in its motional ground state. Due to collectivity, our system is capable of reaching the strong coupling regime of cavity optomechanics, where fluctuations of the mechanical and optical oscillator mutually couple. Experimentally, we observe optical bistability at photon numbers below one, and strongly driven backaction dynamics triggered by only a few photons inside the resonator. We explore the transition from our system to a similar realization of cavity optomechanics [26, 45] where ultracold atoms are tightly confined in a periodic external potential. Our measurements agree very well with *ab-initio* calculations, which we perform in a mean-field approximation.

Previous experiments on resonator-induced light forces with cold atomic ensembles have focused on spatial atomic self-organization [72] and collective cooling [73] in a large volume Fabry-Perot cavity with moderate finesse. The regime of dispersive collective strong coupling has been studied with laser cooled atoms, trapped within a high-finesse ring cavity [74]. Here, the collective cavity resonance shift induced by all atoms was larger than the cavity linewidth, which gave rise to optical bistability and self-induced atomic oscillations at large cavity light intensities. Much stronger light forces per cavity photon were attained in small-volume optical cavities, operating in the single-atom strong coupling regime of cavity QED. Pioneering experi-

ments reported on trapping of single atoms in the light field of single cavity photons [75], as well as continuous sensing [76, 75] and cooling [43, 44] of atomic motion by means of the cavity field.

Our BEC-cavity system (and that reported on in [26, 45]) offers new possibilities for manipulating and sensing the collective motion of ultracold atomic gases at the quantum limit. On a conceptual level it bridges three active research fields: cavity QED, ultracold quantum gases, and cavity quantum optomechanics [32]. Even if some might consider an ensemble of 10^5 atoms not as a macroscopic object, the realization of cavity optomechanical systems with ultracold atoms offers intriguing possibilities to contribute to the development of cavity quantum optomechanics on a fundamental level. A first step along this direction was achieved in [45], where measurement backaction caused by quantum force fluctuations was quantified in a cavity optomechanical system for the first time.

Outline:

- Chapter 2 introduces the experimental apparatus at which the experiments presented in this work were carried out.
- The collective coupling between the electronic degrees of freedom of the BEC and the cavity mode is investigated in Chapter 3. After a brief introduction into collective cavity QED, the measurements of the eigenenergy spectrum of the coupled BEC-cavity system are presented. The data are compared with a quantitative model description, which takes into account several degrees of freedom of the coupled system.
- In Chapter 4 a novel description of the dispersively coupled BEC-cavity system in terms of cavity optomechanics is established. It provides the background for the investigations reported on in Chapters 5 to 7.
- The observation of optical bistability at photon numbers below unity is presented in Chapter 5. The measurements are compared with *ab-initio* calculations in a mean-field description.
- Chapter 6 is concerned with the observation of strongly driven back-action dynamics, triggered by the presence of a few photons inside the cavity. Quantitative understanding of the nonlinear dynamics is provided in terms of mean-field calculations.
- In Chapter 7 we investigate yet another cavity optomechanical system where the collective center of mass motion of ultracold atoms couples to the cavity field. Measurements are presented which clarify about the transition between the two different realizations, in agreement with a simple quantitative mean-field model.

2 The experimental setup

The experiments described in this thesis were performed on an existing apparatus [77] which was designed in 2001 to combine the research fields of ultracold atomic gases and cavity quantum electrodynamics (QED) for the first time. At the heart of the experiment is a small-volume ultrahigh-finesse optical cavity, which operates in the single-atom strong coupling regime of cavity QED. In addition, the apparatus allows to achieve Bose-Einstein condensation (BEC) in a dilute gas of ^{87}Rb atoms.

In a first series of experiments [46, 78, 79, 80] carried out on this setup, ultracold atoms were prepared in a magnetic trap, placed a few centimeters above the cavity. The latter served as a sensitive detector of single atoms, which were extracted from the magnetic trap and propagated downwards through the cavity field. This minimally invasive probing scheme allowed to study the correlations and counting statistics of an atom laser [46], to observe the formation of long-range order during BEC [79], and to explore the critical behavior of a trapped interacting Bose gas [80].

In order to realize the experiments which were performed within the scope of this thesis, the experimental setup was modified. We implemented an optical conveyer belt which allows us to transport ultracold atoms in a controlled way from the magnetic trap into the high-finesse optical cavity. Once overlapping with the cavity mode, the atoms are loaded into a crossed-beam dipole trap where Bose-Einstein condensation is achieved by means of evaporative cooling. The physical properties of the mutually coupled BEC-cavity system are studied by probing the cavity field with a weak laser field, while continuously monitoring the transmitted light intensity.

The experimental apparatus was described in detail in the theses of my predecessors Anton Öttl [81], Stephan Ritter [82] and Tobias Donner [83]. Hence, we will provide the reader in this chapter only with a brief overview of the main experimental setup and the preparation of ultracold atoms in the magnetic trap. A more detailed description will be given on the properties of the high-finesse cavity, the optical transport and trapping within the cavity, as well as the optical probing techniques used in the experiments.

2.1. Overview of the experimental setup

The experimental setup consists basically of two parts: an ultrahigh-vacuum system where the actual experiments take place, and a laser setup where the laser light is generated, used for cooling, manipulating and trapping the atoms, as well as for probing and stabilizing the high-finesse cavity. The whole setup is installed on two separated optical tables which are connected by several optical fibers, delivering the light from the laser table to the main experiment table. The experimental cycle is computer controlled with the help of a software, developed in our research group [84].

The preparation of a Bose-Einstein condensate in dilute atomic gases requires sophisticated vacuum conditions in order to reduce wasteful collisions with background atoms. At the same time, a sufficient vapor pressure is needed to efficiently load a magneto-optical trap (MOT) for pre-cooling the atoms with laser light. In our setup this problem was solved by means of a double-vacuum chamber design, with the two chambers being connected by a differential pumping tube (see Figure 2.1).

The MOT chamber operates at a pressure of a few 10^{-9} mbar and provides the necessary vapor pressure from a dispenser source [85] for collecting and laser cooling ^{87}Rb atoms in a three-dimensional MOT. Typically, a few billion atoms are collected during a loading time of 18 s, and subsequently sub-Doppler cooled and optically pumped into the low-field seeking state $|F = 1, m_F = -1\rangle$. A differential pumping tube allows to magnetically transport [86] the laser cooled atoms afterwards over a distance of 82 mm into the main chamber which is operated at a pressure of a few 10^{-11} mbar. Here, the atomic sample is trapped and evaporatively cooled in a magnetic QUIC (quadrupole Ioffe configuration) [87] trap, and finally transported into the optical cavity. All magnetic coils, used for transporting and trapping the atoms, are installed in vacuum, and are cooled down to -90° C in order to prevent unwanted outgassing while operating them at high currents. The ultrahigh-finesse optical cavity is placed 36 mm below the QUIC trap inside the main chamber, and can be optically accessed via several vacuum windows.

2.2. The optical high-finesse cavity

The heart of the experimental setup consists of an ultrahigh-finesse optical cavity, operating in the single-atom strong coupling regime of cavity QED. This section collects necessary information about the physical properties of the cavity, and the way how its resonance frequency is optically probed and actively stabilized during the experiments.

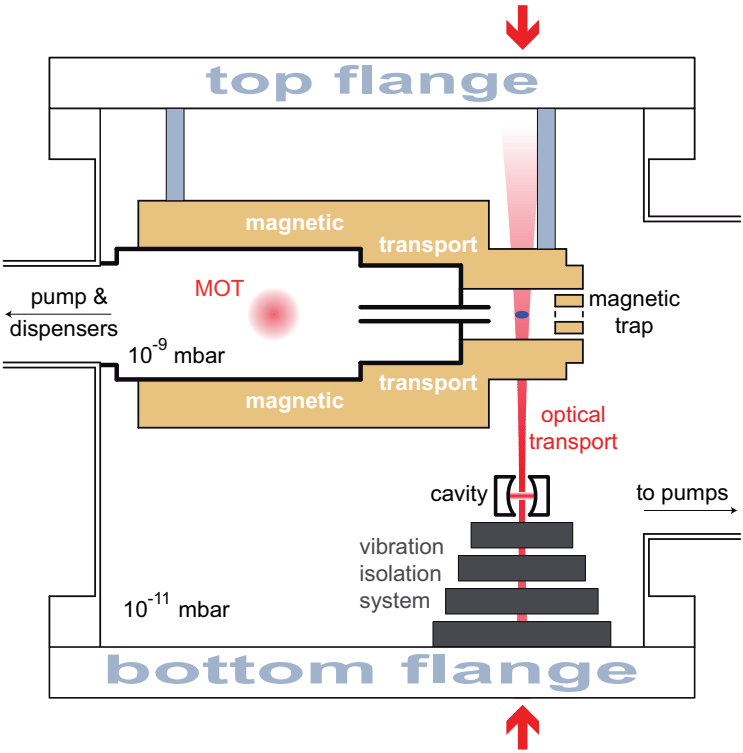

FIGURE 2.1.: Schematic drawing of the vacuum system. Atoms are laser cooled inside the MOT chamber at a pressure of a few 10^{-9} mbar and subsequently transported into the main chamber operating at a pressure of a few 10^{-11} mbar. Here, the cold atoms are evaporatively cooled within a magnetic trap close to quantum degeneracy. 36 mm below the magnetic trap the ultrahigh-finesse optical cavity is positioned on a vibration isolation stage. To prepare a BEC inside the cavity mode, ultracold atoms are optically transported from the magnetic trap into the cavity. Figure adopted from [77].

2.2.1. General properties and characteristics

Our science cavity consists of two highly reflecting mirrors facing each other at a distance of $l_{\mathrm{res}} = 176\,\mu$m. With a radius of curvature of $R = 75$ mm, the mirrors form a near-planar resonator geometry which supports a variety of different eigenmodes of the electromagnetic field. Their spatial field

distribution is obtained by solving the electromagnetic field equations according to the boundary conditions imposed by the mirrors [88]. A general solution is provided by the Hermite-Gaussian modes. The corresponding electric field distribution at the position of the mode waist is given by

$$E_{lmn}(0,y,z) = E_0\, H_l(\sqrt{2}y/w_0) H_m(\sqrt{2}z/w_0) e^{-\frac{y^2+z^2}{w_0^2}} \tag{2.1}$$

with x denoting the cavity axis. Here, H_l denotes the l^{th} Hermite polynomial, and w_0 is the waist radius of the transversally fundamental cavity mode. For a near-planar cavity the corresponding mode frequencies are given by [89]

$$\nu_{lmn} = \Delta\nu_{\text{FSR}}\Big(n + \frac{1+l+m}{\pi}\sqrt{\frac{2l_{\text{res}}}{R}}\Big). \tag{2.2}$$

The transversally fundamental modes ($l = m = 0$), labelled by the integer n, are characterized by a Gaussian mode profile along the transverse directions, and are separated in frequency by the free spectral range $\Delta\nu_{\text{FSR}} = \frac{c}{2l_{\text{res}}}$. For given n, the higher-order transverse modes (TEM_{lm}) differ in frequency from the corresponding fundamental mode by an integer multiple of the transverse mode spacing $\Delta\nu_{\text{T}} = \frac{\Delta\nu_{\text{FSR}}}{\pi}\sqrt{\frac{2l_{\text{res}}}{R}} \ll \Delta\nu_{\text{FSR}}$. Modes which fulfill the condition $l + m = \text{const}$ (for given n) are degenerate in frequency space (see Figure 2.2).

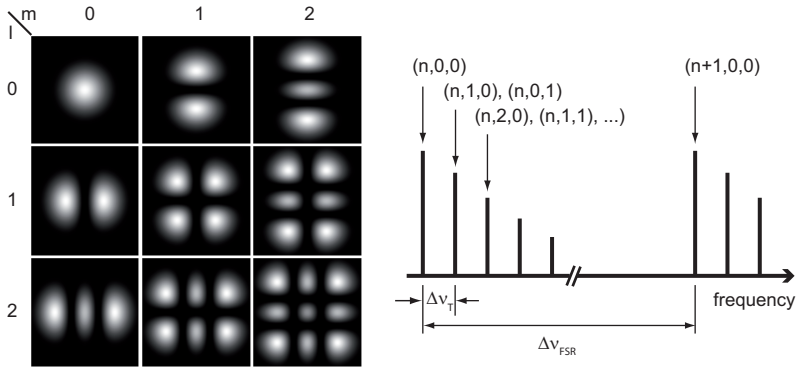

FIGURE 2.2.: Shown is the intensity distribution of the lowest order transverse TEM_{lm}-modes (left) as well as their arrangement in frequency space (right). For every longitudinal mode number n there exists a comb of higher-order transverse modes labelled by (n, l, m).

cavity length l_{res}	$176\,\mu$m
free spectral range $\Delta\nu_{\mathrm{FSR}}$	852 GHz
transverse mode spacing $\Delta\nu_{\mathrm{T}}$	18.5 GHz
linewidth $\Delta\nu$	2.4 MHz
finesse $\mathcal{F}$	342×10^3
mirror transmission $\mathcal{T}$	2.3 ppm
mirror losses $\mathcal{L}$	6.9 ppm
mirror radius of curvature R	75 mm
mode waist radius w_0	$25.3\,\mu$m
(fundamental) mode volume V	$88 \times 10^3\,\mu\mathrm{m}^3$
decay rate of the atomic dipole moment γ	$2\pi \times 3.0$ MHz
decay rate of the intracavity field κ	$2\pi \times 1.3$ MHz
(effective) atom-cavity coupling constant g_0	$2\pi \times 10.6$ MHz
cooperativity parameter $C = g_0^2/(2\gamma\kappa)$	14.7

TABLE 2.1.: Parameters of the ultrahigh-finesse optical cavity for probe light at $\lambda_p = 780$ nm. Data taken from [82].

The mirrors, even though among the best available ones, have a finite transmittivity and surface roughness which eventually gives rise to a loss of the stored cavity light. The cavity finesse $\mathcal{F}$, which determines – up to a factor of π – the mean number of round trips of light, before it gets lost at the mirrors, is defined by the ratio between free spectral range and cavity linewidth (FWHM) $\Delta\nu$:

$$\mathcal{F} = \frac{\Delta\nu_{\mathrm{FSR}}}{\Delta\nu}. \tag{2.3}$$

In case of very high mirror reflectivities, the finesse relates to the mirror transmission $\mathcal{T}$ and mirror losses $\mathcal{L}$ via

$$\mathcal{F} = \frac{2\pi}{2\mathcal{L} + 2\mathcal{T}}. \tag{2.4}$$

In our setup we use dielectric Bragg mirrors with a reflection coating, being optimized for light with a wavelength of 780 nm. This results in a finesse of $3.4 \cdot 10^5$ and a cavity linewidth of 2.4 MHz. Possibly due to mounting-induced strain on the mirror substrates, a slight birefringence splits the two orthogonal, principal polarization axes of the TEM_{00} cavity mode by 1.7 MHz. A list of relevant cavity parameters is given in Table 2.1.

2.2.2. Probing the cavity resonance

Experimentally, we probe the resonance frequency of the coupled BEC-cavity system by shining a weak laser beam with a wavelength of $\lambda_p = 780\,\mathrm{nm}$ onto one of the cavity mirrors, while monitoring the transmitted light intensity on a single photon counter. The probe laser beam profile is mode matched to the Gaussian TEM_{00} mode profile. The relative frequency between the empty cavity resonance and the probe laser is controlled by means of a stabilization laser which operates at a wavelength of $\lambda_s = 830\,\mathrm{nm}$. This laser is frequency stabilized relative to the probe laser via two independent Pound-Drever-Hall locks [90] onto a common transfer cavity [91] with a cavity linewidth of approximately 1 MHz (see Figure 2.3). The length of the science cavity can be controlled with a piezo tube, and is actively stabilized via a Pound-Drever-Hall lock onto the stabilization laser. The relative frequency between the empty cavity resonance and the probe laser can be fine-tuned within the transfer cavity free spectral range of 1 GHz, by using an additional pair of 780 nm and 830 nm lasers onto which the probe and stabilization lasers are phase-locked, respectively (see Figure 2.3).

This "lock chain" provides us with a relative frequency stability between empty cavity resonance and probe laser well below the linewidth of the

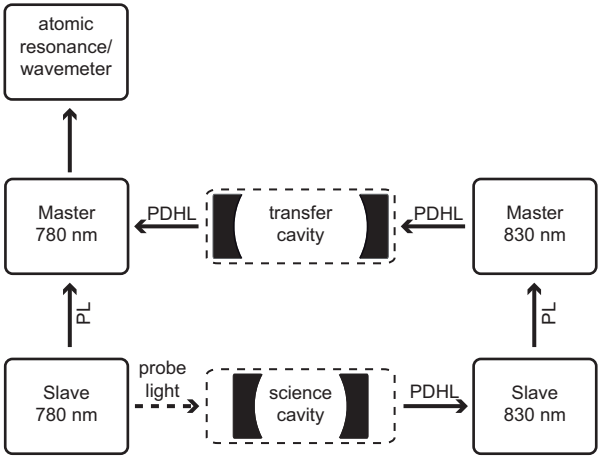

FIGURE 2.3.: Simplified schematics of the cavity lock chain. Components which are connected by solid lines are frequency stabilized to each other (PDHL: Pound-Drever-Hall lock, PD: phase lock). The component where the arrow points to serves as the frequency reference.

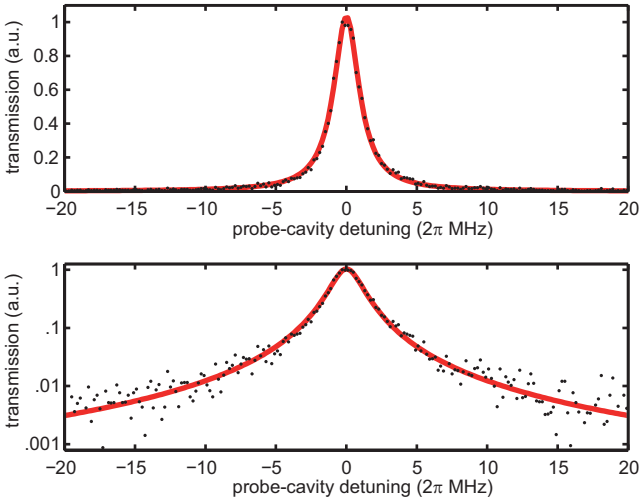

FIGURE 2.4.: Characterization of the empty cavity resonance. Shown is the transmitted light intensity (in arbitrary units) while scanning the probe laser frequency ω_p at a rate of 2 MHz/ms across the empty cavity resonance with a maximum mean intracavity photon number of 1.5. The data points are obtained by averaging over 41 shots. The solid line is obtained by fitting a Lorentzian line shape to the data which results in a cavity linewidth of $\kappa = 2\pi \times 1.2\,\mathrm{MHz}$.

science cavity, as we infer from probe frequency scans across the empty cavity resonance (Figure 2.4). To probe the system in the vicinity of the atomic D_2 transition line we additionally frequency stabilize one of the 780 nm lasers via Doppler-free RF spectroscopy onto an atomic resonance, providing us with an absolute frequency stability below the MHz scale. For experiments in the dispersive regime, where the probe laser frequency is detuned by several tens of GHz from the atomic resonance, we actively frequency stabilize the cavity lock chain on a wavelength meter (see Figure 2.3).

2.2.3. Cavity QED parameters

With a mode waist radius of $w_0 = 25.3\,\mu\mathrm{m}$ the TEM_{00} mode of our cavity has a mode volume of $V = 88 \times 10^3\,\mu\mathrm{m}^3$. Correspondingly, the maximum electric field strength $E_1 = \sqrt{\frac{\hbar\omega_c}{2\epsilon_0 V}}$ of a single intracavity photon with frequency ω_c is sufficiently large to reach the single-atom strong coupling regime of cavity

QED. With the effective dipole moment d_{eff} (isotropic light polarization) for the $|F = 2\rangle \rightarrow |F' = 3\rangle$ transition of ^{87}Rb we find an atom-cavity coupling rate of $g_0 = \frac{d_{\text{eff}} E_1}{\hbar} = 2\pi \times 10.6\,\text{MHz}$ which exceeds both the decay rate of the cavity field, $\kappa = 2\pi \times 1.2\,\text{MHz}$, and the atomic spontaneous decay rate, $\gamma = 2\pi \times 3.0\,\text{MHz}$.

In our experiments, we prepare spin-polarized atomic samples which were optically pumped into the $|F = 1, m_F = -1\rangle$ ground state. Due to a small magnetic field ($B \approx 0.1\,\text{G}$) pointing along the cavity axis, probe photons can only couple to σ_+ or σ_- transitions. The corresponding coupling strengths are obtained by summing the relevant Clebsch-Gordan coefficients [92] in squares. For a single σ_+ or σ_- polarized photon we find coupling strengths of $g_+ = 2\pi \times 14.1\,\text{MHz}$ and $g_- = 2\pi \times 10.9\,\text{MHz}$, respectively. In the experimental setup we use polarization optics and two independent single photon counter modules in order to simultaneously detect the left-handed and right-handed polarized components in the transmitted cavity light.

2.2.4. Photon detection efficiency

Though unwanted in many cavity QED experiments, the unavoidable loss of cavity photons through the cavity mirrors provides us with valuable *in-situ* information about the intracavity light intensity. The quantitative relationship between the photon count rate r_{SPCM} at the single photon counting module (SPCM), and the mean number of intracavity photons is determined by the detection efficiency ϵ of a single intracavity photon. This probability depends on the transmission $\mathcal{T} = 2.3\,\text{ppm}$ and the losses $\mathcal{L} = 6.9\,\text{ppm}$ at the cavity mirrors, the total losses $1 - \epsilon_{\text{op}} \approx 0.15$ at the optics (mirrors, spatial and spectral filters) used to direct the light onto the SPCM, and the quantum efficiency $\epsilon_{\text{SPCM}} \approx 0.5$ of the SPCM itself:

$$\epsilon = \frac{\mathcal{T}}{2\mathcal{T} + 2\mathcal{L}}\, \epsilon_{\text{op}}\, \epsilon_{\text{SPCM}} \approx 0.05. \tag{2.5}$$

The count rate r_{SPCM} of the SPCM for a mean intracavity photon number $\bar{n}$ is given by

$$r_{\text{SPCM}} = 2\kappa\epsilon\bar{n}. \tag{2.6}$$

This relationship is only valid as long as saturation effects at the SPCM (which can be corrected for) are negligible. We estimated the overall systematic uncertainty in determining the intracavity photon number to be 25 %.

2.3. Preparing a Bose-Einstein condensate inside the optical cavity

With a duty cycle of about 60 s, atoms are pre-cooled and collected in the magneto-optical trap, optically pumped into the low-field seeking state $|F = 1, m_F = -1\rangle$, and magnetically transported into the QUIC trap. Here, evaporatively cooled samples of typically a few 10^6 atoms are prepared close to the critical temperature where Bose-Einstein condensation sets in. Experimentally we found, that further decreasing the temperature of the gas within the magnetic trap does not increase the final number of condensed atoms within the cavity.

To transport the atoms in a controlled way into the science cavity, we implemented an optical conveyor belt [93, 94] formed by two counter-propagating, red-detuned laser beams (Figure 2.1, 2.5). Due to the optical dipole forces, atoms can be loaded into the antinodes of the vertically aligned standing-wave potential forming a stack of pancake-shaped atom clouds. By applying a frequency difference between the upwards and the downwards propagating wave, the optical standing-wave pattern is converted into a moving pattern, and the confined atoms are transported downwards. Once the atoms reached the position of the cavity mode, they are loaded into a crossed-beam dipole trap, and evaporatively cooled down to quantum degeneracy.

2.3.1. The optical transport

Optical setup

The light for transporting the atoms into the cavity is provided by two tapered amplifiers seeded by a common diode laser operating at a wavelength of $\lambda_T = 852\,\mathrm{nm}$. Since the overall transport distance depends linearly on this wavelength, we frequency stabilize this laser onto an atomic ^{133}Cs resonance. The frequencies and intensities of the transport beams are controlled using acousto-optical modulators, which are driven by two home-built, computer controlled direct digital synthesizers [95].

We use two independent optical fibers to guide the transport light from the laser table to the main experiment table. To reduce relative phase noise between the different optical paths, the optical fibers are passively stabilized by guiding them inside a passively vibration isolated tube. From the beat-note of the two transport beams (aligned in the final transport configuration) we infer a residual relative phase jitter below π per second.

After shaping the transport beams with telescopes, they are focused down to beam waist radii of $(w_x, w_y) = (25, 50)\,\mu\mathrm{m}$ at the position of the cavity

mode. This beam parameters were chosen in order to minimize cutting of the beams at the cavity mirror edges and mounting apertures, and to minimize the beam divergence at the position of the magnetic trap. The beam radii at the position of the magnetic trap are $(W_x, W_y) = (390, 200)\,\mu$m, and the maximum available power per transport beam (within the chamber) is about 85 mW.

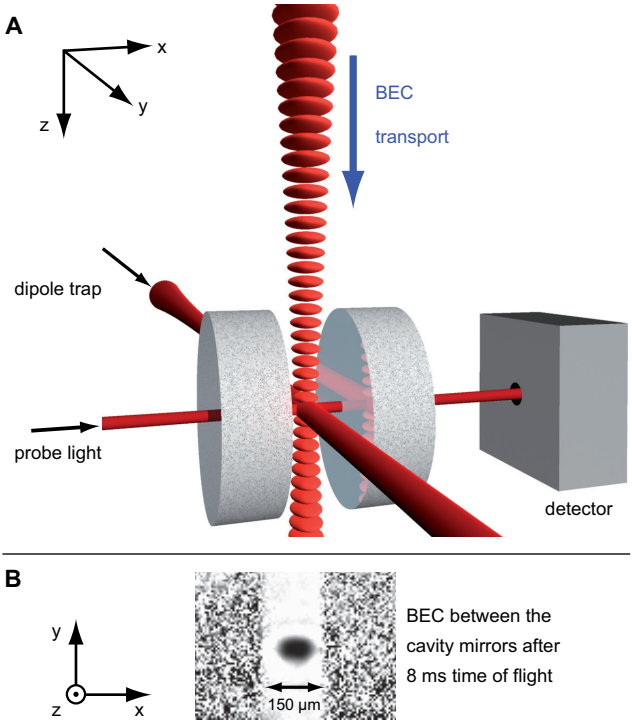

FIGURE 2.5.: Preparation of a BEC inside the cavity. (A) 36 mm above the cavity, 3.5×10^6 ultracold atoms are loaded into the dipole potential of a vertically oriented 1D optical lattice. This trumpet shaped standing wave has its waist inside the ultrahigh-finesse cavity and is composed of two counter-propagating laser beams. A translation of the lattice pattern transports the atoms into the cavity mode. There they are loaded into a crossed-beam dipole trap formed by a focused beam oriented along the y-axis and one of the transport beams. (B) Almost pure condensates with up to 2×10^5 atoms overlapping with cavity mode are obtained.

Transport sequence

After preparing ultracold atoms in the magnetic QUIC trap, we load them within 100 ms into a $7.5E_{\mathrm{rec}}$ deep transport lattice, with the recoil energy defined by $E_{\mathrm{rec}} = \frac{\hbar^2 k_{\mathrm{T}}^2}{2m}$, and the wave number $k_{\mathrm{T}} = 2\pi/\lambda_{\mathrm{T}}$. After the magnetic trap is switched off, the atoms are transported into the cavity within $T = 100\,\mathrm{ms}$. The frequency difference $\delta(t)$ between the two counter-propagating waves follows $\delta(t) = \frac{\delta_{\max}}{2}[1-\cos(2\pi t/T)]$, with a maximum detuning of $\delta_{\max} = 1.7\,\mathrm{MHz}$. Correspondingly, the atoms travel at a velocity of $v(t) = \lambda_{\mathrm{T}}\delta(t)/2$, and experience a maximum acceleration of $a = 22.4\,\mathrm{m/s^2}$. During the transport, the power in the laser beams is kept constant until the maximum light intensity at the position of the atoms has increased by a factor of 10. Subsequently, this intensity is kept constant by actively controlling the laser power in the two transport beams. Due to intrinsic evaporation during the transport, the number of atoms arriving in the cavity is reduced to typically 10^6. During the transport a small magnetic field serves as a quantization axis which keeps the sample highly spin polarized in the $|F = 1, m_F = -1\rangle$ state. However, due to off-resonant scattering in the transport beams, a small fraction of the atoms undergoes spontaneous transitions into the $|F = 2\rangle$ hyperfine ground state manifold. The transport beams are linearly polarized along the cavity axis, which rules out potential light scattering into the cavity mode [96].

2.3.2. The crossed-beam dipole trap

At the position of the cavity mode, the atoms are loaded into a crossed-beam dipole trap formed by one of the transport beams and an additional, horizontally propagating laser beam with a waist radius of $w_x = w_z = 27\,\mu\mathrm{m}$ (see Figure 2.5). A final stage of evaporative cooling is performed by suitably lowering the laser powers, ending up with an almost pure condensate of up to 2×10^5 atoms, as we infer from absorption imaging (see Figure 2.5). The final trapping frequencies are $(\omega_x, \omega_y, \omega_z) = 2\pi \times (290, 43, 277)\,\mathrm{Hz}$. We adjust the transverse position of the beams forming the dipole trap in order to optimize the overall coupling strength between the condensate and the cavity field.

2.3.3. The cavity dipole trap

A different far off-resonant dipole trap is provided by the laser light, which is used to frequency stabilize the science cavity. Its spatial structure is determined by the TEM_{00} mode profile of the cavity, and can be considered

to first order as a one-dimensional standing-wave potential. At the corresponding wavelength of $\lambda_t = 830\,\mathrm{nm}$ the cavity has a finesse of 38×10^3 and a linewidth of 22 MHz. We determine the depth of the trapping potential from the light intensity which is transmitted through the cavity, by taking into account a measured cavity mirror transmittance of 58 ppm.

Usually, we actively control the stabilization light intensity during the experiments at a minimal value which still allows a robust stabilization of the cavity resonance. The corresponding lattice potential has a depth which is on the order of $1E_{\mathrm{rec}}$. An exception are the experiments performed in Chapter 7, where the stabilization light is used to tightly confine the atoms in a one-dimensional, periodic lattice potential.

3 Cavity QED with a Bose-Einstein condensate

Cavity quantum electrodynamics (cavity QED) describes the coherent interaction between matter and an electromagnetic field confined within a resonating structure. By using high-quality resonators, a strong coupling regime can be reached experimentally in which atoms coherently exchange energy with a single light-field mode many times before dissipation sets in. This led to fundamental studies with both microwave [39, 38] and optical resonators [40]. To meet the challenges posed by quantum state engineering [37] and quantum information processing, recent experiments have focused on laser cooling and trapping of atoms inside an optical cavity [44, 97, 94]. However, the tremendous degree of control over atomic gases achieved with Bose-Einstein condensation [98] has so far not been used for cavity QED.

In this chapter we explore the strong coupling between the electronic degrees of freedom of a Bose-Einstein condensate and the quantized field of an ultrahigh-finesse optical cavity. We present a measurement of the eigenenergy spectrum, which is in perfect agreement with a theoretical model description. This experiment provides access to a conceptually new regime of cavity QED, in which all atoms occupy a single mode of a matter-wave field and couple identically to the light field, sharing a single excitation. It opens possibilities ranging from quantum communication [33, 34, 35] to a wealth of new phenomena proposed in the many-body physics of quantum gases with cavity-mediated interactions [31, 99].

The chapter is organized as follows. After an introduction into cavity QED with many atoms (Section 3.2), we show in Section 3.3 that the use of a Bose-Einstein condensate provides an ideal realization of the Tavis-Cummings model where all atoms are coupled identically to the cavity field. We generalize the generic Tavis-Cummings model to multi-level atoms and multi-mode cavities in the presence of a single excitation (Section 3.5). A measurement of the internal excitation spectrum of the coupled condensate-cavity system is presented in Section 3.6. We find very good agreement

between our data and a quantitative model description (Section 3.7), which confirms the excellent control over the experimental system.

The experimental results of this chapter have been published in [100]: F. Brennecke, T. Donner, S. Ritter, T. Bourdel, M. Köhl, and T. Esslinger. *Cavity QED with a Bose-Einstein condensate.* Nature 450, 268 (2007).

3.1. Introduction

The coherent coupling of a single two-level atom with a single mode of the electromagnetic field leads to a splitting of the energy eigenstates of the combined system, and is described by the Jaynes-Cummings model [101]. For its experimental realization the strong coupling regime has to be reached, where the maximum coupling strength g_0 between atom and light field is larger than both the amplitude decay rate of the excited state γ and the intracavity field κ. For a thermal ensemble of atoms coupled to a cavity mode, the individual, position-dependent coupling strengths of the atoms have to be taken into account.

To capture the basic physics of a Bose-Einstein condensate (BEC) coupled to the quantized field of a cavity, consider N atoms occupying a single wave function. Since the atoms are in the same motional quantum state, the single atom coupling g to the cavity mode is identical for all atoms. Moreover, bosonic stimulation into the macroscopically populated ground state should largely reduce the scattering of atoms into higher momentum states during the coherent evolution. This situation is well described by the Tavis-Cummings model [28], where N two-level atoms are assumed to identically couple to a single light field mode. A single cavity photon resonantly interacting with the atoms leads to a collective coupling of $g\sqrt{N}$.

An ensemble of thermal atoms would not fulfill the requirement of identical coupling, but it shows a similar energy spectrum, which can be modeled by the Tavis-Cummings Hamiltonian with an effective collective coupling [102]. In previous measurements [103, 104] and also in a very recent report [27], these eigenenergies have been measured for thermal atoms coupled to a cavity. Besides the sensitivity of the spectrum to the precise spatial distribution of the atoms, the differences between a BEC and a thermal cloud, or between a BEC and a Mott-insulator, should be accessible through the fluctuations of the coupling, i.e. in the width of the resonances [105].

3.2. Collective cavity QED

To understand the physics underlying the collective interaction between an atomic ensemble and light, we consider N identical two-level atoms with transition frequency ω_a coupled to a single cavity mode with resonance frequency ω_c. The atomic ground and excited states are denoted by $|g\rangle$ and $|e\rangle$, respectively. The individual positions $\mathbf{r}_i$ of the atoms within the TEM_{00} cavity mode structure $\phi(\mathbf{r}) = E_{00n}(\mathbf{r})/E_0$ (see Equation (2.1)) are considered to be fixed. The maximum coupling strength $g_0 = \frac{dE_1}{\hbar}$ between one atom and a single cavity photon is determined by the atomic dipole matrix

element $d = \langle g|\hat{d}|e\rangle$ and the "electric field strength per photon" $E_1 = \sqrt{\frac{\hbar\omega_c}{2\epsilon_0 V}}$, which depends on the cavity mode volume $V = \int |\phi(\mathbf{r})|^2 \mathrm{d}^3 r$.

The Hamiltonian describing the coherent coupling between N atoms and a single cavity mode reads [106, 2]

$$\hat{H} = \hbar\omega_c \hat{a}^\dagger \hat{a} + \hbar\omega_a \sum_{i=1}^{N} |e\rangle_{ii}\langle e| + \hbar \sum_{i=1}^{N} \left(g_i |e\rangle_{ii}\langle g|\hat{a} + g_i^* |g\rangle_{ii}\langle e|\hat{a}^\dagger \right), \quad (3.1)$$

with $\hat{a}(\hat{a}^\dagger)$ denoting the annihilating (creation) operators of cavity photons, and $g_i = g_0\phi(\mathbf{r}_i)$ the field coupling strength for atom i.

3.2.1. Eigenspectrum for a single excitation

The analysis of the eigenspectrum of Hamiltonian (3.1) is considerably simplified by the fact that $\hat{H}$ commutes with the total number of excitations in the system $\hat{n}_{\mathrm{tot}} = \hat{a}^\dagger\hat{a} + \sum_{i=1}^{N} |e\rangle_{ii}\langle e|$. Therefore, the diagonalization can be performed within the eigenspaces of constant excitation number n_{tot}. The only eigenstate with $n_{\mathrm{tot}} = 0$ equals the lowest energy state $|g \ldots g; 0\rangle$ where all atoms are in the ground state and the cavity mode contains no photon.

A basis of uncoupled states (bare states) in the state manifold $n_{\mathrm{tot}} = 1$ is provided by the state $|g \ldots g; 1\rangle$ and the N different states $|g \ldots e_i \ldots g; 0\rangle$, where only atom i is excited. Due to the coherent interaction between light and atoms the eigenstates of $\hat{H}$ are coherent superpositions of the bare states. Diagonalization of the Hamiltonian in this bare state basis yields the two eigenstates (dressed states)

$$\begin{aligned} |+\rangle &= \cos\phi\, |g \ldots g; 1\rangle + \sin\phi \sum_i \frac{g_i}{\bar{g}\sqrt{N}} |g \ldots e_i \ldots g; 0\rangle \\ |-\rangle &= -\sin\phi\, |g \ldots g; 1\rangle + \cos\phi \sum_i \frac{g_i}{\bar{g}\sqrt{N}} |g \ldots e_i \ldots g; 0\rangle \end{aligned} \quad (3.2)$$

with corresponding eigenenergies

$$E_\pm^{(1)} = \hbar\frac{\omega_a + \omega_c}{2} \pm \hbar\sqrt{\Delta_{ca}^2/4 + \bar{g}^2 N}. \quad (3.3)$$

Here, we introduced the cavity-atom detuning $\Delta_{ca} = \omega_c - \omega_a$, the collective coupling constant $\bar{g} = \sqrt{\sum_i |g_i|^2/N}$, and the mixing angle ϕ defined by $\tan(2\phi) = \frac{2\bar{g}\sqrt{N}}{\Delta_{ca}}$. The remaining $N-1$ eigenstates with eigenenergy $\hbar\omega_a$ are antisymmetric combinations of the N bare states $|g \ldots e_i \ldots g; 0\rangle$ without admixture of state $|g, \ldots, g; 1\rangle$. Since these states cannot be excited directly from the ground state $|g, \ldots, g; 0\rangle$ by driving the cavity mode, they are

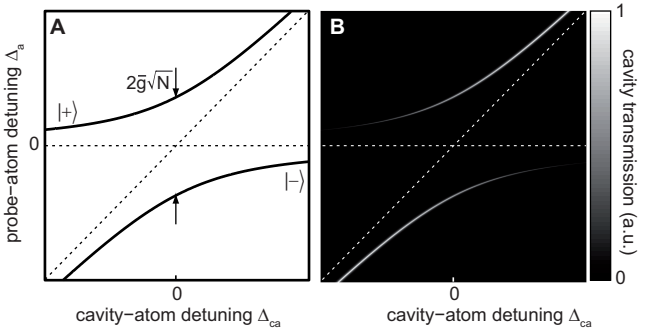

FIGURE 3.1.: (A) Excitation spectrum of the collectively coupled atoms-cavity system in presence of a single excitation (see Equation 3.1). The solid lines depict the two coupled resonances $|\pm\rangle$ which split around the crossing of the corresponding bare states $|g\ldots g;1\rangle$ and $|g\ldots e_i\ldots g;0\rangle$ depicted by the angular and horizontal dashed lines, respectively. (B) Cavity transmission spectrum in the low excitation limit, according to Equation (3.16). The amount of transmission is a measure for the admixture of the bare cavity state $|g\ldots g;1\rangle$ in the coupled eigenstates $|\pm\rangle$.

usually referred to as dark states [102, 107]. In what follows we will ignore all dark states.

From Equation (3.3) one infers about an enhanced coupling strength of the atomic ensemble to the single cavity mode by a factor of $\sqrt{N}$, compared to the single-atom case with mean coupling strength $\bar{g}$. This enhancement, which is not a consequence of quantum statistics, refers to the fact that a single atomic excitation is coherently shared between all atoms (see Equation (3.3)). In particular, collectivity does not require identical coupling strength of all atoms to the cavity mode. In general, such coherent superposition states of N identical subsystems are called Dicke states. Their collective behavior has been theoretically studied for the first time by Dicke in 1954 [49], and recently gained renewed interest in the context of the realization of a quantum memory [34, 50].

The energy spectrum of the coupled system in presence of a single excitation is shown in Figure 3.1A as a function of cavity-atom detuning. The two dressed states $|+\rangle$ and $|-\rangle$ show a characteristic anti-crossing around the crossing of the bare state energies. The splitting, which is commonly referred to as the vacuum Rabi splitting, is given by twice the collective coupling strength. For large cavity-atom detuning Δ_{ca} the dressed state

energies converge to the bare state ones, and the excitation is dominantly found in the corresponding subsystem, as expressed by the mixing angle ϕ in Equations (3.2).

3.2.2. Nonlinearity and the second excitation manifold

A characteristic property of the Jaynes-Cummings model, which refers to the single-atom version of Hamiltonian (3.1), is a nonlinearity of the energy spectrum, which arises when passing to higher excited state manifolds $n_{\mathrm{tot}} > 1$. Basically, it originates from the fact that a single two-level system (in contrast to a harmonic oscillator) cannot carry more than one excitation at once. This nonlinearity in the excitation number of the Jaynes-Cummings model prevents one from climbing the excitation spectrum with a single laser frequency [7, 108], and leads to collapse and revival phenomena in the cavity field intensity [109, 3].

In the case of $N \gg 1$ two-level systems collectively coupled to the cavity mode, this nonlinearity is strongly suppressed. Here, many excitations can be put into the atomic ensemble until saturation gets relevant. For low excitation numbers this corresponds to the situation of two mutually coupled harmonic oscillators – a system which has a purely linear energy spectrum. Quantitatively, this can be understood from the diagonalization of the Hamiltonian (3.1) within the second excited state manifold $n_{\mathrm{tot}} = 2$. For $\Delta_{ca} = 0$, the three relevant eigenstates have eigenenergies given by

$$E_{\pm}^{(2)} = 2\hbar\omega_a \pm 2\hbar\bar{g}\sqrt{N - 1/2} \tag{3.4}$$

$$E_{0}^{(2)} = 2\hbar\omega_a. \tag{3.5}$$

All other eigenstates are dark ones. The result shows that in case of large atom number N the second excited manifold can be excited resonantly (up to an error on the order of $1/N$) via the first excited state manifold, which holds true for even higher excited state manifolds as along as $n_{\mathrm{tot}} \ll N$ [28]. This is in contrast to the single-atom case, where the splitting between the two coupled states in the second excited state manifold is given by $2\sqrt{2}\bar{g}$.

3.3. Coupling a BEC to a single cavity mode: Tavis-Cummings model

A substantial simplification of the collective atom-cavity system is introduced by taking all coupling constants to be identical, $g_i = g$, as was originally considered by Tavis and Cummings in 1968 [28]. A true experimental

realization of this situation with thermal atoms inside a standing wave optical resonator would require very elaborate trapping techniques. Instead, using the ultimate control over the external degree of freedom provided by Bose-Einstein condensation, allows to realize the Tavis-Cummings model with large atom number N in the optical domain. In a condensate all atoms are prepared in the same motional quantum state characterized by the wave function $\psi(\mathbf{r})$. Thus, all atoms share the same spatial overlap with the cavity mode structure and couple identically to the cavity field.

Formally, the coupled BEC-cavity system can be described within a many-body formalism. Denoting by $\hat{\Psi}_g$ and $\hat{\Psi}_e$ the matter-field operators for atoms in the ground state and the excited state, respectively, the coherent coupling between a BEC of two-level atoms and a single cavity mode is captured by the Hamiltonian [110]

$$\hat{H}_{\mathrm{BEC-cav}} = \hbar\omega_c \hat{a}^\dagger \hat{a} + \int \Big(\hbar\omega_a \hat{\Psi}_e^\dagger(\mathbf{r}) \hat{\Psi}_e(\mathbf{r}) + \hbar g_0 \big(\hat{\Psi}_e^\dagger(\mathbf{r}) \hat{\Psi}_g(\mathbf{r}) \phi^*(\mathbf{r}) \hat{a} + \mathrm{h.c.} \big) \Big) \mathrm{d}^3 r, \tag{3.6}$$

where h.c. denotes the hermitian conjugate. As we are interested in the internal atom dynamics only, the terms describing atomic motion and the atom-atom interactions have been omitted.

Within a mean-field model, all condensate atoms can be considered to occupy the same spatial matter-wave mode described by the wave function $\psi(\mathbf{r})$, which is obtained as the lowest energy solution of the Gross-Pitaevskii equation [111]. In our experiment, the condensate wave function extends over about ten optical wavelengths, i.e. the atoms are delocalized over several nodes and antinodes of the cavity mode structure. In the following we aim to find the relevant bare states of the system in the first excited state manifold.

With a single photon occupying the cavity mode, the first excited bare cavity state is denoted by

$$|1_c\rangle \equiv \Psi(\mathbf{r}) |g \ldots g; 1\rangle, \tag{3.7}$$

with the many-body wave function denoted by $\Psi(\mathbf{r}) = \prod_{i=1}^{N} \psi(\mathbf{r}_i)$. Condensate atoms which absorb a photon from the cavity field are transferred, according to the spatial mode structure $\phi(\mathbf{r})$, into the spatial mode $\psi(\mathbf{r})\phi^*(\mathbf{r})$. The light-matter interaction couples the state $|1_c\rangle$ to the coherent superposition

$$|1_e\rangle \equiv \mathcal{N}_1 \sum_{i=1}^{N} \phi^*(\mathbf{r}_i) \Psi(\mathbf{r}) |g \ldots e_i \ldots g; 0\rangle, \tag{3.8}$$

where the prefactor $\mathcal{N}_1$ accounts for proper normalization. Applying the interaction term again on the state $|1_e\rangle$ yields the state

$$|1'_c\rangle \equiv \mathcal{N}_2 \sum_{i=1}^{N} |\phi(\mathbf{r}_i)|^2 \Psi(\mathbf{r}) |g \dots g; 1\rangle, \tag{3.9}$$

where all atoms are in their electronic and motional ground state except one being transferred into the spatial mode $\psi(\mathbf{r})|\phi(\mathbf{r})|^2$. However, this state differs only up to terms of order $1/\sqrt{N}$ from the initial state $|1_c\rangle$

$$|1'_c\rangle = \langle 1_c|1'_c\rangle |1_c\rangle + \mathcal{O}(1/\sqrt{N}). \tag{3.10}$$

This confirms that for large atom numbers the BEC-cavity excitation spectrum in presence of a single excitation can effectively be deduced within the basis spanned by the bare states $|1_c\rangle$ and $|1_e\rangle$.

To formally show the relationship to the Tavis-Cummings model, we expand the matter wave operators in the relevant spatial modes

$$\begin{aligned} \hat{\Psi}_g(\mathbf{r}) &= \psi^*(\mathbf{r})\hat{g} \\ \hat{\Psi}_e(\mathbf{r}) &= \psi^*(\mathbf{r})\phi(\mathbf{r})\hat{e} \end{aligned}$$

with ground and excited state annihilation operators $\hat{g}$ and $\hat{e}$, respectively. Accordingly, the many-body Hamiltonian (3.6) simplifies to

$$\hat{H}_{\mathrm{BEC-cav}} = \hbar\omega_c \hat{a}^\dagger \hat{a} + \hbar\omega_a \hat{e}^\dagger \hat{e} + \hbar g\big(\hat{e}^\dagger \hat{g} \hat{a} + \mathrm{h.c.}\big). \tag{3.11}$$

Thus, every condensate atom couples identically to the cavity field with an average coupling strength given by

$$g = g_0 \sqrt{\int |\phi(\mathbf{r})|^2 |\psi(\mathbf{r})|^2 \mathrm{d}^3 r}. \tag{3.12}$$

For large atom number the Bogoliubov approximation $\hat{g} = \sqrt{N}$ applies. This turns Hamiltonian (3.11) via the identification $\hat{e} \equiv \sum_i |g\rangle_{ii}\langle e|/\sqrt{N}$ into the Tavis-Cummings Hamiltonian

$$\hat{H}_{\mathrm{TC}} = \hbar\omega_c \hat{a}^\dagger \hat{a} + \hbar\omega_a \sum_{i=1}^{N} |e\rangle_{ii}\langle e| + \hbar g\Big(\sum_{i=1}^{N} |e\rangle_{ii}\langle g| \hat{a} + \mathrm{h.c.}\Big). \tag{3.13}$$

3.4. Dissipation

In any experimental cavity QED realization the unitary Hamiltonian dynamics is accompanied by decoherence processes: both the cavity field and the atomic excited state can decay into vacuum field modes which are not supported by the resonator. The appropriate description of such open quantum systems is provided by a density matrix formalism. In case of the Tavis-Cummings model, the density matrix $\hat{\rho}$ of the coupled system evolves in time according to the Master equation [112, 113]

$$\dot{\hat{\rho}} = -\frac{i}{\hbar}[\hat{H}_{\mathrm{TC}}, \hat{\rho}] - \frac{i}{\hbar}[\hat{H}_p, \hat{\rho}] + \kappa \mathcal{D}[\hat{a}]\hat{\rho} + \gamma \sum_{i=1}^{N} \mathcal{D}[\sigma_i^-]\hat{\rho}. \tag{3.14}$$

Here, γ and κ denote the amplitude decay rates of the atomic excited state and the cavity field, respectively, and the super-operators [114] $\mathcal{D}[\hat{c}]$ (for any operator $\hat{c}$) act on the density matrix according to $\mathcal{D}[\hat{c}]\hat{\rho} = 2\hat{c}\hat{\rho}\hat{c}^\dagger - \hat{c}^\dagger\hat{c}\hat{\rho} - \hat{\rho}\hat{c}^\dagger\hat{c}$. The Tavis-Cummings Hamiltonian $\hat{H}_{\mathrm{TC}} = -\hbar\Delta_c\hat{a}^\dagger\hat{a} - \hbar\Delta_a \sum_i \hat{\sigma}_i^+\hat{\sigma}_i^- + \hbar g \sum_i (\hat{\sigma}_i^+\hat{a} + \hat{\sigma}_i^-\hat{a}^\dagger)$ is written in a frame which rotates at the probe frequency ω_p, with probe-cavity detuning $\Delta_c = \omega_p - \omega_c$ and probe-atom detuning $\Delta_a = \omega_p - \omega_a$. Coherently driving the cavity mode at amplitude rate η is described by the probe term $\hat{H}_p = -i\hbar\eta(\hat{a} - \hat{a}^\dagger)$. For notational simplicity, the pseudo-spin operators $\hat{\sigma}_i^+ \equiv |e\rangle_{ii}\langle g|$, $\hat{\sigma}_i^- \equiv |g\rangle_{ii}\langle e|$ and $\hat{\sigma}_i^z \equiv |e\rangle_{ii}\langle e| - |g\rangle_{ii}\langle g|$ for atom i have been introduced.

According to the Master equation (3.14), the time evolution of the expectation values of the cavity field and the atomic dipoles is determined by

$$\begin{aligned} \langle \dot{\hat{a}} \rangle &= (i\Delta_c - \kappa)\langle \hat{a} \rangle + \eta - ig \sum_i \langle \hat{\sigma}_i^- \rangle \\ \langle \dot{\hat{\sigma}}_i^- \rangle &= (i\Delta_a - \gamma)\langle \hat{\sigma}_i^- \rangle + ig\langle \hat{\sigma}_i^z \hat{a} \rangle. \end{aligned} \tag{3.15}$$

In the weak-probe limit $\eta \ll \kappa$ the states with more than one excitation present in the system can be neglected, which implies $\langle \hat{\sigma}_i^z \hat{a} \rangle = -\langle \hat{a} \rangle$ [113]. This allows to analytically solve equations (3.15) for the steady-state cavity mean-field:

$$\langle \hat{a} \rangle = \frac{\eta}{(\kappa - i\Delta_c) + Ng^2/(\gamma - i\Delta_a)}. \tag{3.16}$$

Figure 3.1B shows the cavity transmission $\propto |\langle \hat{a} \rangle|^2$ in steady state, according to Equation (3.16). The dressed cavity transmits light only close to the eigenfrequencies of the coupled system (shown in Figure 3.1A). Namely, in the absence of spontaneous emission, $\gamma = 0$, the field amplitude $\langle \hat{a} \rangle$ takes its local maxima along the lines $\omega_p = E_\pm^{(1)}/\hbar$ (see Equation (3.3)). The

corresponding amount of transmission reflects the probability to find the excitation in the cavity field, which in the limit $\kappa = \gamma = 0$ is given by the mixing factors in the dressed state expansion (Equation (3.2)).

3.5. Multilevel atoms coupled to a multi-mode cavity

To quantitatively describe the internal energy spectrum of 10^5 Rubidium atoms coupled to the field of an optical Fabry-Perot cavity, we have to consider several generalizations of the model system studied before, in order to account for the atomic multilevel structure and the different modes supported by the cavity.

In our experiments the collectively enhanced coupling strength between condensate and cavity field is on the order of several GHz. Therefore, all optical dipole transitions of the D_2 line in ^{87}Rb can potentially contribute to the energy spectrum [114], and induce a coupling of the two principal polarizations of the empty cavity field.

Furthermore, a spatially inhomogeneous atomic ensemble can significantly modify the spatial cavity mode structure. This corresponds to the fact that excited atoms can emit light into different empty cavity modes giving rise to mode cross coupling. In principle, the new eigenmodes of the coupled atoms-cavity system are obtained by solving the field equations, containing the atomic polarizability as a source term. In our BEC-cavity system, the transverse mode structure of the empty cavity gets significantly affected since the collective coupling is comparable to the transverse mode spacing. This can be viewed as a variant of the superstrong coupling regime studied in [115], where the atom-light coupling strength was considered to be on the order of the free spectral range of the cavity.

In order to better understand how these different effects influence the BEC-cavity eigenspectrum, we consider in the following several extensions of the Tavis-Cummings model separately. A model description of the measured BEC-cavity spectrum which takes into account all effects mentioned above, is summarized in Section 3.7.

3.5.1. Two atomic ground states

The energy spectrum of our BEC-cavity system crucially depends on the initial population of the hyperfine ground states in ^{87}Rb. To demonstrate this, we consider an atomic level structure with only two ground states[1] $|g_1\rangle$

[1] In particular, we have in mind the $|F = 1\rangle$ and the $|F = 2\rangle$ state manifolds neglecting their Zeeman sublevels.

and $|g_2\rangle$, and a single excited state $|e\rangle$. The two ground states are separated by Δ_{12}, and couple with strength g_1 and g_2 to the excited state (Figure 3.2).

The collective interaction between N of these three-level atoms and one cavity mode is described by the generalized Tavis-Cummings Hamiltonian

$$\hat{H} = \hbar\omega_c \hat{a}^\dagger \hat{a} + \hbar\Delta_{12} \sum_{i=1}^{N} |g_2\rangle_{ii}\langle g_2| + \hbar\omega_a \sum_{i=1}^{N} |e\rangle_{ii}\langle e| + \hbar \sum_{i=1}^{N} \Big(g_1 |e\rangle_{ii}\langle g_1|\hat{a} + g_2 |e\rangle_{ii}\langle g_2|\hat{a} + \text{h.c.} \Big), \quad (3.17)$$

where ω_a denotes the transition frequency between $|g_1\rangle$ and $|e\rangle$.

Initially the system is prepared in the ground state $|g_1 \dots g_1; g_2 \dots g_2; 0\rangle$ with N_1 ($N_2 = N - N_1$) atoms in state $|g_1\rangle$ ($|g_2\rangle$), respectively, and without excitation in the cavity mode. Possible coherences between state $|g_1\rangle$ and $|g_2\rangle$, which are present for example in spinor condensates [116], are not captured by this state description. However, it mimics incoherent spin mixtures as we deal with in our experiments.

Weakly driving the cavity field populates the state $|0\rangle = |g_1 \dots g_1; g_2 \dots g_2; 1\rangle$ which owing to the interaction Hamiltonian $\hat{H}_{\text{int}}$ (the last term in Equation (3.17)) is coupled to the following two Dicke-type states

$$\begin{aligned} |1\rangle &= \frac{1}{\sqrt{N_1}} \sum_{i=1}^{N_1} |g_1 \dots \underset{\substack{\uparrow \\ i}}{e} \dots g_1; g_2 \dots g_2; 0\rangle \\ |2\rangle &= \frac{1}{\sqrt{N_2}} \sum_{i=1}^{N_2} |g_1 \dots g_1; g_2 \dots \underset{\substack{\uparrow \\ i}}{e} \dots g_2; 0\rangle. \end{aligned} \quad (3.18)$$

where the excitation is being taken either by a $|g_1\rangle$- or a $|g_2\rangle$-atom. The coupling matrix elements between the states $|c\rangle$ and $|1\rangle$ ($|2\rangle$) are given by $g_1\sqrt{N_1}$ ($g_2\sqrt{N_2}$), respectively.

The interaction Hamiltonian couples the states $|1\rangle$ and $|2\rangle$ either back to the state $|c\rangle$, or to the two states

$$\begin{aligned} |0'\rangle &= \frac{1}{\sqrt{N_1}} \sum_{i=1}^{N_1} |g_1 \dots \underset{\substack{\uparrow \\ i}}{g_2} \dots g_1; g_2 \dots g_2; 1\rangle \\ |0''\rangle &= \frac{1}{\sqrt{N_2}} \sum_{i=1}^{N_2} |g_1 \dots g_1; g_2 \dots \underset{\substack{\uparrow \\ i}}{g_1} \dots g_2; 1\rangle, \end{aligned} \quad (3.19)$$

where one atom was transferred from $|g_1\rangle$ to $|g_2\rangle$, or vice versa. Though these transitions are off-resonant, they can in principle contribute in terms

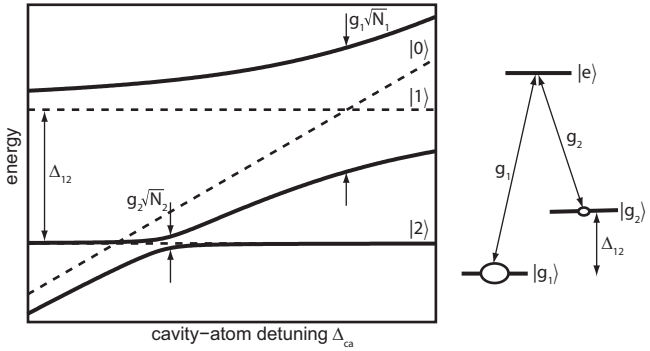

FIGURE 3.2.: Eigenspectrum in the presence of a single excitation of a generalized Tavis-Cummings model corresponding to the atomic level scheme shown to the right. The dressed (bare) states are depicted by the solid (dashed) lines. The incoherent state populations of the two ground states $|g_1\rangle$ and $|g_2\rangle$ are given by N_1 and $N_2 = 0.01N_1$, respectively.

of virtual photon processes to the final energy spectrum. However, since we assume coherences between the two ground state populations to be negligible, the corresponding transition probabilities are not collectively enhanced. This can be shown by calculating the corresponding transition matrix elements

$$\langle 1|H_{\rm int}/\hbar|0'\rangle =$$

$$\frac{g_2}{N_1}\sum_i^N\sum_j^{N_1}\sum_k^{N_1}\langle g_1\ldots\underset{\uparrow}{e}_j\ldots g_1;g_2\ldots g_2;0|e\rangle_{ii}\langle g_2|\hat{a}|g_1\ldots\underset{\uparrow}{g_2}_k\ldots g_1;g_2\ldots g_2;1\rangle$$

$$= g_2. \tag{3.20}$$

In summary, we can restrict the calculation of the energy spectrum of Hamiltonian (3.17) within the first excited state manifold to the bare states basis $|0\rangle$, $|1\rangle$ and $|2\rangle$.

Figure 3.2 shows the resulting energy spectrum for a relative state population of $N_1 = 100N_2$. As for the case of N two-level atoms, the eigenstates exhibit vacuum Rabi splittings which are proportional to the square root of the atom number in the corresponding state. For a strong imbalance between N_1 and N_2 the splitting of the minority component is – caused by dispersive shift of the majority component – horizontally shifted with respect to the crossing of the corresponding bare states (see Figure 3.2).

3.5.2. Two orthogonally polarized cavity modes

Our high-finesse cavity supports two linearly polarized TEM_{00} modes, labelled as horizontal (h) and vertical (v) polarized modes. The cavity birefringence splits their resonance frequencies by about 1.7 MHz. In general, the two bare cavity modes get mixed by their coupling to the different atomic dipole transitions. Experimentally, we eliminate possible π-transitions by applying a small magnetic field pointing along the cavity axis.

To illustrate the mixing of the two linear polarized bare cavity modes, we consider a simplified atomic level scheme consisting of a single ground state and two degenerate excited states $|e_+\rangle$ and $|e_-\rangle$, that couple to the ground state via σ_+ and σ_- transitions, respectively. The corresponding Hamiltonian reads

$$\begin{aligned}\hat{H} = \hbar \sum_{p=h,v} \omega_c^p \hat{a}_p^\dagger \hat{a}_p + \hbar\omega_a \sum_{i=1}^{N} \Big(|e_+\rangle_{ii}\langle e_+| + |e_-\rangle_{ii}\langle e_-| \Big) \\ + \hbar \sum_{i=1}^{N} \Big(g_+ |e_+\rangle_{ii}\langle g| (\hat{a}_h + i\hat{a}_v)/\sqrt{2} + g_- |e_-\rangle_{ii}\langle g| (\hat{a}_h - i\hat{a}_v)/\sqrt{2} + \text{h.c.} \Big)\end{aligned} \tag{3.21}$$

with empty cavity frequencies ω_c^h and ω_c^v and coupling constants $g_\pm$. Switching to field operators for circular polarized modes $\hat{a}_\pm = (\hat{a}_h \pm i\hat{a}_v)/\sqrt{2}$, one can rewrite this Hamiltonian as

$$\hat{H} = \hat{H}_+ + \hat{H}_- + \hat{H}_{\text{couple}} \tag{3.22}$$

with the two-level Tavis-Cummings systems

$$\hat{H}_\pm = \hbar\bar{\omega}_c \sum_{\pm} \hat{a}_\pm^\dagger \hat{a}_\pm + \hbar\omega_a \sum_{i=1}^{N} |e_\pm\rangle_{ii}\langle e_\pm| + \hbar \sum_{i=1}^{N} \Big(g_\pm |e_\pm\rangle_{ii}\langle g| \hat{a}_\pm + \text{h.c.} \Big), \tag{3.23}$$

and a coupling term between the two circular polarized modes

$$\hat{H}_{\text{couple}} = \hbar\delta(\hat{a}_+^\dagger \hat{a}_- + \hat{a}_-^\dagger \hat{a}_+). \tag{3.24}$$

Here, the mean resonance frequency $\bar{\omega}_c = \frac{\omega_h + \omega_v}{2}$ and the birefringence splitting $\delta = \frac{\omega_h - \omega_v}{2}$ have been introduced. For a collective coupling strength which by far exceeds the birefringence δ the mode coupling term can be neglected. Therefore, the final energy spectrum is given by the superposition of two Tavis-Cummings spectra with different vacuum Rabi splittings corresponding to the different coupling strengths $g_\pm$.

3.5.3. Higher-order transverse cavity modes

The large collective atom-field coupling present in our system causes a significant coupling between the different transverse cavity modes. In case of non-degenerate cavity modes this coupling becomes visible in the energy spectrum as long as the collective atom-light coupling strength is comparable to the frequency difference between the cavity modes.

To be more quantitative, we generalize the Master equation approach in Section 3.4, Equations (3.15), to the case of N two-level atoms and several cavity modes with bare resonance frequencies ω_k, $k \geq 0$, and mode functions $\phi_k(\mathbf{r})$. Eliminating the atomic polarizations $\langle \dot{\hat{\sigma}}_i \rangle$, the steady-state amplitude of mode k is determined by [105, 117]

$$0 = (i\Delta_k - \kappa)\langle \hat{a}_k \rangle + \delta_{k0}\eta + \sum_l \frac{g_k g_l}{i\Delta_a - \gamma} N \mathcal{O}_{kl} \langle \hat{a}_l \rangle. \tag{3.25}$$

Here, $\Delta_k = \omega_p - \omega_k$ is the probe-cavity detuning for mode k, and the Kronecker symbol δ_{k0} takes into account that only the zero-order mode (in the experiment the TEM_{00} mode) is driven with amplitude rate η. The maximum coupling strengths between a single atom and the individual cavity modes are given by $g_k = \frac{d}{\hbar}\sqrt{\frac{\hbar\omega_k}{2\epsilon_0 V_k}}$, and differ mainly due to the different cavity mode volumes V_k. All atoms are assumed to occupy the motional ground state $\psi(\mathbf{r})$ which enters the mode overlap integrals $\mathcal{O}_{kl} = \int \mathrm{d}^3 r |\psi(\mathbf{r})|^2 \phi_k^*(\mathbf{r})\phi_l(\mathbf{r})$.

The set of coupled equations (3.25) is equivalent to the classical field equations, which describe a driven multi-mode cavity containing a polarizable medium with density distribution given by $|\psi(\mathbf{r})|^2$ [118]. The cross coupling between the bare cavity modes is determined by the off-diagonal overlap integrals $\mathcal{O}_{kl}$ which – due to orthogonality of the modes ϕ_k – vanish for the case of a uniform density distribution. In our experiments the mean transverse size of the condensate is smaller than the cavity mode waist which results in a significant coupling of the different transverse cavity modes.

In the following we take the detunings of the higher-order modes, $k > 0$, from the zero-order mode, $\omega_k - \omega_0$, to be larger than the collective coupling strength. To lowest order the presence of the higher-order cavity modes then gives rise to an energy spectrum of the zero-order mode which is dispersively shifted with respect to the bare atomic transition line. We solve the coupled set of equations (3.25) in the limit $|\langle \hat{a}_k \rangle|^2 \ll |\langle \hat{a}_0 \rangle|^2$ for all $k > 0$, and obtain

$$\langle \hat{a}_k \rangle \approx \frac{g_0 g_k}{(\Delta_a - i\gamma)\Delta_k} \mathcal{O}_{k0} \langle \hat{a}_0 \rangle \qquad \forall k > 0. \tag{3.26}$$

Inserting this result into Equation (3.25), the zero-order mode spectrum is approximately described by the relation

$$0 = (i\Delta_0 - \kappa)\langle\hat{a}_0\rangle + \eta - \frac{Ng_0^2\mathcal{O}_{00}}{i(\Delta_a + \delta_{\text{eff}}) - \gamma}\langle\hat{a}_0\rangle \tag{3.27}$$

with an overall dispersive frequency shift given by $\delta_{\text{eff}} = \frac{N}{\mathcal{O}_{00}}\sum_{k\neq 0}\frac{g_k^2\mathcal{O}_{0k}^2}{\Delta_k}$. Correspondingly, the vacuum Rabi splitting of the zero-order mode is shifted by δ_{eff} with respect to the bare atomic transition frequency (see Section 3.6).

3.6. Measurements

To experimentally investigate the internal excitation spectrum of the coupled BEC-cavity system, we prepare almost pure condensates of up to 2.2×10^5 atoms in a crossed-beam dipole trap with trapping frequencies $(\omega_x, \omega_y, \omega_z) = 2\pi \times (290, 43, 277)\,\text{Hz}$, where x denotes the direction along the cavity axis. The atoms are prepared in the $|F = 1, m_F = -1\rangle$ ground state with respect to a small magnetic field of 0.1 G oriented along (within 10 %) the cavity axis. The position of the optical trap is adjusted to optimize the overlap between the atomic density and the TEM_{00} mode.

While probing the system, the intensity of the laser light which is used to stabilize the empty cavity resonance[2] is minimized in order to reduce the effect of the corresponding lattice potential on the atoms. This is achieved by operating the science cavity Pound-Drever-Hall lock on one of the sidebands of the stabilization light whose phase is modulated at a frequency of 364 MHz. This results in a one-dimensional lattice depth of $2.4\,E_{\text{rec}}$, with the recoil energy defined by $E_{\text{rec}} = h^2/(2m\lambda^2)$. The chemical potential $\mu = 1.8\,E_{\text{rec}}$ of 2.2×10^5 trapped atoms is comparable to the depth of this one-dimensional lattice, so that long-range phase coherence is well established in the atomic gas. The 1/e-lifetime of the atoms in the combined trap was measured to be 2.8 s.

3.6.1. Excitation spectrum in the weak-probe limit

To find the eigenenergies of the coupled BEC-cavity system for a single excitation, we perform transmission spectroscopy using a weak probe laser with frequency ω_p. The probe beam is mode matched to the Gaussian TEM_{00} mode profile of the empty cavity, and polarization matched to one of the cavity's principal axis. The stabilized resonance frequency ω_c of the

[2] The overall dispersive shift of the corresponding far-detuned cavity mode, caused by the presence of the atoms, is below 1MHz.

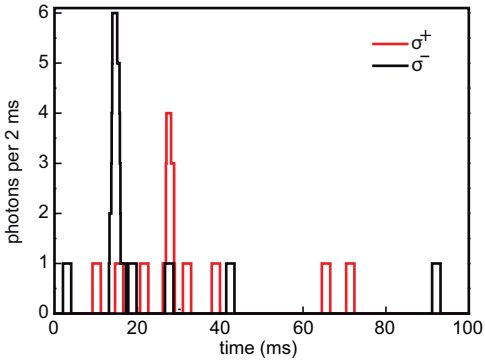

FIGURE 3.3.: Cavity transmission for the σ^+ and σ^- polarization component. The probe laser frequency is scanned at a speed of 25 MHz/ms while the cavity detuning is fixed. The original transmission data, recorded with a resolution of 0.4 μs, is averaged over 2 ms using a sliding average. A single peak for each polarization can clearly be distinguished from the background of about 60 dark counts per second.

(empty) TEM_{00} cavity mode is detuned by a variable frequency $\Delta_{ca} = \omega_c - \omega_a$ with respect to the frequency ω_a of the $|F = 1\rangle \rightarrow |F' = 2\rangle$ transition of the D_2 line of ^{87}Rb. The transmission of the probe laser through the cavity is monitored as a function of its detuning $\Delta_a = \omega_p - \omega_a$ (see Figure 3.3). The two circular polarization components of the transmitted light are separated and detected with independent single-photon counting modules. The overall detection efficiency for an intracavity photon was determined to be $5 \pm 1\,\%$. To probe the system in the weak excitation limit, the probe laser intensity is adjusted such as to excite a coherent state with mean intracavity photon number below the critical photon number $n_0 = \gamma^2/(2g_0^2) = 0.04$. With this the probability to find one photon in the cavity is more than 50 times larger than the probability to find two photons at once. From individual recordings of the cavity transmission as shown in Figure 3.3 we map out the low excitation spectrum of the coupled system as a function of Δ_{ca} (see Figure 3.4). After single scans across the coupled resonance we do not detect a significant influence on the BEC in absorption imaging for large atom numbers. For small BECs on the order of 5000 atoms we observe a loss of 50% of the atoms after resonant probing. The normal mode splitting at $\Delta_{ca} = 0$ amounts to 7 GHz for σ^+ polarization, which results in a collective cooperativity of $C = Ng^2/(2\gamma\kappa) = 1.6 \times 10^6$. The splitting for the σ^- component is smaller, because the overall dipole matrix

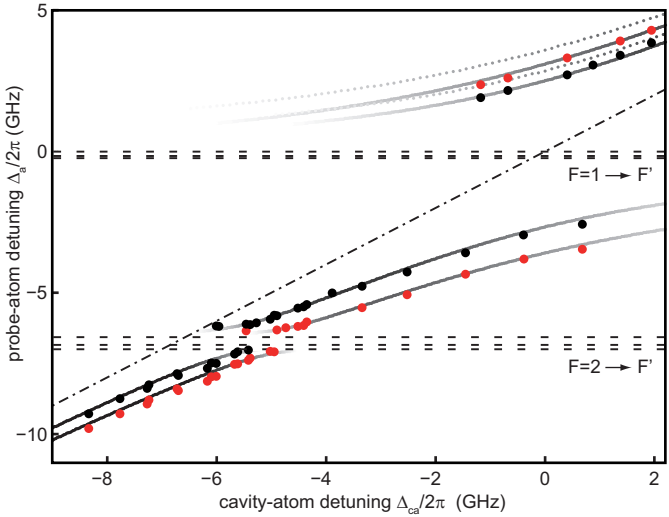

FIGURE 3.4.: Energy spectrum of the coupled BEC-cavity system. The data points are measured detunings of resonances for σ^+ (red) and σ^- (black) polarized light. Each data point is the average of three measurements with an uncertainty of about 25 MHz. Bare atomic resonances are depicted by the dashed horizontal lines, whereas the empty cavity resonance of the TEM_{00} mode is indicated by a dashed-dotted line. The solid lines show the result of a theoretical model (see Section 3.7) which takes into account all relevant dipole transitions and several higher-order cavity modes. Free fit parameters are the atom numbers N_{F,m_F} in the $|F=1,m_F=-1\rangle$ state and the Zeeman states in the $|F=2\rangle$ state manifold, respectively, as well as a transverse shift r of the trap center with respect to the cavity axis (for details see Section 3.7). Good agreement with our data is found for $N_{1,-1}=157\times10^3$, $\sum_k N_{2,k}=3.4\times10^3$ and $r=7\,\mu$m. The level of gray indicates the cavity transmission. The asymmetry in the splitting at $\Delta_{ca}=0$ is caused by the influence of higher-order transverse modes. Neglecting this influence the eigenenergies shown by the dotted lines would be expected, where the free parameters were adjusted to fit the spectrum for $\Delta_a<0$.

element for transitions starting in state $|F=1,m_F=-1\rangle$ driven by this polarization is smaller than that for σ^+ transitions.

A striking feature of the energy spectrum in Figure 3.4 is a second avoided crossing at probe frequencies resonant with the bare atomic transitions $|F=2\rangle\rightarrow|F'=1,2,3\rangle$. It is caused by the presence of atoms in the $|F=2\rangle$ hyperfine ground state (see Section 3.5.3). This avoided crossing is located

at a cavity detuning where the eigenenergy branch of the BEC-cavity system with no atoms in the $|F = 2\rangle$ would intersect the energy lines of the atomic transitions $|F = 2\rangle \rightarrow |F' = 1, 2, 3\rangle$. Accordingly the avoided crossing is shifted by approximately $Ng^2/\Delta_a = 2\pi \times 1.8\,\mathrm{GHz}$ with respect to the intersection of the empty cavity resonance with the bare atomic transition frequencies. From a theoretical analysis (see Section 3.7), we find the atom number of the $|F = 2\rangle$ minority component to be about 2 % of the total number of atoms.

Our near-planar cavity supports higher-order transverse modes equally spaced by 18.5 GHz, which is on the order of the collective coupling $g\sqrt{N}$ in our system. Due to atom-induced mode coupling (see Section 3.5.3) this results in a clearly visible asymmetry of the energy spectrum with respect to the bare atomic transition lines (see Figure 3.4).

3.6.2. Scaling with atom number

To test the square root dependence of the normal mode splitting on the number of atoms in the BEC, a second measurement was conducted. We set the cavity frequency to $\Delta_{ca} = 0$ and record the detuning $|\Delta_a|$ of the lower coupled state from the bare atomic resonance $|F = 1\rangle \rightarrow |F' = 2\rangle$ as a function of atom number, as displayed in Figure 3.5. The atom number was varied between 2.5×10^3 and 200×10^3, determined from separately taken absorption images with an estimated statistical error of $\pm 10\,\%$; possible systematic shifts are not accounted for. Our data is well described by a square root dependence, as expected from the Tavis-Cummings model. However, for a weakly interacting BEC the size of the atomic cloud – and thus the spatial overlap with the cavity mode – also depends on the atom number. Taking this effect into account, as well as the influence of higher-order cavity modes, results in a slightly better description of our data (Figure 3.5). It yields maximum single-atom couplings of $g_{\sigma^+} = 2\pi \times (14.4 \pm 0.3)\,\mathrm{MHz}$ and $g_{\sigma^-} = 2\pi \times (11.3 \pm 0.2)\,\mathrm{MHz}$ for the two polarization components. These values agree within our systematic uncertainties (dominated by atom number determination) with the expected coupling strengths of $g^{\mathrm{th.}}_{\sigma^+} = 2\pi \times 14.1\,\mathrm{MHz}$ and $g^{\mathrm{th.}}_{\sigma^-} = 2\pi \times 10.9\,\mathrm{MHz}$, which have been obtained by adding the coupling strengths of the different dipole transitions starting from $|F = 1, m_F = -1\rangle$ [92] in squares.

3.7. Quantitative modelling of the excitation spectrum

To quantitatively compare the measured energy spectrum with the one expected from theory, we take into account all optical dipole transitions within

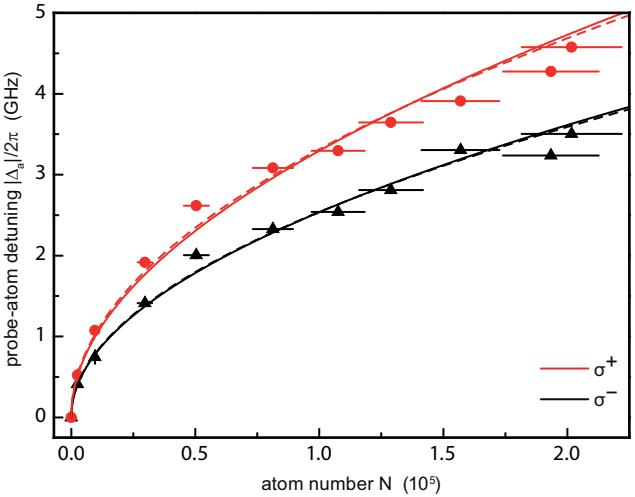

FIGURE 3.5.: Shift of the lower resonance of the coupled BEC-cavity system from the bare atomic resonance. The cavity was locked at $\Delta_{ca} = 0$. σ^+ and σ^- polarizations are shown as red circles and black triangles, respectively. Each data point is the average of three measurements. The atom number was determined separately from absorption images with an estimated error of $\pm 10\%$; the vertical statistical error bars are too small to be resolved. The solid lines are fits of the square root dependence on the atom number, as predicted by the Tavis-Cummings model. The dashed lines correspond to a more detailed theoretical model (see text) resulting in maximum coupling rates $g_{\sigma^+} = 2\pi \times (14.4 \pm 0.3)$ MHz and $g_{\sigma^-} = 2\pi \times (11.3 \pm 0.2)$ MHz. The ratio of the two coupling rates, 1.27 ± 0.03, agrees with the expected ratio of 1.29.

the D_2 line which couple to the two linear polarizations of the empty cavity field. We label the different atomic states in the $5^2S_{1/2}$ ground and the $5^2P_{3/2}$ excited state manifold by $|F, m_F\rangle$ and $|F', m'_F\rangle$, respectively. The transverse cavity modes are referenced by the double index $k \equiv (x, y)$ and the polarization index p, taking values h (horizontal) and v (vertical). Generalizing Equations (3.25) to the case of several optical transitions we arrive at the following set of coupled equations for the expectation values $\alpha_{j,p} \equiv \langle \hat{a}_{j,p} \rangle$

$$\dot{\alpha}_{k,p} = (i\Delta_k - \kappa)\alpha_{k,p} + \eta_{k,p} - \sum_{k',q} \Delta_{k,p}^{k',p'} \alpha_{k',p'}. \tag{3.28}$$

Here, the total dispersive and absorptive effect of the atoms on the empty cavity modes is given by

$$\Delta_{k,p}^{k',p'} = \sum_{F,m_F} N_{F,m_F} \sum_{F',m'_F} \frac{g_{F,m_F,p}^{F',m'_F\,*} g_{F,m_F,p'}^{F',m'_F}}{\gamma - i\Delta_{F,F'}} \mathcal{O}_{kk'} \frac{V_0}{\sqrt{V_k V_{k'}}}. \tag{3.29}$$

It depends on the spatial overlap integral $\mathcal{O}_{kk'} = \int \mathrm{d}^3 r |\psi(\mathbf{r})|^2 \phi_k^*(\mathbf{r}) \phi_{k'}(\mathbf{r})$ between atomic density distribution and cavity mode k and k', where V_k is the volume of mode k. $g_{F,m_F,p}^{F',m'_F}$ denotes the maximum coupling strength between the TEM_{00} mode with polarization p and the dipole transition connecting the states $|F, m_F\rangle$ and $|F', m'_F\rangle$ with transition frequency $\omega_p - \Delta_{F,F'}$. The number of atoms occupying the state $|F, m_F\rangle$ is given by N_{F,m_F}. Due to mode matching between the cavity probe beam and the fundamental mode in our experiment all driving amplitudes $\eta_{k,p}$ except the one with $k = (0,0)$ and $p = h$ can be set to zero. The higher-order cavity mode detuning $\Delta_{(x,y)} = \Delta_{(0,0)} - (x+y)\Delta\nu_\mathrm{T}$ differs from the zero mode detuning $\Delta_{(0,0)}$ by a multiple of the transverse mode spacing $\Delta\nu_\mathrm{T}$.

In our trapping geometry the condensate extends along the cavity axis over about 15 periods of the standing wave field intensity. We split the overlap integrals $\mathcal{O}_{kk'}$ into a product of a longitudinal part which equals approximately 1/2, and a pure transverse part $\mathcal{O}_{kk'}^\mathrm{tr}$. For a given trapping geometry the transverse overlap integrals depend only on the total atom number (which determines the condensate size) and the transverse position r of the trap center with respect to the cavity axis. For modelling the measured spectrum we include all transverse modes up to TEM_{xy} with $x + y = 4$. The influence of even higher transverse modes which are detuned by more than 90 GHz from the fundamental mode was numerically checked to be minor. Good agreement with our data is achieved by introducing a slight offset between condensate and cavity axis of $r = 7\,\mu\mathrm{m}$, which is on the order of our trap alignment accuracy. This increases the coupling to the closest detuned $\mathrm{TEM}_{(0,1)}$ and $\mathrm{TEM}_{(1,0)}$ modes, and is necessary to explain the distinct asymmetry of the splitting around the transition frequencies starting in $|F = 1\rangle$ (see Figure 3.4).

Starting with the overlap matrix $\mathcal{O}_{kk'}^\mathrm{tr}$, we numerically solve the linear system of equations (3.28) for steady state of $\alpha_{(0,0),h}$ and $\alpha_{(0,0),v}$. The solid curves in Figure 3.4 display the points where the intensity of the two circular polarizations $\alpha_{(0,0),h} \pm i\alpha_{(0,0),v}$ are locally maximal.

3.8. Summary

We presented a measurement of the internal excitation spectrum of a strongly coupled BEC-cavity system. Our model description includes several optical transitions as well as higher-order transverse cavity modes, and provides a very good understanding of our measurements, confirming the tremendous control achieved in this novel system.

The coupling of a single matter-field mode to a single cavity mode opens a route to new experiments. It facilitates the manipulation and study of statistical properties of quantum-degenerate matter-wave fields by a quantized optical field, or further the generation of entanglement between these two fields [105, 110]. The detection of single atoms falling through the cavity has already been demonstrated with this setup, providing valuable insight into the counting statistics of an atom laser [46]. In principle, the detection of small impurity components embedded in a large BEC presented here can also be extended to single atoms. This is an important step towards the realization of schemes aiming at the cooling of qubits immersed in a large BEC [119].

4 Cavity optomechanics with a Bose-Einstein condensate

In the remaining part of this thesis we study the dispersive coupling between a trapped Bose-Einstein condensate and the optical field inside a high-finesse Fabry-Perot cavity. In contrast to the near-resonant case where the coupled BEC-cavity system is dominated by the coherent exchange of excitations between the atomic internal degrees of freedom and the cavity field (see Chapter 3), here the system is governed by dipole forces and the atoms-induced phase shift of the cavity field. Correspondingly, both atomic motion and cavity field amplitude act as dynamical and mutually coupled degrees of freedom.

In this chapter we show that the dispersive coupling between condensate and cavity field can be described in the framework of cavity optomechanics. A collective density excitation of the BEC, matching the cavity mode profile, serves as a mechanical oscillator which strongly couples to the cavity field. After a brief introduction into cavity optomechanics, we present a theoretical description of the coupled BEC-cavity system in the dispersive limit. In a uniform and non-interacting limit the system is directly mapped to a cavity optomechanical model system. The influence of atom-atom interactions and the external trapping potential on the system's dynamics is discussed. This chapter provides the reader with the necessary background for understanding the experimental investigations, reported on in Chapters 5 to 7.

The main results of this chapter have been published in [120]: F. Brennecke*, S. Ritter*, T. Donner, and T. Esslinger. *Cavity Optomechanics with a Bose-Einstein condensate.* Science 322, 235 (2008).

4.1. A short introduction to cavity optomechanics

Light affects the motional degrees of freedom of a mechanical system through radiation pressure, which is caused by the exchange of momentum between light and matter. Besides the *scattering force* which results from momentum transfer whenever light is reflected at e.g. a mirror, spatial variations of the light intensity give rise to the *dipole force*, which nowadays is routinely used to trap atoms in optical dipole traps [56] and optical lattices [57, 121], or to manipulate micro-sized particles with optical tweezers [53].

Radiation pressure sets an ultimate limit on the precision at which the position of an object (e.g. a mirror) can be measured using light [61, 122]. In general, the tiny wavelength λ of optical fields is uniquely suited to measure distances with ultrahigh precision, as it is done in gravitational wave detectors or in Fabry-Perot cavities with a demonstrated sensitivity of $10^{-19}\,\mathrm{m}/\sqrt{\mathrm{Hz}}$ [123]. Here, the purpose is to determine tiny changes in the distance between the two end mirrors of a Fabry-Perot interferometer. This can be achieved, for example, by detecting the phase shift which a resonant laser beam experiences depending on the mirror distance. For a given relative displacement $\mathrm{d}X$ of the mirrors this phase shift $\mathrm{d}\varphi$ is enhanced by the cavity finesse $\mathcal{F}$, which determines the number of photon round trips in the cavity (see Figure 4.1B).

As was noted already in the 1980s by V.B. Braginsky [124], the radiation-pressure induced back-action of light on the motion of the cavity mirrors sets an ultimate limit on the precision of gravitational wave detectors. The optimum sensitivity is reached at the so called standard quantum limit [70] (SQL) which is a direct consequence of the Heisenberg principle. The SQL represents a tradeoff between two sources of imprecision: 1. *shot noise* at the detector used for measuring the phase shift in the light field, and 2. *quantum back-action* which causes mirror-displacement noise due to random momentum kicks of reflected photons. In principle, the effect of the former, to lower the signal-to-noise ratio, can be arbitrarily reduced by using more light power. However, this inevitably increases the noise arising from quantum back-action. This results in an optimum operation point where both noise sources contribute equally to the overall measurement imprecision.

The generic cavity optomechanical model system [60], depicted in Figure 4.1A, consists of a Fabry-Perot cavity with one fixed and one harmonically bound mirror. The coupling between the mechanical motion and the cavity light field arises from the radiation pressure force acting on the mirror, and the dependence of the cavity resonance frequency on the mirror displacement. Experimental realizations of this model system range from fibre-suspended macroscopic mirrors [66], mirror coated AFM-cantilevers [125],

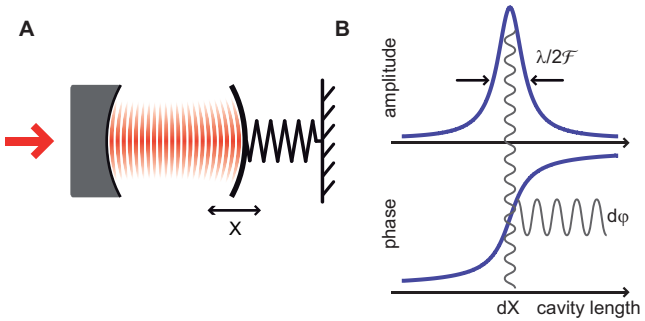

FIGURE 4.1.: Cavity optomechanical model system. (A) A Fabry-Perot cavity with one fixed and one harmonically bound mirror realizes an optomechanical coupling between the cavity light field and the mechanical mirror motion. Intracavity photons impinging on the movable mirror exert a radiation pressure force which sets the mirror into motion. The resulting change of the cavity length provides a feedback onto the cavity field. The intrinsically nonlinear coupling gives rise to phenomena like optical bistability and dynamical backaction, which can be used to amplify and cool the mechanical motion. (B) Principle of ultra-sensitive position measurement. Laser light which is tuned in resonance with the Fabry-Perot cavity experiences a phase-shift $\mathrm{d}\varphi$ caused by the mirror displacement $\mathrm{d}X$ which can be detected on the reflected light. The conversion of mechanical displacement to phase modulations of the light field is enhanced by the finesse $\mathcal{F}$ of the cavity which measures the number of round trips ($\mathcal{F}/\pi$) a photon undergoes before leaving the cavity.

micro morrors [64, 65], microtoroidal cavities [126], harmonically suspended SiN_3 membranes [67], down to nano-sized beams coupled to coplanar waveguides [127, 128]. The corresponding mechanical oscillator masses range from kilograms to picograms, and the oscillation frequencies from tens of megahertz down to the hertz level. Yet, the underlying physics of all these systems basically is described by the same model system.

The broad interest in optomechanical systems originates from their rich dynamics caused by the mutual coupling between the light field and the mechanical motion. In the limit where the light field adiabatically follows the mechanical motion, the system effectively behaves like a cavity with fixed mirrors containing a nonlinear optical medium. This gives rise to a mechanical kind of optical bistability, which experimentally was observed for the first time in [129]. At the same time, the radiation pressure force affects the frequency of small mechanical oscillations around the steady-state displacement. In the literature this effect is referred to as the "optical

spring effect", observed for the first time in [130]. Retardation effects start to play a dominant role once the lifetime of intracavity photons is comparable to or larger than the mechanical oscillator period. The radiation pressure force then contains a significant component in quadrature with the mechanical motion. The resulting friction force allows to cool or amplify the mirror motion in close analogy to atomic laser cooling [131]. Experimentally, radiation pressure cooling, originally proposed by Braginsky, was observed in recent years in various different optomechanical systems, ranging from kilogram-scale mirrors down to nano-scale mechanical oscillators [132, 63, 64, 65, 66, 67]. A major goal of these experiments is to reach the quantum regime of cavity optomechanics, where the mechanical oscillator is prepared in its quantum mechanical ground state. This would open up the avenue to observe quantum phenomena of macroscopic objects, and to investigate the border between classical and quantum physics [32, 70, 133, 134].

Before we return to our BEC-cavity system, we shortly review the Hamiltonian description of a generic cavity optomechanical model system, as depicted in Figure 4.1A. To this end, we identify how the cavity resonance frequency $\omega_c(X)$ changes as a function of the mirror displacement X, considered to be small compared to the cavity length L. Denoting the bare cavity frequency by $\omega_c \equiv \omega_c(0)$, a linear expansion of the cavity resonance frequency in the mirror displacement results in

$$\omega_c(X) = \omega_c \frac{L}{L+X} \approx \omega_c(1 - \frac{X}{L}). \tag{4.1}$$

The corresponding quantum mechanical system is described by the Hamiltonian

$$\hat{H} = \hbar\omega_m \hat{c}^\dagger \hat{c} + \hbar(\omega_c - G\hat{X})\hat{a}^\dagger \hat{a} + \hat{H}_{\text{in}} \tag{4.2}$$

where $\hat{c}$ denotes the annihilation operator for the mechanical oscillator mode with frequency ω_m, and $\hat{a}$ that for the cavity mode. External driving of the cavity mode is taken into account by the term $\hat{H}_{\text{in}}$.

The optomechanical coupling between the cavity field and the mechanical oscillator is captured by the term $-\hbar G\hat{X}\hat{a}^\dagger\hat{a}$, with the cavity optomechanical coupling constant $G = \frac{\omega_c}{L}$. Depending on the point of view, this term quantifies the change in the cavity resonance frequency as a function of the mirror displacement, or the radiation pressure force acting with a strength of $\hbar G$ per cavity photon on the mirror. This relates to the fact, mentioned before, that radiation pressure effects are inevitably linked to the sensitivity at which mirror displacements can be observed via the cavity field.

4.2. Dispersive coupling between a BEC and a cavity field

The forces exerted by laser light on atoms have been used extensively in atomic physics since the invention of laser cooling in 1975 [54]. In the dispersive limit, where the laser frequency is far detuned from any atomic dipole transition, the interaction between the light-induced atomic dipole and the electric field results in the optical dipole force. This conservative force is commonly used to trap and manipulate cold and ultracold atoms in various light beam geometries. In contrast to the free space situation, the dipole forces inside a high-finesse cavity are accompanied by a significant phase shift which is imprinted on the cavity field by the induced atomic dipoles. The incidence of dipole forces and the atomic retroaction on the light field originate from a common interaction term, which is at the heart of the BEC-cavity dynamics in the dispersive regime.

4.2.1. Dispersive atom-light interaction

Before we describe the dispersive coupling between BEC and cavity field, we first consider the case of a single two-level atom moving within the field of an optical cavity. In general, this situation is captured by the Jaynes-Cummings model [101, 106] (see also Chapter 3). In the dispersive limit, where the cavity resonance frequency is far detuned from the atomic transition frequency, the atomic excited state population is very small and spontaneous emission can be neglected. Correspondingly, the fast internal state dynamics can be adiabatically eliminated from the equations of motion, resulting in an effective Hamiltonian which describes the purely dispersive atom-light interaction [135, 136].

For this to be a valid approximation, the atomic saturation parameter $s = g_0^2\bar{n}/(\Delta_a^2 + \gamma^2)$ has to be much smaller than one. Here, g_0 denotes the atom-photon coupling strength, γ the atomic spontaneous emission rate, and $\bar{n}$ the mean intracavity photon number. The cavity field is considered to be driven by a probe laser at frequency ω_p, which also is far detuned from the atomic transition frequency ω_a by $\Delta_a = \omega_p - \omega_a$. Typically, we work at a probe-atom detuning of $\Delta_a > 2\pi \times 30\,\mathrm{GHz} \sim 10^4\gamma$, and with a mean intracavity photon number on the order of one. This results in a saturation parameter of about $s \sim 2 \cdot 10^{-7}$. For an atom number of 10^5, this corresponds to an overall spontaneous emission rate of $\frac{N}{2}\gamma s$ (see also Equation (3.16)), which is about 40 times less than the cavity decay rate κ. Correspondingly, we will neglect the effect of atomic spontaneous emission in the following.

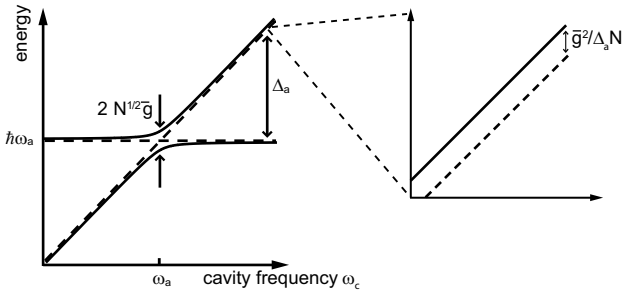

FIGURE 4.2.: Simplified energy diagram of the coupled BEC-cavity system. We work in the dispersive regime where the probe laser frequency ω_p is far detuned from the atomic transition frequency ω_a. The collective coupling between the atomic ensemble and the cavity mode leads to dressed states (solid). In the dispersive regime their energy is shifted with respect to the bare state energies (dashed) by an amount which is given by the light shift of a single atom $\tilde{g}^2/\Delta_a$ times the atom number N. Here, the effective single atom coupling constant involves the overlap integral between the atomic density distribution and the cavity mode. Correspondingly, the atoms are subject to a dynamic lattice potential whose depth depends non-locally on the atomic density distribution.

In a frame rotating at the pump laser frequency ω_p, the effective Hamiltonian describing the dispersive interaction between atom and light reads [135]

$$\hat{H}_1 = \hat{H}_a + \hat{H}_c + \hat{H}_{a-c} \tag{4.3}$$

with

$$\hat{H}_a = \frac{\hat{\mathbf{p}}^2}{2m} + V_{\text{ext}}(\mathbf{r}) \tag{4.4}$$

$$\hat{H}_c = -\hbar\Delta_c \hat{a}^\dagger \hat{a} - i\hbar\eta(\hat{a} - \hat{a}^\dagger) \tag{4.5}$$

$$\hat{H}_{a-c} = \hbar U_0 |\phi(\mathbf{r})|^2 \hat{a}^\dagger \hat{a}. \tag{4.6}$$

The term $\hat{H}_a$ describes atomic motion in the external trapping potential V_{ext}, which experimentally is provided by a crossed beam dipole trap. The bare energy of the cavity field is accounted for by the first term in $\hat{H}_c$, with the photon creation operator $\hat{a}^\dagger$ and the pump-cavity detuning $\Delta_c = \omega_p - \omega_c$. The coherent driving of the cavity field at amplitude η by an external probe laser field is described by the second term in $\hat{H}_c$.

The dispersive interaction term $\hat{H}_{a-c}$ acts twofold: For the atom it represents an optical potential whose spatial dependence is determined by the

standing-wave cavity mode function $\phi(\mathbf{r})$, and whose potential depth is proportional to the number of cavity photons. Physically, this potential originates from the spatially dependent light shift experienced by the atom in the far detuned cavity field. From the light field point of view, the atom induces a position-dependent phase shift on the cavity field. For the atom sitting at an antinode of the cavity field, this results in a frequency shift of the empty cavity resonance given by $U_0 = \frac{g_0^2}{\Delta_a}$. Correspondingly, the atom moves in a dynamic lattice potential [135] whose depth depends on the atomic position.

4.2.2. The many-body system

In a many-body description the dispersive interaction of an ensemble of bosonic atoms with the cavity mode can be described by the Hamiltonian [137]

$$\hat{H} = \int \hat{\Psi}^\dagger(\mathbf{r})\big(\hat{H}_a + \hat{H}_{a-c}\big)\hat{\Psi}(\mathbf{r})\mathrm{d}^3r + \hat{H}_c + u\int \hat{\Psi}^\dagger(\mathbf{r})\hat{\Psi}^\dagger(\mathbf{r})\hat{\Psi}(\mathbf{r})\hat{\Psi}(\mathbf{r})\mathrm{d}^3r. \tag{4.7}$$

Here, the atomic field operators $\hat{\Psi}$ and $\hat{\Psi}^\dagger$ obey the usual bosonic commutation relations. The atom-atom interaction via s-wave scattering is taken into account by the last term, with the interaction constant $u = \frac{4\pi\hbar^2 a}{m}$ and the scattering length a.

If the atomic ensemble is cooled below the critical temperature where Bose-Einstein condensation sets in, a single quantum state starts to get macroscopically populated. Within a mean-field picture, this is the ground state of the effective potential formed by the external trapping potential and the mean-field potential caused by the repulsive atom-atom interactions. This situation provides ultimate control over the atomic motion, and serves as an ideal starting point to study the dispersive interaction between atoms and the cavity light field.

4.3. Uniform limit and equivalence to cavity optomechanics

In order to get an intuitive understanding of the condensate motion in the dynamic cavity lattice potential, we will focus in this section on a one-dimensional situation with uniform condensate density along the cavity axis. This simplification is motivated by the fact that in our experimental realization the condensate extends along the cavity axis over more than 15 periods of the cavity lattice potential. In this limit the system can be mapped directly onto a cavity optomechanical model system which was introduced in

Section 4.1. This analogy provides us with qualitative and intuitive interpretations of our experimental observations, and allows to compare the system to other cavity optomechanical systems.

4.3.1. The two-mode model

The limit of a uniform one-dimensional condensate without atom-atom interactions is describe by the simplified Hamiltonian

$$\hat{H} = \int_0^L \hat{\Psi}^\dagger(x)\Big(-\frac{\hbar^2}{2m}\frac{\mathrm{d}^2}{\mathrm{d}x^2} + \hbar U_0 \cos^2(kx)\hat{a}^\dagger\hat{a}\Big)\hat{\Psi}(x)\mathrm{d}x - \hbar\Delta_a\hat{a}^\dagger\hat{a} - i\hbar\eta(\hat{a}-\hat{a}^\dagger) \tag{4.8}$$

with $L \equiv \pi/k$ and cavity field wave number k. Initially, all atoms are prepared in the zero-momentum state $|p=0\rangle$. Probe light entering the cavity gives rise to a periodic lattice potential at which condensate atoms are scattered into a discrete set of higher momentum modes $|p = \pm 2n\hbar k\rangle$, $n \in \mathbb{N}$. This corresponds to virtual photon absorption and emission processes by the atoms. For moderate lattice depths, only a small percentage of atoms is transferred out of the zero-momentum state, predominantly into the symmetric superposition of the states $|p = \pm 2\hbar k\rangle$. Correspondingly, we expand the atomic field operator in the linear space spanned by the motional modes $\psi_0(x) = \sqrt{1/L}$ and $\psi_2(x) = \sqrt{2/L}\cos(2kx)$,

$$\hat{\Psi} = \hat{c}_0\psi_0 + \hat{c}_2\psi_2, \tag{4.9}$$

with mode creation operators $\hat{c}_0^\dagger$ and $\hat{c}_2^\dagger$, obeying $\hat{c}_0^\dagger\hat{c}_0 + \hat{c}_2^\dagger\hat{c}_2 = N$.

After inserting ansatz (4.9) into Hamiltonian (4.8), we find the interaction term to be given by

$$\hbar U_0/\sqrt{8}(\hat{c}_0^\dagger\hat{c}_2 + \hat{c}_0\hat{c}_2^\dagger)\hat{a}^\dagger\hat{a}. \tag{4.10}$$

We now introduce collective ladder operators $\hat{c}^\dagger = \hat{c}_0\hat{c}_2^\dagger/\sqrt{N}$ and $\hat{c} = \hat{c}_2\hat{c}_0^\dagger/\sqrt{N}$, which obey the commutation relation $[\hat{c}, \hat{c}^\dagger] = 1 - 2\hat{c}_2\hat{c}_2^\dagger/N$. In case where most of the atoms remain in the ground state $\hat{c}_2^\dagger\hat{c}_2 \ll N$, the collective (spin) operators $\hat{c}$ and $\hat{c}^\dagger$ approximately describe a harmonic oscillator mode which couples via the 'displacement' operator[1] $\hat{X} = (\hat{c}+\hat{c}^\dagger)/\sqrt{2}$ to the cavity field. With these definitions, the Hamiltonian (4.8) simplifies to

$$\hat{H} = 4\hbar\omega_{\mathrm{rec}}\hat{c}^\dagger\hat{c} - \hbar(\tilde{\Delta}_c - G\hat{X})\hat{a}^\dagger\hat{a} - i\hbar\eta(\hat{a}-\hat{a}^\dagger), \tag{4.11}$$

with the effective detuning $\tilde{\Delta}_c = \Delta_c - \frac{1}{2}U_0N$ and the recoil frequency $\omega_{\mathrm{rec}} = \frac{\hbar k^2}{2m}$.

[1] Here, the displacement X is defined in units of the harmonic oscillator length.

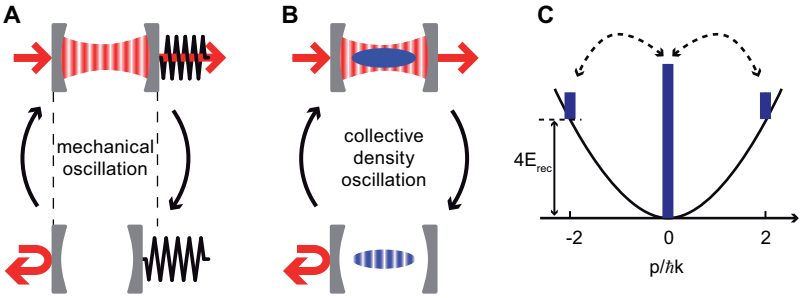

FIGURE 4.3.: (A) Cavity optomechanical model system. A mechanical oscillator, here one of the cavity mirrors, is coupled via radiation pressure to the field of the cavity whose length depends on the oscillator displacement. (B) Coupling a Bose-Einstein condensate dispersively to the field of an optical high-finesse cavity constitutes an equivalent optomechanical system. Here, a collective density excitation of the condensate acts as the mechanical oscillator which couples via the dipole force to the cavity field. Feedback on the cavity resonance frequency is accomplished by the refractive index of the atomic density distribution within the spatially periodic cavity mode structure. In contrast to opto-mechanical systems presented so far this mechanical oscillator is not based on the presence of an external harmonic potential (e.g. a spring). It is rather provided by kinetic evolution of the condensate density excitation. (C) Matter-wave dynamics in momentum space. Atoms initially prepared in the zero-momentum state are partially scattered off the cavity lattice potential into the higher momentum states $|p = \pm 2\hbar k\rangle$. Due to matter-wave interference with the remaining macroscopic zero-momentum component the relative phase evolution results in collective density oscillations.

From Equation (4.11) we infer about a direct analogy between the coupled condensate-cavity system in the uniform limit and the cavity optomechanical model system introduced in Section 4.1. The role of the mechanical oscillator is played by a collective density oscillation mode of the condensate, which couples to the cavity field with optomechanical coupling constant $G = U_0\sqrt{N}/2$. The mechanical oscillation frequency, $4\omega_{\mathrm{rec}}$, is determined by the relative phase evolution of the two mode operators $\hat{c}_0$ and $\hat{c}_2$.

4.3.2. Mean-field description

Intuitively, the equivalence to cavity optomechanics can be understood within a mean-field picture, describing the atomic sample by a single macroscopic

wave function ψ normalized to one (see Figure 4.3). For moderate cavity lattice potential the condensate wave function is given by the coherent superposition $\psi(x,0) \propto \psi_0(x) + \epsilon\psi_2(x)$, with $|\epsilon|^2 \ll 1$. The resulting atomic density distribution forms – due to matter-wave interference – a standing wave pattern which oscillates in time at $4\omega_{\rm rec}$, owing to the energy difference of the two matter field modes ψ_0 and ψ_2,

$$|\psi(x,t)|^2 \propto 1 + 2\sqrt{2}\epsilon\cos(4\omega_{\rm rec}t)\cos(2kx) + \mathcal{O}(\epsilon^2). \tag{4.12}$$

This density oscillation periodically modulates the spatial overlap integral between matter field and cavity field according to

$$\mathcal{O}(t) \equiv \langle\psi(x,t)|\cos^2(kx)|\psi(x,t)\rangle = \frac{1}{2} + \frac{\sqrt{2}}{2}\epsilon\cos(4\omega_{\rm rec}t). \tag{4.13}$$

Therefore, the condensate acts like a wavelike refractive index medium which periodically modulates the cavity resonance frequency $\omega_c + U_0 N\mathcal{O}(t)$, similar to a harmonically oscillating cavity mirror affecting the physical cavity length (see Figure 4.3).

4.3.3. Equations of motion

The coupled condensate-cavity dynamics is captured by the two mutually coupled equations of motion

$$\ddot{\hat{X}} + (4\omega_{\rm rec})^2\hat{X} = -4\omega_{\rm rec}G\hat{a}^\dagger\hat{a} \tag{4.14}$$

$$i\dot{\hat{a}} = -(\tilde{\Delta}_c - G\hat{X} + i\kappa)\hat{a} + i\eta, \tag{4.15}$$

obtained from Hamiltonian (4.11), and including the cavity field decay with rate κ. The first equation describes the motion of the mechanical oscillator driven by the radiation pressure force, being proportional to the cavity photon number. The second equation governs the evolution of the cavity field whose resonance frequency depends linearly on the oscillator's displacement $\hat{X}$.

The atomic mean-field description, considered before, corresponds to replacing the displacement operator $\hat{X}$ by its classical analog X. It measures the deviation of the spatial overlap integral between matter field and cavity field from its mean value, corresponding to a flat atomic density distribution. In the following, we will describe the cavity field by the coherent state variable α. This simplification can be justified by the huge difference in timescales governing cavity decay and atomic motion (see Section 5.3). Thus, we will henceforth replace the photon operator $\hat{a}$ in the equations of motion by the classical variable α.

4.3.4. Cavity quantum optomechanics in the strong coupling regime

The dispersively coupled condensate-cavity system features distinctive properties which point into a so far unexplored regime of cavity optomechanics. Using the collective motion of ultracold atoms as a mechanical degree of freedom, offers direct access to the quantum regime where the harmonic oscillator is prepared in its quantum mechanical ground state. We have estimated the expectation value for thermal excitations in this mode to be below 0.01 for a realistic condensate fraction of 90% (see Section 4.4.4). The ultimate control in preparing our mechanical oscillator serves as an ideal starting point to explore the motion of an atomic ensemble at the quantum limit.

A second property which makes our system very different as compared to previous cavity optomechanical realizations is related to the coupling strength between the mechanical motion and the cavity field. Typically, the radiation pressure forces of single photons exerted onto a macroscopic object (like e.g. a micro-sized cantilever) are tiny, even if enhanced by many thousand roundtrips inside the cavity. Realizing an optomechanical system at the atomic scale, allows us to reach a novel regime of cavity optomechanics, where the effect of single cavity photons on the collective atomic motion becomes relevant. Quantitatively, this can be characterized by the "quantum parameter" $\zeta = G/\kappa$ [138], sometimes also referred to as the "granularity parameter" [45]. It measures the coupling strength between quantum fluctuations of the collective atomic motion and of the cavity light field.

Strong optomechanical coupling is characterized by a quantum parameter on the order of one. Here, a mechanical displacement of $\Delta X = 1$ (in units of the harmonic oscillator length) induces a shift of the cavity resonance by κ, which in principle could be detected on the transmitted or reflected probe light field. On the other hand, a single cavity photon with a mean life time of $\frac{1}{2\kappa}$ imparts an impulse of $\frac{4\omega_{\mathrm{rec}}G}{2\kappa}$ on the oscillator, displacing it by $X = \zeta/2$. Correspondingly, mechanical and optical quantum fluctuations couple in a non-trivial way for $\zeta \gtrsim 1$, while in the non-granular regime, $\zeta \ll 1$, they can be considered as independent. The dependence of the optomechanical coupling strength G on the probe-atom detuning Δ_a provides tunability of the quantum parameter over a wide range. This could be used to perform studies on cavity optomechanics both in a classical and quantum regime. Experimentally, the strong coupling regime $\zeta = 1$ is reached in our system with a detuning of $\Delta_a = 2\pi \times 24\,\mathrm{GHz}$ and a typical atom number of $N = 10^5$.

4.4. Beyond the uniform two-mode model

The equivalence to cavity optomechanics shown above provides us with a simple and intuitive understanding of the coupled BEC-cavity system. In this section we discuss the influence of atom-atom interactions and the external trapping potential onto the dynamics of the system.

4.4.1. Atom-atom interactions

The elementary excitation spectrum of a weakly interacting uniform Bose gas close to $T = 0$ is described within the Bogoliubov theory [139]. By introducing quasi-particle operators defined as linear combinations of the free particle operators for momenta $\pm\mathbf{p}$ the corresponding many-body Hamiltonian

$$\hat{H} = \int \hat{\Psi}^\dagger(\mathbf{r})\Big(-\frac{\hbar^2\nabla^2}{2m} + u\hat{\Psi}^\dagger(\mathbf{r})\hat{\Psi}(\mathbf{r})\Big)\hat{\Psi}(\mathbf{r})\mathrm{d}^3r \tag{4.16}$$

including atom-atom interactions can be diagonalized after separating the condensate part [111]. Correspondingly, the lowest excitations of a weakly interacting Bose gas are described in terms of non-interacting quasi-particles, which obey the Bogoliubov dispersion law

$$\epsilon(p) = \sqrt{c^2p^2 + \Big(\frac{p^2}{2m}\Big)^2}. \tag{4.17}$$

Here, $c = \sqrt{un/m}$ denotes the sound velocity in the Bose gas with mean particle density n.

Depending on their momentum $p = |\mathbf{p}|$, one distinguishes between phonon-like and particle-like excitations (see Figure 4.4). For small momenta, $p \ll mc$, the dispersion relation is linear, $\epsilon(p) = cp$, and the elementary excitations behave like sound waves. In the opposite limit, $p \gg mc$, the dispersion relation follows $\epsilon(p) = p^2/2m + un$, corresponding to particle-like excitations. The energy offset with respect to the free-particle dispersion law equals the chemical potential, $\mu = nu$, and reflects the fact that atoms moving at large momenta feel twice the mean-field energy of those at rest, due to the exchange term in the interatomic potential [140]. Taking into account the inhomogeneity of a trapped Bose condensate, one finds the mean-field shift for particle-like excitations to be approximately given by $\frac{4}{7}un_0$, where n_0 denotes the peak density.

With a peak density of $\sim 3\times10^{14}\,\mathrm{cm}^{-3}$ in our experiment, we deduce in the trap center a sound velocity of $c \sim 3\,\mathrm{mm/s}$, corresponding to a healing length of $\xi = \frac{\hbar}{\sqrt{2}mc} \sim 160\,\mathrm{nm}$ [111]. The sound velocity being four times smaller than the velocity of atoms recoiling at two-photon momenta

$v = \frac{2\hbar k}{m} \sim 12\,\mathrm{mm/s}$, justifies to treat excitations at $p = \pm 2\hbar k$ as particle-like. Accordingly, the atom-atom interactions give rise to an increase of the bare mechanical oscillation frequency, $4\omega_{\mathrm{rec}}$, by an amount of $\frac{4\mu}{7\hbar}$, with the chemical potential, $\mu/\hbar \sim 2\pi \times 2.4\,\mathrm{kHz}$, calculated in the Thomas-Fermi limit.

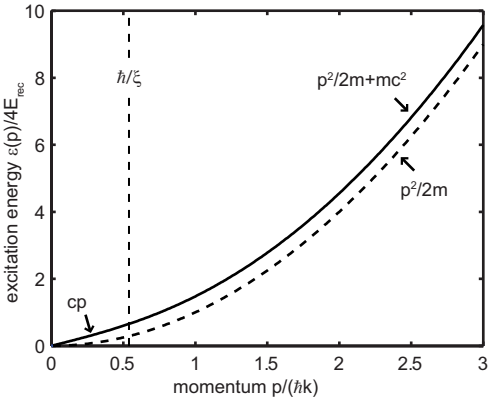

FIGURE 4.4.: Bogoliubov dispersion of elementary excitations (solid line) and free-particle dispersion law (dotted line). The transition between the phonon regime and the particle regime is indicated by the vertical dashed line located at momentum $\hbar/\xi$, with the healing length ξ.

4.4.2. Harmonic confinement along the cavity axis

The uniform two-mode model (Section 4.3) predicts the condensate to perform density oscillations at a timescale which is set by the two-photon recoil frequency $4\omega_{\mathrm{rec}} = 2\pi \times 15.1\,\mathrm{kHz}$. For a harmonically trapped condensate, one expects an additional superimposed dynamics along the cavity axis, occurring at a timescale which is given by the corresponding trapping frequency ω_x. Namely, scattered atoms with momentum $p = \pm 2\hbar k$ get reflected at the external trapping potential which results in a collapse and revival behavior of atomic density oscillations.

To study this in more detail, we numerically simulate the free mean-field dynamics of a trapped Bose condensate, described by the time-dependent 1D Gross-Pitaevskii equation [111]

$$i\hbar\frac{\partial}{\partial t}\psi(x,t) = \Big(-\frac{\hbar^2}{2m}\frac{\partial^2}{\partial x^2} + V_{\mathrm{ext}}(x) + u_{1\mathrm{D}}|\psi(x)|^2\Big)\psi(x). \tag{4.18}$$

Here, the condensate wave function ψ is considered to be normalized to the total atom number N, and the effective atom-atom interaction constant u_{1D} is determined by the chemical potential in the corresponding three-dimensional trapping potential [141]. The external trapping potential along the cavity axis is given by $V_{ext} = \frac{1}{2}m\omega_x^2 x^2$, with m denoting the atomic mass.

To determine the time evolution of free density oscillations of a trapped condensate, we first numerically solve the Gross-Pitaevskii equation (4.18) in imaginary time in order to obtain the ground state wave function ψ_0. Subsequently, density oscillations at wave vector $2k$ are excited by multiplying this ground state with the phase factor $\exp(iK\cos^2(kx))$ with $K = 0.3$, corresponding to a transfer of $\sim 2\%$ of the total number of atoms into the

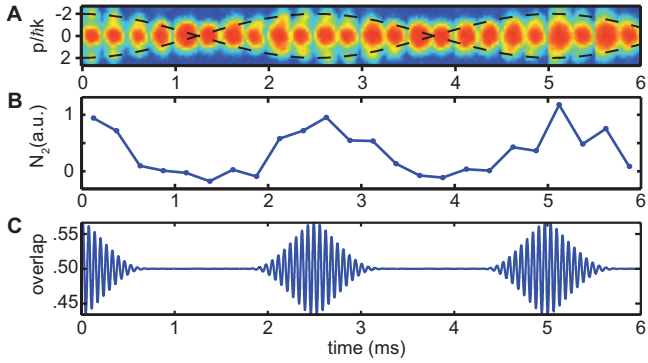

FIGURE 4.5.: Matter-wave dynamics induced by the trapping potential along the cavity axis. (A) Shown is a series of absorption images (obtained from single shots) revealing dipole oscillations of the higher-momentum wave packets in the external dipole trapping potential (see text). The time axis indicates the holding time in the dipole trap after a fraction of atoms was transferred into the higher momentum states $|p = \pm 2\hbar k_t\rangle$ at $t = 0$. The time interval between adjacent images is $125\,\mu$s. The dashed lines are sinusoidal curves with an oscillation frequency of 200 Hz (close to the trapping frequency ω_x) and an oscillation amplitude, corresponding to the distance which atoms with momentum $p = \pm 2\hbar k_t$ travel within the free expansion time of 4.5 ms. (B) The number N_2 of atoms at momentum $p = \pm 2\hbar k_t$ was extracted from the absorption images in A, and serves as a measure for the modulation amplitude of the condensate density at wave vector $2k_t$. Qualitatively, this agrees with a numerical simulation of free oscillations of the spatial overlap between atomic density and cavity intensity profile, as shown in graph C (see text).

recoiling mode $\psi_0(x)\cos(2kx)$. Finally, the time evolution of this state is calculated according to (4.18). Figure 4.5C shows the resulting time dependence of the per-atom mode overlap $\langle\psi(x,t)|\cos^2(kx)|\psi(x,t)\rangle/N$. The fast density modulations at frequency $4\omega_{\rm rec}$ originating from matter-wave interference are clearly visible. However, in contrast to the uniform situation we find a superimposed amplitude modulation at half the trapping period $2\pi/2\omega_x = 2.5\,\mathrm{ms}$. This is caused by dipole oscillations performed by the recoiling matter-wave packets within the harmonic trapping potential.

Experimentally, we observed such dynamics by flashing on a far-detuned laser beam at $\lambda_t = 830\,\mathrm{nm}$ for $100\,\mu\mathrm{s}$. The laser frequency was stabilized to a certain TEM_{00} mode of the cavity by means of a Pound-Drever-Hall lock. This generates out of the initial condensate two matter-wave packets with momentum $p = \pm 2\hbar k_t$, where $k_t = 2\pi/\lambda_t$. After holding the atoms for a certain time in the harmonic trapping potential, we suddenly switch off the trap and image the atoms after a free expansion time of 4.5 ms, getting directly access to the initial momentum distribution of the atomic sample (see Figure 4.5A). We observe clear dipole oscillations of the wave packets in momentum space at the external trapping frequency ω_x, corresponding to collapses and revivals of atomic density oscillations at wave vector $\pm 2k$ (Figure 4.5B). In addition, we observe a spreading of the higher-momentum wave packets at a timescale of about 10 ms, probably caused by the presence of atom-atom interactions. This puts severe limits on the quality factor of our mechanical oscillator.

4.4.3. Transverse degrees of freedom

Until now we restricted our considerations to the light forces pointing along the cavity axis. This was justified by the fact that the maximum force acting along the transverse directions of the Gaussian TEM_{00} cavity mode profile is about 300 times smaller than the maximum force pointing along the cavity axis. Therefore, for moderate intracavity photon numbers we can treat the transverse atomic degrees of freedom as to be unaffected by the cavity probe light. For larger probe strength, however, the atoms start to experience a significant change in their transverse trapping potential, which induces a superimposed dynamics along the directions perpendicular to the cavity axis.

Concerning our particular experimental situation, such dynamics first becomes relevant along the weakest confining transverse direction, where the external trapping frequency is about 40 Hz. For blue-detuned probe light the atoms are pushed out of the cavity interaction region which results in a decrease of the matter-light overlap.

4.4.4. Ground state preparation of the mechanical oscillator

To estimate the number of thermal excitations in the mechanical oscillator mode, we calculate the broadening of the operator $\hat{u} = \int dx \cos^2(kx)\hat{\Psi}^\dagger(x)\hat{\Psi}(x)$ caused by thermal depletion of the condensate, and compare the result with the zero-point fluctuations of $\hat{u}$. We restrict the discussion to the direction along the cavity axis since only density fluctuations along this axis contribute. The atomic annihilation operator $\hat{\Psi}(x)$ is split into a condensate part and a thermal part

$$\hat{\Psi}(x) = \psi_0(x)\sqrt{N_0} + \sum_{i\neq 0} \psi_i(x)\hat{a}_i.$$

Here ψ_0 denotes the condensate wave function obtained in the Thomas-Fermi approximation for N_0 condensed atoms, and ψ_i the harmonic oscillator eigenfunctions in the external trapping potential. For simplicity we neglect the effect of atom-atom interactions on the thermal atoms. We evaluate the variance of $\hat{u}$ in a thermal state at temperature T where the uncondensed atoms $N_T = N - N_0$ are distributed over the excited state levels according to a Bose distribution with chemical potential $\mu = 0$. The total number of atoms N is kept fixed and the condensate fraction is given by $N_0/N = 1 - (T/T_c)^3$, with the critical temperature T_c calculated using the external trapping frequencies. Apart from trivial autocorrelations, we find for the variance of $\hat{u}$

$$\Delta u^2 \equiv \langle \hat{u}^2 \rangle - \langle \hat{u} \rangle^2 = 2N_0 \sum_{i\neq 0} M_{0i}^2 \langle \hat{a}_i^\dagger \hat{a}_i \rangle + \sum_{i,j\neq 0} M_{ij}^2 \langle \hat{a}_i^\dagger \hat{a}_i \rangle \langle \hat{a}_j^\dagger \hat{a}_j \rangle, \quad (4.19)$$

with the matrix elements $M_{ij} = 0.5\langle \psi_i | \cos(2kx) | \psi_j \rangle$. The first term on the right hand side of Equation (4.19) originates from interference between thermal atoms and the condensate. For $N_T < N_0$ this contribution by far exceeds the second term which corresponds to purely thermal density fluctuations at wave vector $2k$. Comparing Δu^2 with the zero-point fluctuations of the overlap $\langle 0|(\hat{u} - N/2)^2|0\rangle = N/8$ at $T = 0$, provides us with an estimation of the average number $n_T = 8\frac{\Delta u^2}{N}$ of thermal excitations in the mechanical oscillator mode. Numerically we find a thermal occupation n_T below 0.01 for a condensate fraction of 90%.

4.4.5. Atomic multilevel structure

The multilevel structure of ^{87}Rb atoms, and the polarization of the cavity field require a description which goes beyond the simple two-level approximation assumed in Section 4.2. As for the experiments described in Chapter

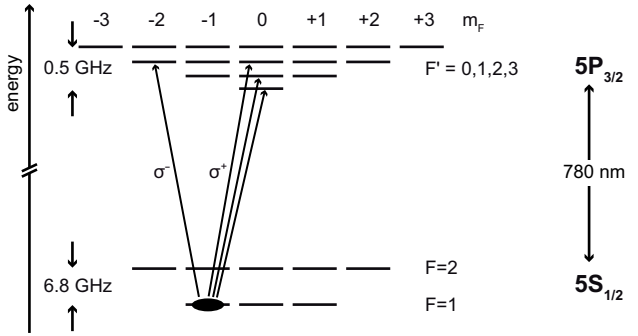

FIGURE 4.6.: Energy spectrum of ^{87}Rb atoms for the D_2 transition line. The arrows indicate possible $\sigma^{\pm}$ transitions starting from the initially prepared spin state $|F = 1, m_F = -1\rangle$. The magnetic Zeeman splitting is not shown.

3, we prepare a spin polarized condensate in the $|F = 1, m_F = -1\rangle$ hyperfine state, and suppress π transitions by applying a small magnetic field of about 0.1 G along the cavity axis. Taking into account all possible transitions for circular polarized cavity photons (see Figure 4.6), we find single-atom coupling constants of $g_+ = 2\pi \times 14.1\,\mathrm{MHz}$ for σ^+ polarized photons, and of $g_- = 2\pi \times 10.9\,\mathrm{MHz}$ for σ^- polarized photons. In order to excite a single polarization component only, we either probe the cavity field with a one particular circular polarization, or make use of the fact that the two dressed cavity resonances for $\sigma^{\pm}$ transitions are separated by $N(g_+^2 - g_-^2)/2\Delta_a \gg \kappa$ (see Section 3.6).

4.5. Summary

A novel and intuitive description of the dispersively coupled, uniform BEC-cavity system was established in terms of cavity optomechanics. Density oscillations of the condensate are excited by the cavity-induced dipole forces, and provide – via the atomic index of refraction – a retroaction on the cavity resonance frequency. The dynamics of the uniform system gets enriched by the presence of atom-atom interactions and the external trapping potential. In the following chapters, the cavity optomechanical interpretation of the BEC-cavity system will provide us with intuitive and qualitative understanding of our experimental observations.

5 Optical bistability at low photon number

A bistable optical system exhibits two different steady transmission states for the same input intensity [142, 143]. A typical realization is given by a Fabry-Perot resonator containing a material whose refractive index is intensity dependent. The simplest case is a Kerr medium, showing a linear dependence of its refractive index on light field intensity. The corresponding input-output characteristics shows differential gain and hysteresis which makes bistable devices desirable for realizing e.g. an optical switch [144]. An extensively studied system which shows bistable behavior is given by an atomic gas placed within an optical resonator [145]. Here, bistability can arise either due to saturation of an optical transition (absorptive optical bistability) or due to a change in the index of refraction with light intensity (dispersive bistability).

Typically, such nonlinear optical phenomena occur only for very large light intensities, since the change of the refractive index (or the degree of saturation of an optical transition) per photon circulating in the resonator is tiny. New possibilities for realizing strong nonlinearities at low photon numbers opened up by placing atomic ensembles into small-volume high-finesse optical resonators, operating in the strong coupling regime of cavity QED. Here, the atom-photon coupling rate overcomes the rates associated with cavity field decay and spontaneous emission. Correspondingly, the single-atom saturation intensity is reached already with a mean intracavity photon number below one. This allowed to observe absorptive optical bistability down to a mean photon number of about 100 [146, 147, 94].

In general, the occurrence of optical bistability at low cavity photon number requires the alteration in the optical property of the medium induced by a single photon to be *strong* enough, and to persist *long* enough, in order to affect subsequent photons. While the former requirement can be met by increasing the light field per photon using a small-volume resonator, the latter asks for coherence times of the nonlinear medium which exceed the cavity photon lifetime.

The motional degrees of freedom of ultracold atomic gases offer coherence times on the order of $\gtrsim 1\,\mathrm{ms}$ which is much longer than the residence time ($< 1\,\mu\mathrm{s}$) of cavity photons in typical small-volume optical high-finesse cavities. Observation of strong optical nonlinearities and bistability with mean intracavity photon numbers below one was achieved for the first time in [26], where the collective motion of tightly confined ultracold atoms was coupled dispersively to an optical cavity field [26]. Here, the optical nonlinearity arises from the cavity-mediated dipole forces which shift the atoms within the spatially dependent mode profile, thereby inducing a change in their refractive index properties.

This type of "mechanical" nonlinearity is typical for cavity optomechanical systems, and was observed with much higher light intensity in [129] for the first time. Instead of changing the effective optical path length of the cavity by some nonlinear medium, here the radiation pressure induced motion of one harmonically bound cavity mirror directly leads to a change of the physical cavity length.

In this chapter, we study the dispersively coupled BEC-cavity system under conditions where the atoms can adiabatically follow the sufficiently slow changes in the cavity light intensity. In this limit the condensate acts like a Kerr medium. Experimentally, we observe optical bistability and hysteretic behavior already with mean intracavity photon numbers below one. We compare our observations with ab-initio calculations in a mean-field approximation.

The experimental results of this chapter have been published in [148]: S. Ritter, F. Brennecke, K. Baumann, T. Donner, C. Guerlin, and T. Esslinger. *Dynamical coupling between a Bose-Einstein condensate and a cavity optical lattice.* Appl. Phys. B 95, 213 (2009).

5.1. Optical Kerr nonlinearity

In Section 4.3 we showed that a condensate which is coupled dispersively to the field of a high-finesse optical cavity in the uniform limit is equivalent to a generic cavity optomechanical system, describing the radiation pressure coupling between a mechanical oscillator and a cavity field. Here, density oscillations on top of the flat condensate play the role of the mechanical element and couple to the standing wave cavity field via the optical dipole force. In a mean-field description neglecting atom-atom interactions, the corresponding equations of motion read

$$\ddot{X} + (4\omega_{\rm rec})^2 X = -4\omega_{\rm rec} G|\alpha|^2 \tag{5.1}$$

$$i\dot{\alpha} = -(\tilde{\Delta}_c - GX + i\kappa)\alpha + i\eta. \tag{5.2}$$

The oscillator amplitude X measures the spatial overlap of the atomic density with the cavity light intensity. In the following, the cavity field will be assumed to be in a coherent state α. Nonclassical correlations such as entanglement between the cavity field and atomic motion, or light squeezing are not taken into account by this description.

5.1.1. Adiabatic limit

We are interested in the limiting case where the intracavity light intensity $\sim |\alpha|^2$ changes slowly compared to atomic motion, such that the condensate density adiabatically follows the corresponding change in the optical potential[1]. Since the cavity field decay rate κ is two orders of magnitude larger than the mechanical oscillation frequency $4\omega_{\rm rec}$ this implies that both light field and mechanical oscillator are in their steady state. Taking $\ddot{X} = 0$ in (5.1) we find the steady state displacement X to depend linearly on the mean intracavity photon number $\bar{n} = |\alpha|^2$,

$$X = -\frac{G}{4\omega_{\rm rec}}\bar{n}. \tag{5.3}$$

After inserting this relation into the steady state solution of (5.2), we obtain a conditional equation for the mean photon number $\bar{n}$

$$\bar{n} = \frac{\eta^2}{\kappa^2 + (\tilde{\Delta}_c + \frac{G^2}{4\omega_{\rm rec}}\bar{n})^2}. \tag{5.4}$$

[1] The finite retardation between mechanical motion and cavity field which is responsible for cooling and amplification effects will be discussed later on (see Section 6.5).

Using $\tilde{\Delta}_c = \Delta_c - U_0 N/2$ and $G = U_0\sqrt{N}/2$ (see Section 4.3), this equation can be written as follows

$$\bar{n} = \frac{\eta^2}{\kappa^2 + \left(\Delta_c - \frac{U_0 N}{2}(1 + \frac{U_0}{8\omega_{\rm rec}}\bar{n})\right)^2}. \tag{5.5}$$

From Equation (5.5) we infer about motional-induced Kerr nonlinearity of the condensate, with a refractive index given by $1 - \frac{U_0 N}{2\omega_p}(1 + \frac{U_0}{8\omega_{\rm rec}}\bar{n})$. Here, the constant term corresponds to the refractive index of atoms which are homogeneously distributed over the standing-wave cavity mode. The term which is linear in $\bar{n}$ describes the change in the refractive index due to atomic density modulations. For typical experimental parameters of $\Delta_a = 2\pi \times 50\,\mathrm{GHz}$ and $N = 10^5$ the dispersive change of the cavity optical path length for one cavity photon on average $\bar{n} = 1$ is about 10 pm, which is well within our length sensitivity determined by $\frac{\lambda}{2\mathcal{F}} \sim 1\,\mathrm{pm}$ (see Section 4.1).

5.1.2. Bistability

From the equivalence to Kerr nonlinearity we can anticipate bistable behavior of the coupled BEC-cavity system. Being of third order in $\bar{n}$, Equation (5.4) can have three different, real-valued solutions, which correspond to different steady-state configurations. Exemplary steady-state resonance curves versus cavity-probe detuning Δ_c, obtained from a numerical solution of Equation (5.4), are shown in Figure 5.1A. With increasing cavity probe strength η the cavity resonance profile deviates more and more from a Lorentzian shape, and exhibits bistable behavior above a certain critical value $\eta_{\rm cr}$. A detailed analysis of Equation (5.4) results in an analytic expression for the critical probe strength $\eta_{\rm cr}$, at which bistability is about to occur. In terms of the maximum intracavity photon number, $\bar{n}_{\rm cr} = \frac{\eta_{\rm cr}^2}{\kappa^2}$, the condition for bistability reads

$$\bar{n}_{\rm cr} = \frac{8}{3\sqrt{3}}\frac{4\omega_{\rm rec}\kappa}{G^2}. \tag{5.6}$$

From this one expects bistability at the single photon level to occur in our system for $G = 0.13\kappa$, which corresponds to a probe-atom detuning of $\Delta_a = 2\pi \times 130\,\mathrm{GHz}$. Here, the influence of atom-atom interactions is not taken into account (see below).

Qualitatively, the asymmetry of the bistable resonance curves in Figure 5.1A can be understood from the fact that the atoms move within a *dynamic* optical lattice potential [135]: probe light entering the cavity gives rise to an optical lattice potential, which pushes the atoms – depending on the sign of the probe-atom detuning Δ_a – to places of higher or lower cavity field

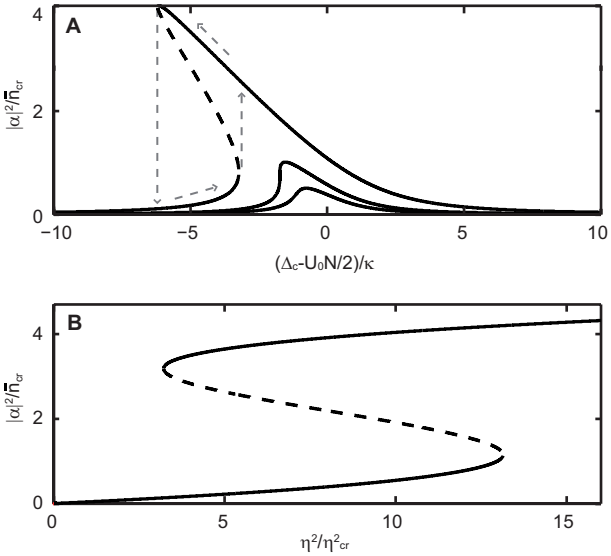

FIGURE 5.1.: (A) Mean intracavity photon number $\bar{n} = |\alpha|^2$ versus cavity-probe detuning Δ_c calculated for three different probe strengths $\eta = (0.7, 1, 2)\eta_{\rm cr}$ (bottom to top curve). The cavity light field, taken to be blue-detuned from the atomic resonance, pushes the atoms to regions of lower coupling strength giving rise to bistability. For increasing probe strength the initially ($\eta \to 0$) symmetric resonance curve centered at $\Delta_c = U_0 N/2$ develops above a critical probe strength $\eta_{\rm cr}$ a bistable region with two stable (solid lines) and one unstable branch (dashed). (B) Mean intracavity photon number of the bistable system versus probe strength for fixed cavity probe detuning $\Delta_c = U_0 N/2 - 5\kappa$. Again, the dashed line indicates the instable steady state solutions.

intensity. Due to the spatial dependence of the atom-light coupling this leads to an overall change of the dispersive shift of the empty cavity resonance frequency. Depending on its frequency, this either tunes the probe laser closer to or further apart from resonance, providing a positive or negative feedback on the intracavity light intensity. This results in asymmetric cavity transmission profiles.

5.1.3. Higher-order Kerr nonlinearity

Due to occupation of higher-order momentum components beyond $|p = \pm 2\hbar k\rangle$ corrections to the Kerr nonlinearity, described above, can be ex-

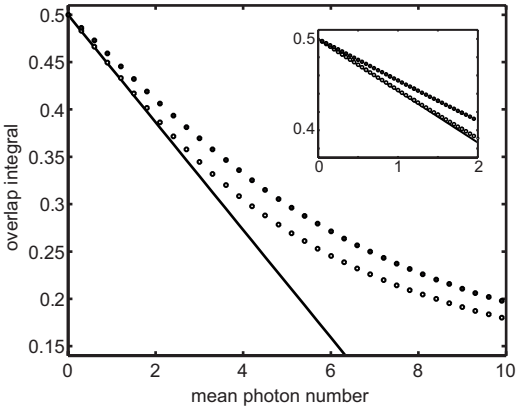

FIGURE 5.2.: Higher-order Kerr nonlinearity. Shown is the spatial overlap integral $\langle\psi_{\bar{n}}|\cos^2(kx)|\psi_{\bar{n}}\rangle$ (per atom) as a function of mean intracavity photon number $\bar{n}$ for a 1D model including external confinement and atom-atom interactions (closed circles). Here, $\psi_{\bar{n}}$ corresponds to the ground state wave function according to the Gross-Pitaevskii equation (5.7). For comparison, open circles depict the overlap integral in the 1D non-interacting case, including higher-order momentum modes which, in the limit of low photon number, resembles the cavity optomechanical two-mode model (solid line), corresponding to normal Kerr nonlinearity. The parameters used for the plots correspond to the experimental settings in Section 5.2.

pected for larger probe light intensity. In addition, atom-atom interactions, which try to flatten out density modulations, will influence the nonlinear response of the atoms upon probing. To be quantitative, we determine the ground state wave function of the condensate according to the Gross-Pitaevskii equation, taking into account the combined potential of the harmonic dipole trap and the dynamic cavity lattice potential. For simplicity we restrict ourselves to a 1D situation along the cavity axis, described by

$$\Big(-\frac{\hbar^2}{2m}\frac{d^2}{dx^2}+V_{\rm ext}(x)+\hbar U_0\bar{n}\cos^2(kx)+u_{\rm 1D}|\psi(x)|^2\Big)\psi(x)=\mu\psi(x) \quad (5.7)$$

with effective atom-atom interaction constant $u_{\rm 1D}$. From the family of ground state solutions $\{\psi_{\bar{n}}\}_{\bar{n}}$ we can deduce the dependence of the overlap integral $\mathcal{O}(\bar{n})=\langle\psi_{\bar{n}}|\cos^2(kx)|\psi_{\bar{n}}\rangle$, which determines the index of refraction as a function of mean intracavity photon number $\bar{n}$ (see Figure 5.2). Direct comparison with a non-interacting model, including higher-order momentum

components (up to $p = \pm 10\hbar k$), clearly shows the tendency of atom-atom interactions to avoid density modulations, thereby lowering the effective Kerr index of the condensate. For low intracavity photon numbers $\bar{n} \leq 2$, which for the chosen parameter settings corresponds to an optical lattice depth of about $2E_{\mathrm{rec}}$, the numerical simulation resembles the linear dependence of the refractive index on photon number, though with a different slope as compared to the non-interacting case. For deeper lattice potentials the occupation of higher-momentum components gives rise to higher-order nonlinearity, which goes beyond the normal Kerr nonlinearity. This causes an additional bending of the bistable resonance curves for large probe strength, and reflects the fact that the per-atom overlap integral $\mathcal{O}$ is bounded within the interval $[0, 1]$.

5.2. Experimental observation of optical bistability

To observe bistable behavior in our system, we probe the cavity field with a weak circularly polarized laser beam, whose frequency is blue-detuned by $\Delta_a = 2\pi \times 58\,\mathrm{GHz}$ from the atomic transition frequency ω_a. Due to a weak magnetic field oriented along the cavity axis, probe photons induce σ^+ transitions starting form the initial ground state $|F = 1, m_F = -1\rangle$. Taking into account all accessible hyperfine levels in the $5P_{3/2}$ excited state manifold, we obtain a maximum coupling strength between a single atom and a σ^+ polarized intracavity photon of $g_0 = 2\pi \times 14.1\,\mathrm{MHz}$. We prepare almost pure condensates containing typically $N = 10^5$ atoms in a harmonic dipole trap with trapping frequencies $(\omega_x, \omega_y, \omega_z) = 2\pi \times (220, 48, 202)\,\mathrm{Hz}$, where x denotes the cavity axis and z the vertical axis. From this we deduce Thomas-Fermi radii of $(R_x, R_y, R_z) = (3.2, 19.3, 3.4)\,\mu\mathrm{m}$.

After preparing a condensate, the probe laser frequency is scanned at a rate of $\dot{\omega}_p = 2\pi \times 1\,\mathrm{MHz/ms}$ across the coupled resonance, while recording the cavity transmission on a single photon counter. The scan speed is chosen to be slow compared to the timescale of atomic motion, in order to guarantee adiabaticity, but still fast compared to the atom loss rate. Typical resonance curves obtained for different probe strengths are shown in Figure 5.3. For maximum intracavity photon numbers well below the critical photon number $\bar{n}_{\mathrm{cr}}$ the resonance curve is Lorentzian shaped and does not depend on the scan direction of the probe laser (A). When increasing the probe strength beyond the critical value, we observe a pronounced asymmetry of the resonance and hysteretic behavior which indicates bistability of the system (B). The frequency range over which bistability occurs gets enlarged by further increasing the probe strength (C).

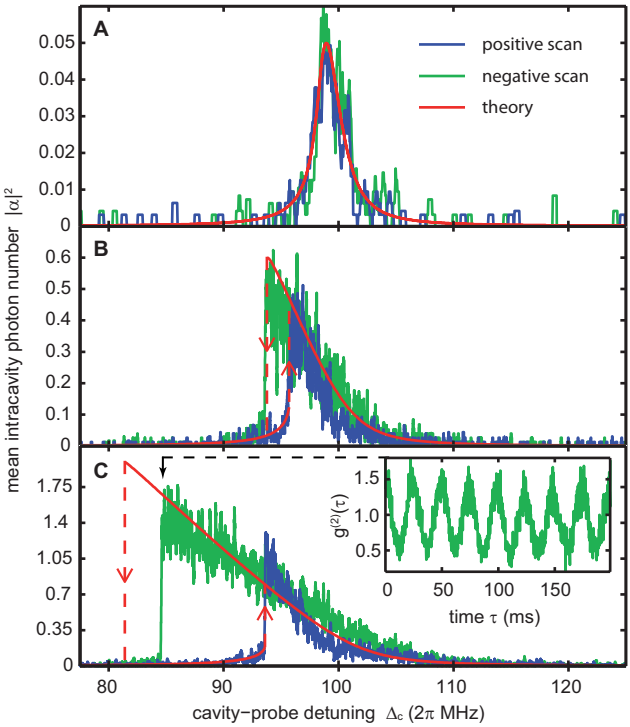

FIGURE 5.3.: Bistable behavior at low photon number. The traces show the mean intracavity photon number $|\alpha|^2$ versus the cavity-probe detuning Δ_c. Traces A, B and C correspond to probe strengths of $\eta = (0.22, 0.78, 1.51)\kappa$, respectively. The intracavity photon number is deduced from the detector count rate. Each graph corresponds to a single experimental sequence during which the probe laser frequency was scanned twice across the resonance, first with increasing detuning Δ_c (blue curve) and then with decreasing detuning (green curve). The scan speed was $2\pi \times 1\,\mathrm{MHz/ms}$ and the raw data has been averaged over 400 µs (A) and 100 µs (B and C). We corrected for a drift of the resonance caused by an atom loss rate assumed to be constant during the measurement. The theoretically expected stable resonance branches (red) have been calculated for 10^5 atoms taking a transverse mode overlap at maximum of 0.6 into account. The inset of C shows photon-photon correlations of the green trace calculated from the last 400 µs right before the system transits to the lower stable branch. Due to averaging these oscillations are not visible in the main graph.

Qualitatively, hysteretic behavior is anticipated from the bistable resonance curves shown in Figure 5.1A. If the probe laser frequency is varied, the system adiabatically moves along the steady state branch. Once the cavity-probe detuning reaches the upper or lower turning point of the bistable resonance curve, the system gets unstable and is forced to pass into the remaining stable state[2]. Quantitatively, we compare our experimental data with resonance curves (red lines in Figure 5.3), which are obtained from a self-consistent numerical solution of equation

$$\bar{n} = \frac{\eta^2}{\kappa^2 + \left(\Delta_c - U_0 \mathcal{O}(\bar{n})\right)^2}, \tag{5.8}$$

using the overlap integrals $\mathcal{O}(\bar{n})$ of the ground state solutions $\psi_{\bar{n}}$ of Equation (5.7).

From this analysis we find a critical photon number of $\bar{n}_{\mathrm{cr}} = 0.21$, in accordance with our experimental observations within the systematic uncertainties. The inclusion of atom-atom interactions results in a critical photon number which is slightly larger than the value 0.18, expected from the analytical interaction-free model. For very low photon numbers (Figure 5.3 A and B) we find good agreement between the measured and calculated resonance curves.

For larger probe strengths our data significantly deviate from the predicted steady state curves (Figure 5.3 C). This is visible in a precipitate transition from the upper branch to the lower one while scanning the probe laser frequency with decreasing Δ_c. Such deviations indicate a superposed non-steady state dynamics. Due to the atomic inertia of our refractive index medium this dynamics goes beyond the physics of a pure Kerr medium [149]. Experimentally, this is supported by detecting regular oscillations in the second-order correlation function $g^{(2)}(\tau)$ which was evaluated from the transmission signal right before the system leaves the upper resonance branch (Figure 5.3C inset).

To observe higher-order nonlinearity due to occupation of higher-order momentum states, we conducted a series of resonance scans (with decreasing Δ_c), using up to 20 times more probe light power than in Figure 5.3C. Our observations are shown in Figure 5.4. For increasing input power the observed bistable region extends more and more towards the empty cavity resonance (dashed line), indicating a decrease of the spatial overlap integral almost down to zero. Deviations from the pure Kerr nonlinearity, which is characterized by a linear dependence of the refractive index on light intensity,

[2] Transient oscillations which are excited during this non-adiabatic transition are the subject of Chapter 6.

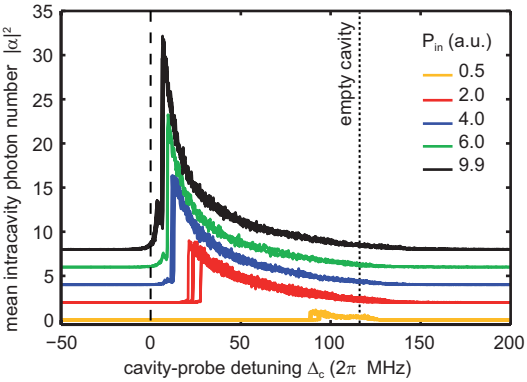

FIGURE 5.4.: Strong bistable behavior and higher-order Kerr nonlinearity. Shown are scans across the bistable resonance with decreasing Δ_c at large input powers, inducing a bistable region which approaches the empty cavity resonance (dashed line). The dressed cavity resonance (dotted line) corresponding to a uniform condensate density was deduced by scanning across the resonance with increasing Δ_c. Each resonance curve corresponds to a different atomic sample with estimated shot-to-shot atom number fluctuations of 10%. Curves with different input power have been offset for better visibility. The rate at which the probe frequency was scanned was $-2\pi \times 2\,\mathrm{MHz/ms}$ for the input powers up to 2 (a.u.), and $-2\pi \times 3\,\mathrm{MHz/ms}$ for the higher input powers. The photon count rates were corrected for saturation occurring at the single photon counter module. The mean atom number was 1.2×10^5, and the probe-atom detuning $\Delta_a = 2\pi \times 58\,\mathrm{GHz}$.

are clearly visible in a pronounced bending of the resonance curves close to the empty cavity resonance. This observation directly reflects the nonlinear behavior of the overlap integral shown in Figure 5.2.

To quantitatively understand the observed resonance curves at large probe power, the 1D model studied above is not sufficient anymore. Additional dipole forces caused by the blue-detuned probe light start to push the atoms also transversally out of the Gaussian cavity mode profile (mainly along the weak trapping axis y), as was confirmed by a numerical simulation based on the full 3D Gross-Pitaevskii equation. This results in an additional decrease of the spatial overlap integral with increasing probe input power. For sufficiently large probe intensities the combined potential provided by the harmonic dipole trap and the repulsive probe potential develops a double-well

structure along the y-axis, which experimentally could be directly observed on the atomic density distribution using absorption imaging.

From the perspective of optical lattice physics with ultracold gases, the presented measurements demonstrate the ability to adiabatically load a condensate into a deep dynamic lattice potential, which is supported by a high-finesse optical cavity. This opens interesting possibilities for studying the superfluid to Mott insulator transition [17] in a situation where the confining lattice potential itself acts as a dynamic degree of freedom. As was studied in the literature, this can give rise to novel overlapping stability regions [22], corresponding to competing insulator-like states, as well as novel lattice physics with cavity-mediated long-range interactions [150, 137].

5.3. Photon number fluctuations and mean-field approximation

The observation of optical bistability with mean intracavity photon numbers $\bar{n}$ below one rises the question about to what extend intracavity photon number fluctuations influence the atomic motion. In order to distinguish between the classical regime, where the cavity field can be described in terms of a coherent state, and the quantum regime, we have to compare the inherent timescales of the coupled system.

The typical response time for atomic motion is given by the mechanical oscillation period, $T_\mathrm{m} = \frac{2\pi}{4\omega_\mathrm{rec}} \sim 66\,\mu\mathrm{s}$, which is three orders of magnitude larger than the typical residence time of photons in the cavity, determined by $T_\mathrm{c} = \frac{1}{2\kappa} \sim 61\,\mathrm{ns}$. For a mean intracavity photon number of $\bar{n} = 1$ this corresponds to about 10^3 photons on average, passing the cavity within one mechanical oscillation period. The relative fluctuations of the resulting light forces, averaged over T_m, are far below one. This justifies a classical description of the coupled system, even for mean photon numbers on the order of one.

A different regime is attained once the mean intracavity photon number $\bar{n}$ is further reduced such that only a few photons pass the cavity during one mechanical oscillation period, while the cavity-optomechanical coupling rate G is appropriately increased in order to induce nonlinearity, $\bar{n} \sim \bar{n}_\mathrm{cr}$. This corresponds to the strong coupling regime of cavity optomechanics where the coupling rate G is on the order of the cavity decay rate κ (see Section 4.3.4). Here, single photons entering the cavity imprint a density modulation in the condensate which is strong enough to tune the system out of resonance. In this regime, the coupling between fluctuations of the cavity field and the atomic motion becomes dominant, which requires a full density matrix description based on the cavity optomechanical Hamiltonian (4.11).

5.4. Summary

The steady-state behavior of a condensate in a dynamic optical lattice potential, supported by a high-finesse optical cavity, was studied theoretically and experimentally. We have observed strong optical nonlinearity at the single-photon level, manifested by bistable and hysteretic behavior. In principle, the strength of nonlinearity could be further increased, by tuning the probe laser frequency closer to atomic resonance, however, with an upper limit provided by the vacuum Rabi splitting on resonance (see Chapter 3) and decoherence due to spontaneous emission. An increased nonlinearity may allow for observation of non-trivial light statistics, or ponderomotive light squeezing in the probe light field [151, 149].

6 Collective atomic motion in a dynamic optical lattice

Optical light fields have been used to measure the position of particles with very high accuracy. For example, the motion of atoms, which are coupled to the field of a high-finesse optical cavity, can be continuously sensed by means of a probe laser field which experiences, depending on the atomic position, a different phase shift. Experimentally, this was realized with single atoms trapped within a small-volume optical high-finesse cavity, operating in the strong coupling regime [76, 75].

Here, we use the dispersive coupling between a condensate and a high-finesse optical cavity to continuously monitor small amplitude density oscillations in the condensate for the first time. Additional dipole forces caused by the probe light, which is used to monitor the dynamically changing cavity resonance, render these oscillations highly nonlinear. A qualitative understanding of the observed dynamics is obtained from a simple cavity optomechanical model, introduced in Chapter 4. We perform mean-field calculations in the adiabatic cavity limit, and find good agreement with our observations. Finally, we discuss the impact of retardation effects, caused by the finite cavity-decay time, on the system's dynamics.

The experimental results of this chapter have been published in [120]: F. Brennecke*, S. Ritter*, T. Donner, and T. Esslinger. *Cavity Optomechanics with a Bose-Einstein condensate.* Science 322, 235 (2008).

6.1. Adiabatic elimination of the cavity field dynamics

The dynamics of our dispersively coupled BEC-cavity system is governed by two important timescales. The time at which the cavity field decays, $\tau_c = \frac{1}{2\kappa}$, determines the typical response time after which the cavity field has reached a new steady state upon a sudden change in the cavity frequency or the input power. In our system this time scale is about three orders of magnitude shorter than the mechanical oscillation period, $T_m = \frac{2\pi}{4\omega_{\mathrm{rec}}}$. Correspondingly, the cavity field quasi-adiabatically follows the changes in cavity resonance frequency, caused by atomic motion. This allows to perform a Born-Oppenheimer type of approximation, which greatly simplifies the analysis of the system's dynamics. In particular, one can eliminate the cavity field degree of freedom from the coupled equations of motion, and derive an effective equation of motion for the atomic degrees of freedom.

Due to their spatially dependent dispersion, the atoms effectively move in a dynamic optical lattice potential provided by the probe light driving the cavity field. In contrast to a normal optical lattice potential, its depth depends non-locally on the spatial atomic distribution which introduces nonlinear behavior and cavity-mediated atom-atom interactions. To some extent, this is comparable to electrons moving within the lattice structure of a crystal. Here, the lattice spacing being determined by the local electron density, provides a dynamical feedback onto the motion of the electrons.

6.2. The optomechanical potential

In order to get a first insight into the non-steady state dynamics of the coupled BEC-cavity system, we start with the classical equations of motion for the equivalent cavity optomechanical system (see Equations (4.14) and (4.15) in Section 4.3)

$$\ddot{X} + (4\omega_{\mathrm{rec}})^2 X = -4\omega_{\mathrm{rec}} G|\alpha|^2 \tag{6.1}$$

$$i\dot{\alpha} = -(\tilde{\Delta}_c - GX + i\kappa)\alpha + i\eta. \tag{6.2}$$

In contrast to Section 5.1, we now consider X as a dynamical variable changing over time. After inserting the adiabatic solution of Equation (6.2)

$$\alpha = \frac{i\eta}{\tilde{\Delta}_c - GX + i\kappa} \tag{6.3}$$

into Equation (6.1), the following effective equation of motion for the mechanical degree of freedom is derived:

$$\ddot{X} + (4\omega_{\mathrm{rec}})^2 X + \frac{4\omega_{\mathrm{rec}} g\eta^2}{\kappa^2 + (\tilde{\Delta}_c - GX)^2} = 0, \tag{6.4}$$

with effective detuning $\tilde{\Delta}_c = \Delta_c - U_0 N/2$ and optomechanical coupling constant $G = U_0\sqrt{N}/2$. The last term in Equation (6.4) corresponds to the radiation pressure force, which mainly acts if X is within a window of width $\Delta X = 2\kappa/G$ centered around $X_0 = \tilde{\Delta}_c/G$. From the total "mechanical force" in Equation (6.4) we can deduce via integration along X the "optomechanical potential"

$$V_{\mathrm{opt}}(X) = 2\hbar\omega_{\mathrm{rec}}X^2 - \frac{\hbar\eta^2}{\kappa}\arctan\Big(\frac{\tilde{\Delta}_c - GX}{\kappa}\Big). \tag{6.5}$$

This potential provides us with an intuitive picture of the mechanical oscillator dynamics when probing the cavity field with probe strength η.

Exemplary potential curves for different values of the probe-cavity detuning Δ_c are shown in Figure 6.1A-D, according to the dashed lines in the steady-state resonance plot, shown in 6.1E. Depending on the particular probe-cavity detuning the optomechanical potential exhibits either a single well or double well structure. The corresponding stable (instable) steady-state solutions are discovered at the points where the optomechanical potential V_{opt} exhibits a local minimum (maximum), as indicated by the closed (open) circles in Figure 6.1B. For probe strengths below the critical value η_{cr} the optomechanical potential always exhibits a single minimum.

6.3. Energy functional for a dynamic optical lattice

Before we proceed with the discussion on the non-steady state dynamics, we elucidate the relationship between the optomechanical potential V_{opt} and the total energy functional of the atomic system, without relying on the cavity optomechanical equations of motion. As before, we can adiabatically solve the cavity light field for its steady state

$$\alpha = \frac{i\eta}{\Delta_c - U_0\mathcal{O} + i\kappa}, \tag{6.6}$$

with spatial overlap integral $\mathcal{O} = \langle\psi|\cos^2(kx)|\psi\rangle$ and condensate wave function ψ, normalized to the total atom number N. Within a mean-field approximation, the condensate motion in the dynamic cavity lattice potential is described by the time-dependent Gross-Pitaevskii equation

$$i\hbar\dot{\psi}(x,t) = \Big(-\frac{\hbar^2}{2m}\frac{d^2}{dx^2} + V_{\mathrm{ext}}(x) + \hbar U_0|\alpha|^2\cos^2(kx) + u_{1\mathrm{D}}|\psi|^2\Big)\psi(x,t). \tag{6.7}$$

Here, the spatial overlap integral $\mathcal{O}$ introduces, besides the usual atom-atom interaction with strength $u_{1\mathrm{D}}$, an additional nonlinear (and nonlocal) term into the Gross-Pitaevskii equation.

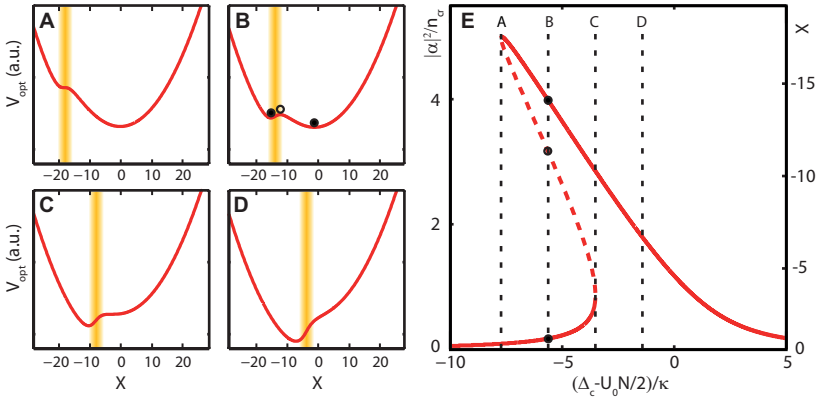

FIGURE 6.1.: (A-D) Shown are plots of the optomechanical potential V_{opt} (see Equation (6.5)) for different probe-cavity detunings corresponding to the dashed lines in the steady state resonance plot E. The yellow bars indicate the resonance profile where maximum cavity transmission occurs. Within the bistable region (detuning A to C) the potential exhibits a double well structure revealing bistability of the system. At the borders of the bistable region (A and C) one of the two local minima changes into a saddle point and the system becomes instable. The parameters used for the plots are $G = 0.42\kappa$ and $\eta = \sqrt{5\bar{n}_{\mathrm{cr}}}\kappa$.

The corresponding time-independent Gross-Pitaevskii equation is obtained from extremalization of the following energy functional

$$E_{\mathrm{GP}}(\psi,\psi^*) = \int\Big[\frac{\hbar^2}{2m}|\psi'(x)|^2 + V_{\mathrm{ext}}(x)|\psi(x)|^2 + \frac{1}{2}u_{1\mathrm{D}}|\psi(x)|^4\Big]dx - \frac{\hbar\eta^2}{\kappa}\arctan\Big(\frac{\Delta_c - U_0\mathcal{O}}{\kappa}\Big).$$

In order to get a rough idea of the characteristics of this energy functional, we restrict the discussion to the uniform density limit, neglecting atom-atom interactions. After expanding the condensate wave function as $\psi(x) = c_0 + c_2\sqrt{2}\cos(2kx)$ with $|c_2|^2 \ll |c_0|^2 \sim N$, we obtain from Equation (??)

$$E_{\mathrm{GP}}(c_2, c_2^*) = 4\hbar\omega_{\mathrm{rec}}|c_2|^2 - \frac{\hbar\eta^2}{\kappa}\arctan\Big(\frac{\tilde{\Delta}_c - G(c_2 + c_2^*)/\sqrt{2}}{\kappa}\Big). \qquad (6.8)$$

The coupling constant G and the effective detuning $\tilde{\Delta}_c$ are defined as before.

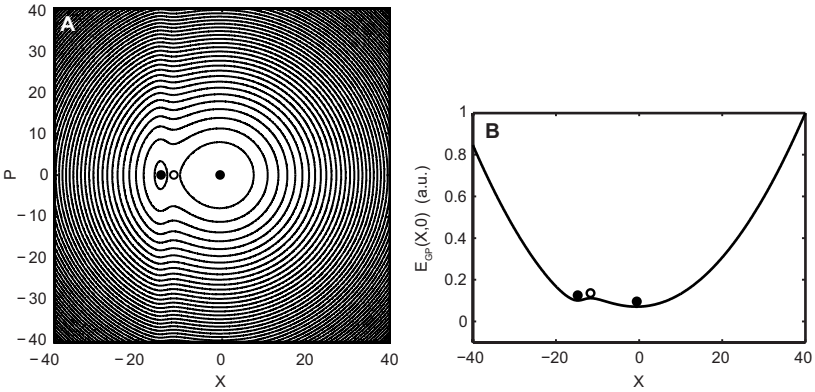

FIGURE 6.2.: (A) Contour plot of the Gross-Pitaevskii energy functional Equation (6.9) in the mechanical "phase space" spanned by the two quadratures X and P. Stable (instable) stationary states are depicted as closed (open) circles. (B) A section of the Gross-Pitaevskii functional along the line $P = 0$ reveals the optomechanical potential V_{opt}. Parameters used for the plots are the same as in Figure 6.1.

In terms of the two quadratures $X = \frac{c_2+c_2^*}{\sqrt{2}}$ and $P = \frac{c_2-c_2^*}{\sqrt{2}i}$ (the position and momentum variables of the equivalent mechanical oscillator) the energy functional can be related to the optomechanical potential V_{opt}:

$$E_{\mathrm{GP}}(X,P) = 4\hbar\omega_{\mathrm{rec}}\frac{P^2}{2} + V_{\mathrm{opt}}(X). \tag{6.9}$$

According to the Bloch theorem, the eigenfunctions in a periodic potential at zero quasi-momentum can always chosen as real functions. Correspondingly, the steady state solutions of (6.9) fulfill the constraint $P = 0$, and the local minima of the optomechanical potential V_{opt} (6.1) agree with the lowest lying energy states of the Gross-Pitaevskii energy functional E_{GP}. Figure 6.2 shows a contour plot of the energy functional (6.9) for the parameters used in Figure 6.1B, as well as the corresponding section at $P = 0$, which agrees with the optomechanical potential V_{opt}.

A swallowtail catastrophe

From the total energy functional E_{GP}, Equation (6.9), one can directly extract the energy of the lowest lying stationary state(s) by means of local minimization. The resulting energy spectrum as a function of the control

parameter Δ_c is plotted in Figure 6.3. It consists of two branches (solid lines) which cross each other and both terminate at the borders of the bistable region, depicted in gray. If the control parameter Δ_c is tuned slowly enough across the bistable region, the system will be able to adiabatically follow one of the two energy branches. However, adiabaticity breaks down, no matter how slowly the control parameter is varied, once the terminus of the energy branch is reached. Such behavior is well known from catastrophe theory which studies and classifies the critical behavior of nonlinear systems under small changes of some control parameter. Here, we are concerned with a variant of the so called "swallowtail catastrophe", according to the shape of the energy diagram. A similar phenomenon was predicted to occur for an interacting Bose-Einstein condensate in a static one-dimensional optical lattice [152]. For densities exceeding a critical value the lowest energy band develops a swallowtail structure at the edge of the first Brillouin zone, which e.g. leads to nonlinear Landau-Zener transitions into higher bands [153].

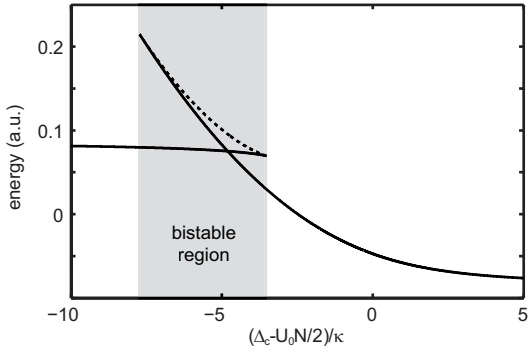

FIGURE 6.3.: Energy landscape of the local extrema of the energy functional E_{GP}, Equation (6.9), versus probe-cavity detuning. The two solid lines crossing each other correspond to the upper and lower stable state branch in the bistable resonance curve shown in Figure 6.1E. The dashed line indicates the energy of the instable state branch. Parameters used for the plot are the same as in Figure 6.1.

6.4. Experimental observation of transient oscillations

To experimentally study the non-steady state dynamics of our system, Bose-Einstein condensates of typically 1.2×10^5 atoms in the $|F = 1, m_F = -1\rangle$ ground state are prepared. Circularly polarized probe photons couple the

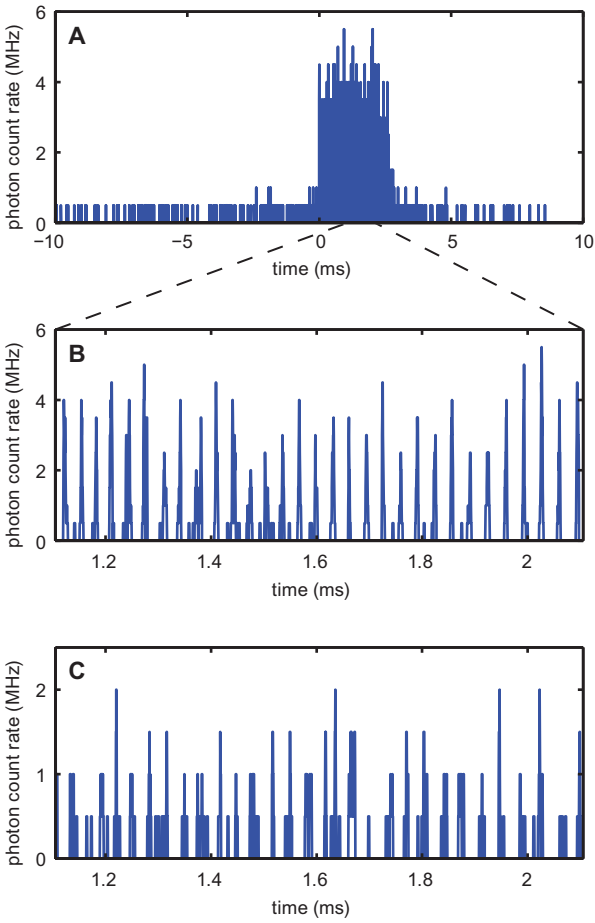

FIGURE 6.4.: (A-C) Response of the continuously driven BEC-cavity system. Shown is a single trace of the cavity transmission (averaged over 2 µs) while scanning the cavity-probe detuning at a rate of $+2\pi \times 2.9\,\mathrm{MHz/ms}$ across its σ^- resonance [100]. The mean intracavity photon number on resonance was 7.3 ± 1.8 (A and detail B) and 1.5 ± 0.4 (C). The photon count rate for one mean intracavity photon is $0.8 \pm 0.2\,\mathrm{MHz}$, and the dead time of the single-photon counter is 50 ns which leads to a saturation of high photon count rates. The probe laser frequency was blue detuned by $\Delta_a = 2\pi \times 32\,\mathrm{GHz}$ with respect to the atomic resonance.

ground state solely to the $|F' = 2, m'_F = -2\rangle$ excited state with a single photon Rabi frequency of $g_0 = 2\pi \times 10.9\,\mathrm{MHz}$. Trapping the condensate within the cavity is accomplished by a crossed-beam dipole trap with trap frequencies $(\omega_x, \omega_y, \omega_z) = 2\pi \times (222, 37, 210)\,\mathrm{Hz}$, where x denotes the cavity axis and z the vertical axis. The cavity mode maximally overlaps with the condensate having Thomas-Fermi radii of $(R_x, R_y, R_z) = (3.3, 20.0, 3.5)\,\mu\mathrm{m}$ which are deduced from a mean field approximation. All experiments presented in this section were performed without active stabilization of the cavity length, which would give rise to an additional weak standing wave potential for the atoms (see Chapter 7).

The cavity field is driven by continuously applying a weak probe laser field along the cavity axis. The light transmitted through the cavity is monitored using a single-photon counter and serves as a probe for the dynamics of the system. With the probe laser frequency ω_p being blue detuned from the atomic resonance frequency ω_a by $\Delta_a = \omega_p - \omega_a \geq 10^4\gamma$, spontaneous emission can be mostly neglected.

Figure 6.4 shows the response of the system while scanning the probe frequency (with increasing Δ_c) across the optical resonance. The transmission signal (A) exhibits a sharp rising edge and subsequently regular and fully modulated oscillations (B) lasting for about 2.5 ms. These oscillations start at a frequency of about 37 kHz which slightly decreases over the train of oscillations and does not depend on the speed at which the probe frequency is varied. Similar responses of the system were measured for lower probe strengths at the same detuning (C) as well as for probe-atom detunings of up to $\Delta_a = 2\pi \times 300\,\mathrm{GHz}$, provided the probe rate was increased sufficiently. Moreover, when continuing the probe frequency scan we observe a further train of oscillations appearing in the vicinity of a second resonance which is driven by σ^+ polarized photons (see Section 3.6). This is in accordance with the observation that the condensate remains intact during probing, which is directly inferred from absorption images taken subsequent to probing. The observed oscillatory behavior is obviously in strong contrast to a Lorentzian shaped resonance curve which would be expected for an atomic ensemble frozen inside the cavity, i.e. when the atomic external degree of freedom is neglected. From absorption images revealing the momentum distribution of the atomic cloud during the oscillatory dynamics, we infer about the occupation of momentum components $|p = \pm 2\hbar k\rangle$, where k denotes the wave number of the probe light (see Figure 6.5).

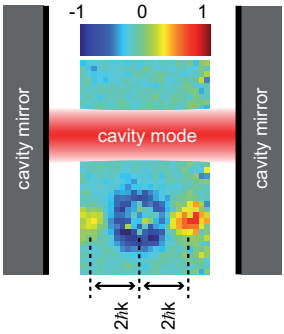

FIGURE 6.5.: Absorption image revealing the population in the $|p = \pm 2\hbar k\rangle$ momentum components during transient oscillations, see Figure 6.4. Once the coherent dynamics was excited, both trapping potential and probe laser were switched off, and the cloud was imaged after 4 ms free expansion. To clearly detect the small $|p = \pm 2\hbar k\rangle$ population we averaged over 9 independent images and subtracted the average of 9 different images without excitation (taken after the oscillations had stopped). The maximum intracavity photon number on resonance was 9.5. The distance between the cavity mirrors and the cavity mode waist are drawn to scale.

Qualitative interpretation

With the optomechanical potential V_{opt} (see Figure 6.2) at hand we gain a direct understanding of the systems response upon an adiabatic scan of the probe laser frequency across resonance. Imagine the system initially is prepared in the steady state $X = 0$ (Figure 6.1A), and the probe laser is subsequently scanned with increasing Δ_c across the resonance curve, shown in Figure 6.1E. Until the terminus of the lower stable branch is reached (C) the system adiabatically follows the changes in the optomechanical potential landscape (A and B). Right at the turning point of the lower branch (C), the system gets unstable and, while scanning the probe laser further, starts to perform transient oscillations within the lower lying potential valley of the optomechanical potential. In doing so it periodically crosses (or strikes) the resonance condition where cavity and probe laser are in resonance, giving rise to a strongly modulated cavity transmission signal (see Figure 6.4).

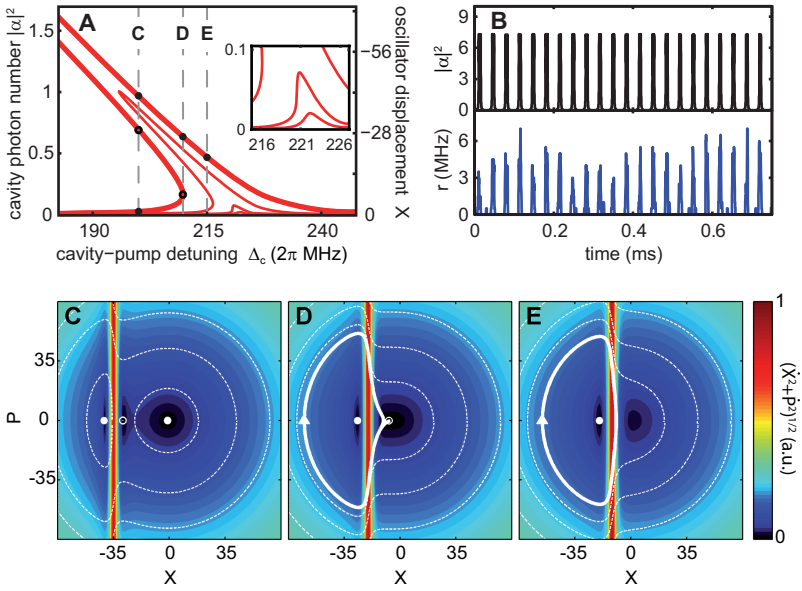

FIGURE 6.6.: Steady state and dynamical behavior of the BEC-cavity system in the two-mode model. (A) Mean intracavity photon number and corresponding oscillator displacement X versus the cavity-probe detuning Δ_c for the steady state solutions of Equations (6.1) and (6.2). The curves correspond to mean intracavity photon numbers on resonance of $\eta^2/\kappa^2 = 0.02, 0.07, 1$ and 7.3, and a probe-atom detuning of $\Delta_a = 2\pi \times 32\,\mathrm{GHz}$. The inset highlights the bistable behavior for probe amplitudes larger than $\eta_{\mathrm{cr}} \approx 0.27\kappa$. (C-E) Evolution of the system in the mechanical phase space depicted for three subsequent situations ($\Delta_c = 2\pi \times (200, 209.7, 215)\,\mathrm{MHz}$) corresponding to the markers in A and $\eta^2/\kappa^2 = 7.3$. The stable and unstable steady state configurations are displayed as filled and open circles respectively. Dashed lines show representative evolutions for different starting conditions. Coloring indicates the modulus of the time evolution field $(\dot{X}, \dot{P})$. The solid lines in D and E correspond to the experimental situation in Fig. 2A and show the evolution of the system while scanning Δ_c at a rate of $2\pi \times 2.9\,\mathrm{MHz/ms}$ across the resonance with the system initially prepared in the lower stable solution. (B) Intracavity photon number $|\alpha|^2$ and corresponding transmission count rate r (including detection shot noise and averaging over 2 µs) for the system circling along the solid line in E.

Further insight is gained by examining the dynamics in the phase space of the mechanical oscillator, spanned by X and P (Figure 6.6C-E). Without cavity field the time evolution would simply correspond to a clockwise rotation at $4\omega_{\mathrm{rec}}$. Yet, when photons enter the cavity the evolution is affected by light forces. This is the case along the vertical resonance line determined by the resonance condition $\tilde{\Delta}_c - GX = 0$, as shown in Figure 6.6C-E (red line). Initially the condensed atoms are prepared at the stable phase-space point $(X, P) = 0$, see Figure 6.6C. Increasing the detuning Δ_c across the resonance renders the system instable and excites transient oscillations, as indicated by the solid line in Figure 6.6D. The evolution along this path is dominated by the free oscillator dynamics which gets periodically interrupted by the interaction with the cavity light field, Figure 6.6D and E. This behavior is closely related to the matter-wave dynamics of a kicked rotor which is operated at an antiresonance where the accumulated phase factor between two kicks inhibits occupation of higher momentum modes [154].

The frequency of transient oscillations decreases continuously over observation time (see Figure 6.7). This is expected when actively scanning the cavity-probe detuning Δ_c which shifts the resonance line in the phase space diagram, and leads to an adiabatic change of the system's circling path (compare Figure 6.6D and E).

Quantitative modelling

A precise quantitative understanding of the observed frequency and its decrease is obtained when taking atom-atom interactions, the external trapping potential and atom losses into account. The atom-atom interactions result in a shift of the bare oscillation frequency $4\omega_{\mathrm{rec}} = 2\pi \times 15.1\,\mathrm{kHz}$ by the mean field energy, which in the Thomas-Fermi limit equals $4/7$ times the chemical potential $\mu = 2\pi \times 2.4\,\mathrm{kHz}$ [11]. The trapping potential gives rise to a Fourier-limited broadening of the initial momentum distribution and accordingly introduces a damping of the free running oscillator dynamics. This suppresses a double peak structure in the transmitted light which would be expected at the onset of oscillations for the homogeneous two-mode model (see Figure 6.6D). An additional decrease in the effectively coupled atom number, possibly caused by optical forces along the transverse directions, accelerates the observed frequency shift by a factor of ~ 2. The numerical integration of the full 1D model (Equations (6.6) and (6.7)) yields very good agreement with our data (Figure 6.7).

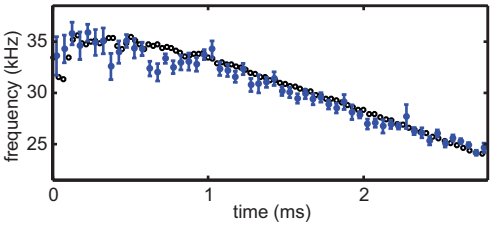

FIGURE 6.7.: Transient oscillation frequency while scanning Δ_c across resonance. The frequency within time bins of $50\,\mu$s was obtained from a peak-detection routine applied to the cavity transmission data averaged over $10\,\mu$s. The data (filled circles) is an average over 23 traces referenced to the start of the oscillations. The error bars indicate the standard deviation of the mean. Open circles show the result of a numerical integration of the 1D system taking atomic interactions and external trapping into account (Equations (6.6) and (6.7)). The mean intracavity photon number on resonance was 3.6 ± 0.9. To fit the slope of the data, the effect of transverse dipole forces during the time of oscillations was taken into account via an effective atom loss of $1.5 \cdot 10^3$ /ms which was added to the experimental frequency chirp of $\dot{\Delta}_c = 2.9\,\mathrm{MHz/ms}$. The background rate of atom loss was measured to be 45/ms, and an atom number of $(116 \pm 18) \times 10^3$ was deduced from absorption images taken after the oscillations.

6.5. Finite cavity lifetime and retardation effects

Until now, the light intensity in the cavity was considered to adiabatically follow the collective motion of the atoms, which corresponds to treating the cavity field decay as infinitely fast. This approximation was justified by the different timescales which underly atomic motion and cavity damping, corresponding to the non-resolved sideband regime of cavity optomechanics. This allowed us to model the atomic dynamics in terms of a conservative potential V_{opt}, in which the effective mechanical element is moving.

In the following, we will be concerned with the first order correction terms to the adiabatic approximation which take into account finite retardation effects between the cavity light intensity and atomic motion. In addition to the conservative light force, these give rise to friction forces, which either stabilize (cool) or destabilize (amplify) atomic motion in the optomechanical potential [60].

Linear analysis around the steady state solutions

To understand the influence of retardation effects on the steady state behavior studied in Chapter 5, we perform a linear analysis around the steady state solutions of the coupled equations of motion (5.1) and (5.2) [155, 60]. Denoting the steady state values as α_0 and X_0, we consider the ansatz

$$\begin{aligned} \alpha &= \alpha_0 + \delta\alpha \\ X &= X_0 + \delta X. \end{aligned}$$

We expand the equations of motion to lowest order in $\delta\alpha$ and δX and arrive at the linearized set of equations

$$\delta\ddot{X} + (4\omega_{\rm rec})^2\delta X = -4\omega_{\rm rec}G(\alpha_0\delta\alpha^* + \alpha_0^*\delta\alpha) \tag{6.10}$$

$$i\delta\dot{\alpha} = -(\Delta_0 + i\kappa)\delta\alpha + G\alpha_0\delta X. \tag{6.11}$$

To approximately solve the light field equation, we perform an expansion in orders of retardation. Terminating the expansion at first order retardation terms, we obtain

$$\delta\alpha \approx \frac{G\alpha_0}{\Delta_0 + i\kappa}\delta X - \frac{iG\alpha_0}{(\Delta_0 + i\kappa)^2}\delta\dot{X} \tag{6.12}$$

with $\Delta_0 = \tilde{\Delta}_c - GX_0$. After plugging this into equation (6.10), we find a harmonic oscillator equation of motion including a friction force term,

$$\delta\ddot{X} + 2\gamma\delta\dot{X} + \omega^2\delta X = 0, \tag{6.13}$$

with oscillation frequency ω, determined by

$$\omega^2 - (4\omega_{\rm rec})^2 = -\frac{G^2\Delta_0}{2\omega_{\rm rec}\eta^2}|\alpha_0|^4, \tag{6.14}$$

and friction coefficient

$$\gamma = 4\omega_{\rm rec}\frac{2G^2\kappa\Delta_0}{\eta^4}|\alpha_0|^6. \tag{6.15}$$

Correspondingly, small amplitude oscillations of the system around the steady state (α_0, X_0) occur with a frequency which differs from the bare oscillation frequency $4\omega_{\rm rec}$. This effect, known under the term 'optical spring', was experimentally observed for the first time in a cavity optomechanical setup involving a mirror mounted on a cantilever [130]. It originates from the conservative part of the radiation pressure force which deforms the harmonic oscillator potential into the optomechanical potential $V_{\rm opt}$, derived in Section 6.2.

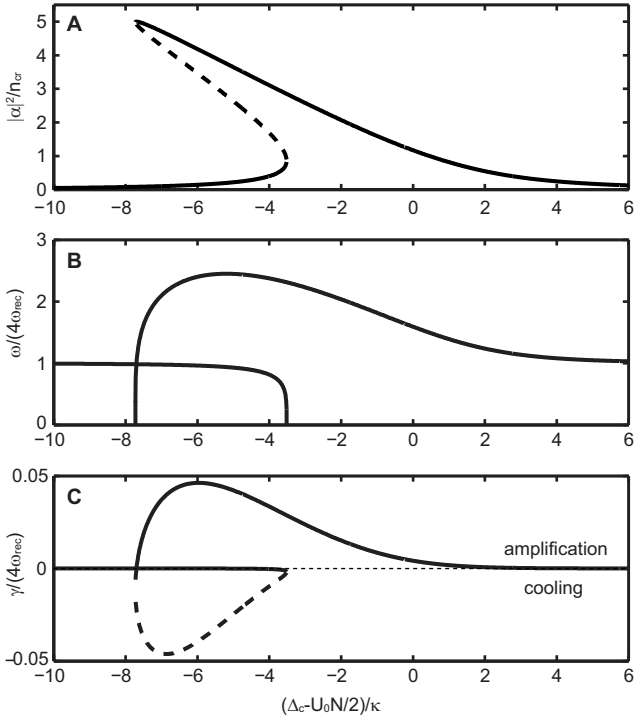

FIGURE 6.8.: Stability analysis in the bistable regime. Displayed are the oscillation frequency (B) and the friction coefficient (C) of small oscillations around the steady state solutions, according to the resonance curve shown in A (see text). The oscillation frequency is obtained from a harmonic analysis of the optomechanical potential (shown in Figure 6.1) around the local minima. The vanishing of ω at the borders of the bistable region indicate the onset of instability.

In contrast, the velocity dependent term in (6.13) relies on the finite response time of the cavity, and causes – depending on whether the probe laser frequency is blue or red detuned with respect to the shifted cavity resonance – amplification or damping of mechanical motion. The behavior of the oscillation frequency ω and the friction coefficient γ as a function of probe frequency is shown in Figure 6.8B and C, corresponding to the steady state curve shown in Figure 6.8A.

From the linear analysis, presented above, we can infer about a dynamical instability of the upper steady state branch, once the amplification rate δ overcomes the intrinsic losses of the mechanical oscillator. Here, tiny oscillations of the system around steady state grow exponentially in time due to positive feedback from the delayed cavity light field. This in particular can induce a precipitate transition from the upper steady state to the lower one, as indicated by the observations in shown Figure 5.3C, and also was verified directly by numerical simulation.

Experimentally, we observed the optical spring effect by scanning the probe laser frequency slowly across the bistable resonance with decreasing probe-cavity detuning, see Figure 6.9. A typical cavity transmission trace, exhibiting the well known abrupt transition from the upper to the

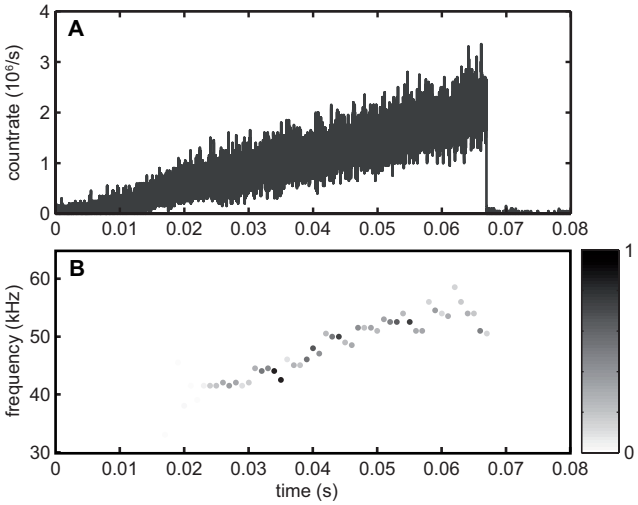

FIGURE 6.9.: Observation of the optical spring effect. (A) Shown is an exemplary trace of the transmitted light intensity while scanning the probe laser with decreasing probe-cavity detuning at a speed of $\dot{\Delta}_c = -2\pi \times 1\,\mathrm{MHz/ms}$ across resonance. The probe laser is blue-detuned by $\Delta_a = 2\pi \times 58\,\mathrm{GHz}$ with respect to the atomic resonance, and the maximum intracavity photon number on resonance is about 5 ± 1. (B) Local frequency analysis of the raw data shown in A. The dots display the oscillation frequency at which the Fourier transform of the transmission data performed within time windows of length 2 ms is maximal. Adjacent time windows overlap by 50 %. The gray shading indicates the corresponding Fourier amplitude in arbitrary linear units.

lower steady state, is shown in Figure 6.9. In the Fourier analysis of the photon data, displayed in B, one clearly notices the onset of oscillations at $t = 20\,\mathrm{ms}$, as well as a subsequent increase of the oscillation frequency up to 55 kHz, which is more than three times larger than the bare oscillation frequency $4\omega_{\mathrm{rec}}$. Qualitatively, this observation is in line with the expectations based on the simple cavity optomechanical model discussed above. However, for a quantitative understanding of the observed frequency response a linear analysis of the full Gross-Pitaevskii equation (6.7) including higher-order momentum modes as well as atom-atom interactions would have to be performed (see e.g. [155]).

6.6. Summary

By coupling a Bose-Einstein condensate dispersively to the field of an optical cavity, we are able to *in-situ* observe small-amplitude condensate density oscillations. The strong collective coupling between atomic motion and cavity field renders these oscillations highly nonlinear, as can be intuitively understood in terms of cavity optomechanics. Due to its high sensitivity to atomic displacement, the system seems to be well suited for sensing collective atomic motion down to the quantum limit. With a mean excitation number of about 10^3, the experiments presented in this chapter are still far away from the quantum regime. In order to decrease the effect of probe light forces, it might be favorable to choose a larger probe-atom detuning, which comes with the expense of a lower displacement sensitivity. Further perspectives to detect small-amplitude oscillations of the condensate density may arise by implementing a phase-sensitive detection method (e.g. a heterodyne detection scheme) for the transmitted or reflected probe light into our setup.

7 Cavity optomechanics with tightly confined ultracold atoms

We have shown in the preceding chapters, that a uniform matter-wave coupled to a standing-wave cavity mode constitutes a cavity optomechanical model system. The role of the mechanical element is played by a density excitation whose eigenfrequency is determined by the matter-wave dispersion relation.

Recently, a different realization of cavity optomechanics with ultracold gases was investigated in the group of D. Stamper-Kurn [26, 45, 71]. Here, non-condensed ultracold atoms are tightly confined within several sites of a static periodic lattice potential, where they perform collective oscillations which strongly couple to the cavity field. In contrast to the uniform situation, the mechanical oscillation frequency, which is determined by the harmonic potential of the individual sites, can be tuned over a wide range. This provides the opportunity, to approach the resolved sideband regime of cavity optomechanics where retardation effects between the optical and the mechanical dynamics play a dominant role [60].

This chapter is concerned with the transition between these two realizations of cavity optomechanics. By loading a condensate into an external optical lattice with variable depth, we are able to continuously pass from the quasi-uniform to the tightly confined regime. We measure the frequency spectrum of transient oscillations, and compare our observations with a simple non-interacting band model. We demonstrate the *in situ* observation of collective atomic oscillations in the tightly confined regime, with an amplitude of about 30 harmonic oscillator lengths.

7.1. Collective motion of tightly confined ultracold atoms

In the following we consider an ultracold gas which is tightly confined at the sites of a one-dimensional lattice potential. This potential is provided by an externally driven TEM_{00} mode of the high-finesse cavity at a wave length of $\lambda_t = 830\,\mathrm{nm}$. Retraction of the atoms upon the trapping light can be neglected. The atoms strongly couple to a different TEM_{00} cavity mode at frequency ω_c which is tuned several tens of GHz from the atomic resonance frequency, and coherently driven by a probe laser with wavelength $\lambda_p = 780\,\mathrm{nm}$. The mismatch between the wavelengths used for trapping and probing the atoms results in a spatial beating between the atomic structure and the probe intensity profile, with a period of about $6\,\mu\mathrm{m}$ (see Figure 7.1).

7.1.1. Hamiltonian description

To obtain a quantitative description of the system, we generalize the dispersive interaction between a single two-level atom and the cavity field (see Section 4.2) to the case of N atoms located at positions $\mathbf{r}_i$. The overall dispersive shift of the cavity resonance frequency ω_c induced by the atomic refractive index is given by [45, 156]

$$\Delta = \sum_{i=1}^{N} \frac{g^2(\mathbf{r}_i)}{\Delta_a}, \tag{7.1}$$

with spatially dependent light-atom coupling $g(\mathbf{r}) = g_0\phi(\mathbf{r})$ and cavity mode profile $\phi(\mathbf{r})$.

The experimental trap geometry permits several approximations, which finally reduces the position dependence of Δ to a single collective variable. The atomic distribution extends along the transverse directions of the cavity much less than the width of the Gaussian mode structure. Accordingly, the position dependence of Δ can be reduced to the direction along the cavity axis x. The trapping frequency ω_m along this direction within a single site of the confining lattice potential is given by

$$\omega_m = 2\sqrt{s}\,\omega_{\mathrm{rec},t}, \tag{7.2}$$

where s denotes the lattice depth in units of $E_{\mathrm{rec},t} \equiv \hbar\omega_{\mathrm{rec},t} = \frac{\hbar^2 k_t^2}{2m}$, and $k_t = \frac{2\pi}{\lambda_t}$ is the wave number of the trapping light. For a typical experimental lattice depth of $s = 50$ the elementary excitation energy $\hbar\omega_m$ within a single site is about one order of magnitude larger than the thermal energy $k_B T$ of the atomic cloud. Correspondingly, the atoms are well prepared in their motional ground state along the cavity axis. The width of the

atomic distribution is determined by the harmonic oscillator length $x_{\mathrm{ho}} = \sqrt{\frac{\hbar}{2m\omega_m}}$, which is about one order of magnitude smaller than the periodicity of the cavity probe lattice. This justifies a linear expansion of the dispersive frequency shift Δ around the atomic equilibrium positions $\bar{x}_i$

$$\Delta = \sum_{i=1}^{N} U_0 \cos^2(k_p x_i) \simeq U_0 N/2 - \sum_{i=1}^{N} U_0 \sin(2k_p \bar{x}_i) k_p \delta x_i \tag{7.3}$$

with displacement variables $\delta x_i = x_i - \bar{x}_i$, and dispersive coupling constant $U_0 = \frac{g_0^2}{\Delta_a}$. The first term in Equation (7.3) accounts for the refractive index of the atoms in equlibrium. The second term quantifies its change when atoms depart from their equilibrium positions $\bar{x}_i$ experiencing, depending on $\bar{x}_i$, a different gradient in probe light intensity (see Figure 7.1).

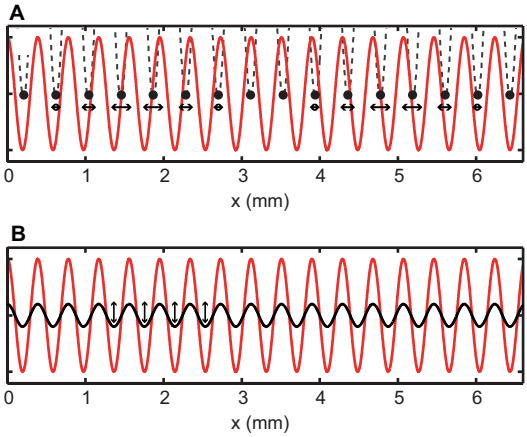

FIGURE 7.1.: Two different realizations of a cavity optomechanical model system using ultracold atoms which are dispersively coupled to a single cavity mode (red solid line). (A) Atoms are tightly confined to the sites of a deep one-dimensional optical lattice potential (dashed) and couple via a particular collective oscillation mode (indicated by arrows) strongly to the cavity field. (B) A uniform matter-wave with initial momentum state $p = 0$ is excited by the periodic cavity field to a coherent density oscillation which periodically changes the cavity optical path length. In contrast to situation A, harmonic "mechanical" oscillation is due to the relative phase evolution of the matter-wave constituents. The atomic density is depicted by the solid black line.

According to Equation (7.3), the cavity-induced dipole forces excite one particular collective motional mode, with the atoms oscillating like $\delta x_i \propto \sin(2k_p\bar{x}_i)$. Any other mode, $\delta x_i \propto \beta_i$, which is orthogonal to the considered one, $\sum_i \beta_i \sin(2k_p\bar{x}_i) = 0$, decouples from the cavity field. In fact, the corresponding dispersive cavity shift vanishes due to orthogonality

$$\sum_{i=1}^{N} U_0 \sin(2k_p\bar{x}_i)k_p\delta x_i \propto \sum_{i=1}^{N} \sin(2k_p\bar{x}_i)\beta_i = 0. \tag{7.4}$$

This motivates to introduce the collective displacement variable

$$X = \frac{1}{\sqrt{N_{\text{eff}}}} \sum_{i=1}^{N} \sin(2k_p\bar{x}_i)\delta x_i \tag{7.5}$$

together with its conjugate momentum

$$P = \frac{1}{\sqrt{N_{\text{eff}}}} \sum_{i=1}^{N} \sin(2k_p\bar{x}_i)p_i. \tag{7.6}$$

The normalization factor $N_{\text{eff}} = \sum_{i=1}^{N} \sin^2(2k_p\bar{x}_i) \approx N/2$ guarantees that the usual commutation relation

$$[\hat{X}, \hat{P}] = i\hbar \tag{7.7}$$

holds true for the corresponding quantum operators. With these definitions the total cavity resonance shift reduces to

$$\Delta = U_0 N/2 - \tilde{G}X, \tag{7.8}$$

where the cavity optomechanical coupling constant $\tilde{G} = U_0 k_p \sqrt{N_{\text{eff}}}$ was intruduced.

Passing now from classical variables to quantum operators, we can write down the total Hamiltonian of the coupled atoms-cavity system in 1D (neglecting atom-atom interactions)

$$\hat{H}_{\text{tot}} = \sum_{i=1}^{N} \hbar\omega_m \hat{c}_i^\dagger \hat{c}_i - \hbar(\Delta_c - \Delta)\hat{a}^\dagger\hat{a} - i\hbar\eta(\hat{a} - \hat{a}^\dagger) \tag{7.9}$$

with harmonic creation operator $\hat{c}_i^\dagger$ for atom i, and cavity photon creation operator $\hat{a}^\dagger$. Defining collective mode operators $\hat{c}, \hat{c}^\dagger$, according to $\hat{X} = x_{\text{ho}}(\hat{c} + \hat{c}^\dagger)$, the total Hamiltonian can be split into two parts. The first one involves the collective mode $\hat{X}$ only

$$\hat{H} = \hbar\omega_m \hat{c}^\dagger\hat{c} - \hbar(\tilde{\Delta}_c + G\hat{X})\hat{a}^\dagger\hat{a} - i\hbar\eta(\hat{a} - \hat{a}^\dagger), \tag{7.10}$$

and is again of cavity optomechanical type (see Section 4.1). As before, the effective detuning between probe laser and dressed cavity resonance is denoted by $\tilde{\Delta}_c = \Delta_c - U_0 N/2$. The second part of $\hat{H}_{\mathrm{tot}}$ describes the free harmonic motion of the remaining $N-1$ orthogonal eigenmodes of the atomic system. Since their motion decouples from the cavity field, we can omit them from the following analysis (see also [156]).

7.1.2. Characteristic properties of the system

The realization of a cavity optomechanical system with tightly confined atoms coupled to the cavity field exhibits similarities but also distinct differences in comparison with the previously studied case of a uniform condensate (Section 4.3). In the following we briefly mention the most important differences.

In the uniform limit, mechanical oscillations originate from matter-wave interference, and happen at a characteristic frequency determined by the free matter-wave dispersion relation. Confining the atom in an external trapping potential allows to tune the mechanical oscillation frequency over a wide range by changing the lattice depth. This could be used to approach the resolved-sideband regime of cavity optomechanics where retardation effects between mechanical motion and the cavity field evolution become dominant.

Working with a tightly confined atomic ensemble relaxes the need for temperatures far below the BEC transition temperature for preparing atomic motion in its ground state. The first excited state energy within a single site of a $50E_{\mathrm{rec},t}$ deep lattice potential corresponds to a temperature of about $2\,\mu$K which is large compared to a BEC transition temperature of about 270 nK in our experiment.

It is instructive to compare the strengths at which mechanical motion and cavity field couple in the two regimes. This is quantified by the cavity resonance shift caused by a mechanical displacement on the order of the harmonic oscillator length[1]. For their ratio we find

$$\frac{G}{\tilde{G}x_{\mathrm{ho}}} = \frac{U_0\sqrt{N}/2}{U_0 k_p \sqrt{N/2}\sqrt{\hbar/2m\omega_m}} = \frac{\lambda_p}{\lambda_t} s^{1/4}. \tag{7.11}$$

Correspondingly, in the tightly confined situation the coupling strength depends only weakly on lattice depth. In particular, in the parameter regime of our experiments, $50 < s < 150$, it is, compared to the uniform case $s = 0$, smaller by a factor of about three.

[1] In the uniform BEC case, the displacement operator was defined in units of the harmonic oscillator length.

7.2. The transition from weak to strong confinement

We considered two limiting cases of a dispersively coupled atoms-cavity system, both representing different realizations of cavity optomechanics. In the first case the atom cloud is quasi-homogeneously distributed over many sites of the cavity probe lattice, while in the second case atoms are tightly confined to the intensity maxima of a static optical lattice.

In this section, we investigate the transition between these two regimes by loading a BEC in an external lattice of variable depth. In particular we aim to understand the intermediate regime where the atomic density is already modulated by the confining periodic potential but tunneling between neighboring lattice sites is still present. To this end, we have to introduce the matter-wave dispersion relation of atoms moving in a periodic trapping potential, which in solid-state physics is referred to as the band structure [157].

7.2.1. Band structure

Consider a particle with mass m moving in a one-dimensional periodic potential of depth s in units of the recoil energy $E_{\mathrm{rec},t}$. The corresponding time-independent Schrödinger equation with eigenenergy E reads

$$\Big(-\frac{\hbar^2}{2m}\frac{d^2}{dx^2} + \frac{s}{2}E_{\mathrm{rec},t}\cos(2k_t x)\Big)\psi(x) = E\psi(x). \tag{7.12}$$

The stationary states of the system can be found by applying Bloch's theorem [158], which states that the eigenfunctions of equation (7.12) are $\lambda_t/2$-periodic, up to a phase factor that can be parameterized by the quasi-momentum q,

$$\psi_{n,q}(x) = e^{iqx}u_{n,q}(x) \tag{7.13}$$

with

$$u_{n,q}(x) = \sum_{m\in\mathbb{Z}} c^m_{n,q} e^{i2mk_p x}. \tag{7.14}$$

The complex coefficients $c^m_{n,q}$ are obtained by diagonalization of the Hamiltonian underlying Equation (7.12) in the free-space momentum basis. The corresponding eigenenergies, $E_n(q)$, form different energy bands which are labelled by the discrete band index $n \geq 0$.

In the limit of vanishing lattice depth, $s \to 0$, the band structure equals the free-space quadratic dispersion relation $E(q) = q^2/2m$ (see the dashed lines in Figure 7.2A). For a deep lattice potential, tunneling between neighboring lattice sites is suppressed, and the band structure reveals the harmonic excitation spectrum of a single lattice site. The energy bands become flat and

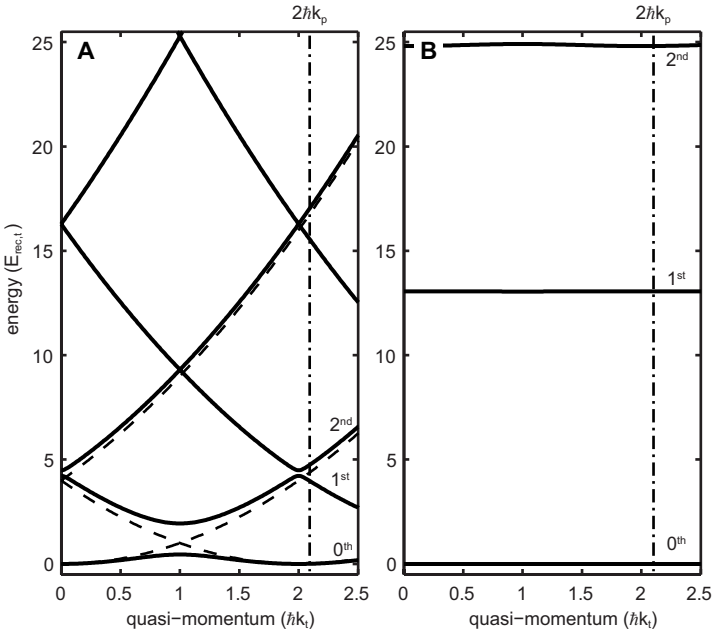

FIGURE 7.2.: Band structure (solid lines) of non-interacting particles in a periodic lattice potential with a depth of $3E_{\rm rec}$ (A) and $50E_{\rm rec}$(B), respectively. The dashed lines in A indicate the free-space dispersion relation. Particles which initially are prepared in the lowest energy band at zero quasi-momentum are transferred by the non-commensurable probe lattice potential to states with quasi-momentum $\pm 2\hbar k_p$, indicated by the dashed-dotted line (see text).

equally spaced by the single site excitation energy $\hbar\omega_m = 2\sqrt{s}E_{{\rm rec},t}$ (see Figure 7.2A).

7.2.2. Interaction with the probe light

We now consider an atomic ensemble which initially is prepared in the lowest energy band, $n = 0$, at quasi-momentum $q = 0$ of the external lattice potential. Experimentally, this is realized by loading a harmonically trapped condensate into an optical lattice of variable depth. The influence of the cavity probe light on the atomic motion is governed by the additional potential term $\hbar U_0|\alpha|^2\cos^2(k_p x)$. To lowest order, it induces transitions from

the initial state $q = 0$ to the quasi-momentum states $q = \pm 2\hbar k_p$. In the limit of vanishing lattice depth, $s = 0$, atoms are scattered off the probe lattice and transferred into states with kinetic energy $4E_{\mathrm{rec},p}$ (with the probe light recoil energy $E_{\mathrm{rec},p} = \frac{\hbar^2 k_p^2}{2m}$). However, in case of a finite lattice depth, $s \neq 0$, several excitation channels exist according to the merging Band structure (see Figure 7.2).

In order to understand this excitation process in more detail, we calculate the transition probabilities p_n into the lowest three energy bands ($n = 0, 1, 2$)

$$p_n = |\langle \psi_{0,0}(x)| \cos^2(k_p x) |\psi_{n,2\hbar k_p}(x)\rangle|^2 \tag{7.15}$$

as a function of lattice depth s (see Figure 7.3B). As expected from the free matter-wave dispersion, only transitions to the second excited band ($n = 2$) can occur in the uniform case $s = 0$. Increasing the lattice depth renders this excitation channel more and more improbable in favor of transitions to the zeroth order and first excited band. In the limit of a very deep lattice potential, the transition probability to the first excited band vanishes asymptotically, as expected from the scaling behavior of the cavity optomechanical coupling strength in (7.11).

The transition energy spectrum corresponding to excitations into the lowest two excited bands ($n = 1, 2$) is plotted in Figure 7.3B (solid and dashed lines). For deep lattices one recognizes the square root dependence on the lattice depth s, reflecting the harmonic excitation spectrum of a single site.

7.2.3. Measurement of the collective excitation spectrum

In order to experimentally investigate the dispersively coupled BEC-cavity system for variable depth of the confining lattice potential, we prepare a Bose-Einstein condensate of typically 1.2×10^5 atoms in a harmonic dipole trap with trapping frequencies $(\omega_x, \omega_y, \omega_z) = 2\pi \times (220, 48, 202)\,\mathrm{Hz}$. The one-dimensional lattice confinement is provided by a laser beam with wavelength $\lambda_t = 830\,\mathrm{nm}$ which pumps a particular TEM_{00} mode of the high-finesse optical cavity. The relative frequency between laser and cavity resonance is actively controlled via a Pound-Drever-Hall lock (see Chapter 2). After preparing the condensate in the dipole trap, the power of the trapping light is ramped within 50 ms from its initially small value, needed for keeping the relative frequency stabilization, to some variable end value. We experimentally deduce the trapping lattice depth from the light intensity being transmitted through the cavity, taking into account the independently measured transmittivity of the cavity mirrors at $\lambda_t = 830\,\mathrm{nm}$.

To measure the excitation spectrum of the system, we non-adiabatically excite atomic transient oscillations, and continuously monitor the corre-

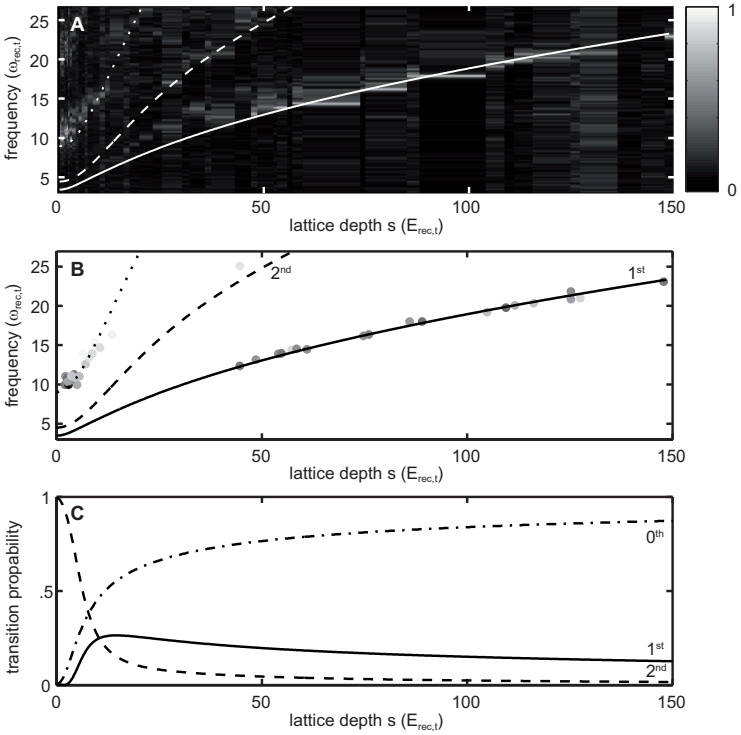

FIGURE 7.3.: Excitation spectrum of the atoms-cavity system. (A) Shown are the Fourier spectra of single frequency scans across the coupled resonance for variable lattice depth (Fourier amplitude increases form black to white). (B) The dots display the frequencies with maximum Fourier amplitude, extracted from the spectra in A. The gray shading indicates the corresponding Fourier amplitude, increasing from white to black. The expected transition frequencies according to the non-interacting band model (see text) are shown by the solid (first excited band) and dashed (second excited band) lines in A and B. The dotted line indicates the doubled transition frequency into the second excited band. The only free parameter in this model is the measured mirror transmittivity, which deviates by 10% from the independently measured value. (C) Transition probabilities p_n from the initial ground state $q = 0$ into the ground (0^{th}), first excited (1^{st}) and second excited (2^{nd}) band as a function of lattice depth (see Equation (7.15)). Transitions to higher excited energy bands are negligible.

sponding dynamical change in cavity resonance. To this end, we probe the cavity resonance frequency with a laser beam which is blue detuned from the atomic D_2 resonance by $\Delta_a = 2\pi \times 58\,\mathrm{GHz}$, while monitoring the transmitted light intensity on a single photon counter. The mean intracavity photon number on resonance is 10 ± 2, which is large compared to the critical photon number where bistability occurs (see Section 5.1). Therefore, transient oscillations are excited while scanning the probe laser frequency across the resonance (see Section 6.4).

From the transmission data we extract the collective oscillation frequencies as a function of lattice depth s (see Figure 7.3A and B). For $s \gtrsim 50$ clear transient oscillations are observed with a frequency that increases with lattice depth, in agreement with the transition energy spectrum into the first excited band (solid curve). In the opposite limit of very shallow lattice potential we observe a rather broad Fourier distribution around twice the expected transition frequency into the second excited band. This refers to probe-induced dipole forces which strongly affect the bare collective atomic oscillations, described by the simple energy band model (see Section 6.4 and the discussion below). From $s = 0$ to about $s = 12$ a clear increase in the oscillation frequency of these driven oscillations can be observed, accompanied by a decrease in Fourier amplitude. This reflects the pronounced drop in the transition probability p_2 into the second excited band (Figure 7.3C). In the intermediate regime, $12 \lesssim s \lesssim 30$, the coupling strengths to the first and second excited band are comparable, which suggests a multi-mode dynamics with the appearance of certain combinations (like e.g. the arithmetic mean) of the bare excitation frequencies. An indication of such dynamics is provided by the hardly visible oscillation branch in between the first and second excited band transition branches (see Figure 7.3A).

7.2.4. Influence of probe light on the collective motion

A direct measurement of the bare excitation spectrum, as presented above, is hindered by the fact that probe-induced dipole forces render atomic motion nonlinear. In the limiting cases in which the atomic collective motion can be described in terms of a single harmonic oscillator, this nonlinearity is expressed by the effective potential V_{opt}, introduced in Section 6.2. From comparing the effective potentials for the two cases $s = 0$ and $s = 80$ (Figure 7.4 A and C), one can expect harmonic oscillations in the uniform case to be much stronger affected by probe light relative to the tightly confined case. Qualitatively, this is in agreement with our observation of well defined oscillation frequencies in the deep lattice situation (Figure 7.4D) compared to the weak lattice case, where the dynamic change of the effective potential

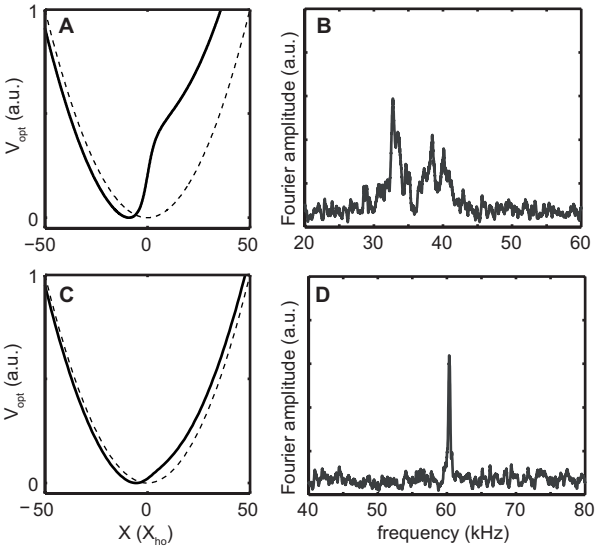

FIGURE 7.4.: Comparison of the optomechanical potentials V_{opt} in the uniform $s = 0$ (A) and the tightly confined situation $s = 80$ (C) for a maximum intracavity photon number of 1.4. The free harmonic potential landscape is indicated by the dashed line. (B and D) Fourier spectra of experimentally obtained photon traces corresponding to situation A and C, respectively (taken from Figure 7.3A).

landscape with probe-cavity detuning results in a varying oscillation frequency around twice the bare harmonic oscillation frequency (Figure 7.4B).

7.3. *In-situ* observation of collective motion

From the above discussion we presume the tightly confined regime to be well suited for continuous observation of quasi-free collective atomic motion via the cavity probe field. For demonstration, we performed resonance scans (like the ones in Figure 7.3) for a lattice depth of $s = 90$ and a maximum intracavity photon number of 4.5 ± 0.9. Non-adiabatically excited transient oscillations modulate the transmitted light intensity as shown in Figure 7.5A. To resolve the dynamics of the system over time, we look at the intensity autocorrelations of the transmitted light, within a moving time

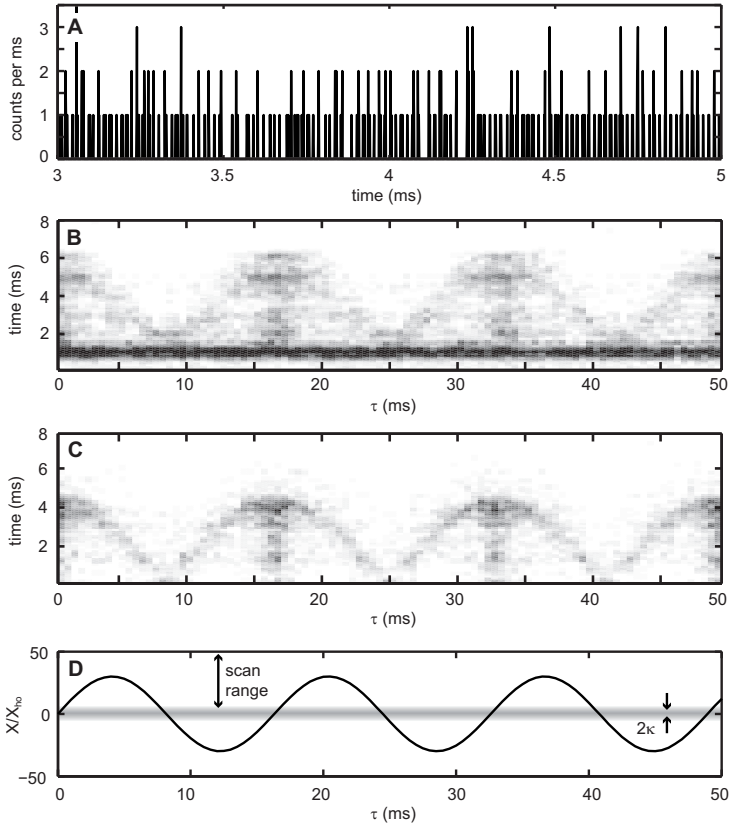

FIGURE 7.5.: Observation of quasi-free collective atomic motion. (A) Shown is a single cavity transmission trace where the probe frequency is scanned across resonance at a speed of $\dot{\Delta}_c = +3\,\mathrm{MHz/ms}$. The maximum intracavity photon number is 1.4 ± 0.3. The probe laser frequency is blue-detuned by $\Delta_a = 2\pi \times 58\,\mathrm{GHz}$ from the atomic resonance. (B) Density plot of local intensity autocorrelations within a moving time window of $200\,\mu\mathrm{s}$ width, deduced from the photon data shown in A. Adjacent windows overlap by $100\,\mu\mathrm{s}$. (C) Intensity autocorrelations (obtained as in B) from numerically generated photon transmission data assuming undamped and harmonic mechanical oscillations as shown in D, taking into account a detection efficiency of 5% and shot noise. The cavity resonance depicted by the gray shaded line was taken to move in X-space across the oscillations region starting at $X = 0$ for $t = 0$.

window of length $T = 200\,\mu$s, as shown in Figure 7.5B. The distinct structure in the autocorrelations (Figure 7.5B) refers to a moving resonance condition caused by scanning the probe laser frequency at a rate of 3 MHz/ms. The transient oscillations are excited about when the probe laser is close to the non-displaced cavity resonance $X = 0$. Correspondingly, the probe laser is in resonance with the coupled system after every half oscillation period (Figure 7.5D). Subsequently, the transmission signal develops am over-period given by the single oscillation frequency until the resonance condition is reached only once per oscillation period.

In order to infer from such *in-situ* measurements about the principle experimental limitations, we compare our data (Figure 7.5B) with a simulation of the expected intensity correlations assuming an undamped harmonic oscillation (Figure 7.5D), including shot-noise and our limited detection efficiency. The qualitative agreement between data and simulations confirms our ability to continuously monitor quasi-free collective atomic motion quite close to the shot-noise limit. Taking into account the optomechanical coupling strength and the speed at which the probe laser frequency was scanned in Figure 7.5A, we conclude about a mechanical oscillation amplitude of about $30x_{\mathrm{ho}}$ (Figure 7.5B).

7.4. Summary

We have investigated the dispersively coupled BEC-cavity system in presence of an underlying periodic trapping potential with variable depth. For tightly confined atoms, this constitutes another realization of cavity optomechanics which offers tunability of the mechanical oscillation frequency. By exciting transient oscillations, we measured the excitation spectrum of the system as a function of lattice depth, and found good agreement with a simple band model. The tightly confined regime was found to be well suited for sensing quasi-free collective oscillations. Future improvements on the signal-to-noise ratio might allow for sensing collective atomic motion close to the quantum limit.

8 Conclusions and outlook

Within the scope of this thesis, the coherent coupling between a Bose-Einstein condensate and the optical field of a small-volume ultrahigh-finesse cavity was experimentally realized for the first time. We investigated the collective interaction between the cavity field and the internal and motional degrees of freedom of a quantum gas both experimentally and theoretically. These experiments are among the first ones [27, 45], which allow to control and sense collective degrees of freedom of ultracold atoms, using coherent optical light fields at the single-photon scale.

Coupling a quantized light field to a single macroscopic matter-wave realizes a novel regime of cavity quantum electrodynamics, where the atom-light coupling strength is highly controllable and identical for all atoms. This situation is described by the Tavis-Cummings model [28], which considers the atomic ensemble as a single quantum system that interacts collectively with the light field. Experimentally, this was confirmed by measuring the energy spectrum of the coupled system, and observing a square-root dependence of the vacuum Rabi splitting on the number of atoms. We developed a theoretical model description of the system which is in very good agreement with our experimental findings.

The large cooperativity inherent in our BEC-cavity system, opens the route to a matter-light interface for quantum information processing or quantum information storage in the atomic internal degrees of freedom. The tremendous control over the external degrees of freedom present in a Bose-Einstein condensate not only reduces motional-induced decoherence effects, but also offers the possibility to efficiently load the atoms into a three-dimensional optical lattice potential. In such a crystalline arrangement, the storage of quantum information, the implementation of local addressability of single qubits via magnetic field gradients, or the coherent cavity-mediated interaction between separated qubits can be envisaged with our experimental setup.

The collective enhancement of the coupling strength between light and the atomic ensemble comes at the expense of the desirable nonlinearity in the excitation number, exhibited by a single two-level system coupled to a single cavity mode. The linear excitation spectrum of our system prevents the study of intrinsic quantum effects, like the generation of non-classical field states, or the implementation of a photon blockade. Possibilities to introduce a nonlinearity at the single-photon level into a collective atoms-cavity system have been discussed in the literature [159, 160, 161], and could be realized by coupling the atomic excited state ($5P_{3/2}$) to a high-lying Rydberg state [162]. Atoms which are excited to the Rydberg state strongly interact via long-ranged dipole-dipole forces. The induced level shifts associated with these interactions prevent the excitation of more than one Rydberg atom within a certain blockade region, which introduces a strong nonlinearity into the excitation spectrum of mesoscopic atomic samples [163]. Providing this nonlinearity exceeds the collective atom-light coupling strength, the atomic ensemble couples like a two-level "super-atom" to the cavity, and the system exhibits a Jaynes-Cummings-type nonlinearity at the single-photon level. Experimentally, we are currently integrating a laser system into our experimental setup for implementing this promising scheme.

In the dispersive regime, the coupled BEC-cavity system allows to manipulate and sense collective motional degrees of freedom of a quantum gas with unprecedented accuracy and – in principle – at the quantum level. The small mode volume of our ultrahigh-finesse cavity results – even at the single photon scale – in large cavity-induced dipole forces. At the same time, single collective density excitations of the atomic ensemble induce a refractive cavity shift on the order of the cavity linewidth, which provides a strong backaction onto the cavity field intensity. Within the scope of this thesis, it was noticed for the first time that this dynamic optical lattice configuration can be mapped onto a cavity optomechanical model system: collective density excitations, matching the cavity mode profile, act like a mechanical element which optomechanically couples to the field intensity. Experimentally, we observed motional-induced optical nonlinearities at the single-photon level. Collective anharmonic density oscillations, triggered by the presence of a few photons in the resonator, have been observed *in-situ* via the transmitted cavity light field. Finally, an additional static lattice potential has been applied, in order to tailor the properties of collective atomic motion, and to tune important system parameters. Our measurements have been compared with quantitative *ab-initio* calculations performed in a mean-field framework. These experiments represent first studies on the interac-

tion between a macroscopic matter-wave and far-detuned light fields at the single-photon scale.

Using collective motional degrees of freedom of an ultracold quantum gas as an optomechanical element [71] opens new possibilities for exploring cavity optomechanics in the quantum regime. The controlled preparation of the mechanical element in its motional ground state, and the ability to tune various system parameters, like the optomechanical coupling strength, the mechanical oscillation frequency, or the oscillator mass over a wide range, make these systems to be well suited for the investigation of harmonic oscillators in the quantum regime or the quantum-to-classical boundary.

The interaction induced entanglement between collective atomic motion and the cavity field offers a novel playground for generating nonclassical motional states, like Schrödinger cat states or squeezed states. As originally proposed in [164], superposition states in the incoming light field could be transferred via the coherent light-matter interaction into a macroscopic superposition of atomic motion. To prevent the intermediate, highly entangled state from decoherence due to cavity field decay, a fast and efficient method for erasing the which-path information of the cavity field is required, which poses challenging limitations on the cavity linewidth [164]. Furthermore, situations can be envisaged where the cavity field induces a strong interaction between motional and electronic degrees of freedom in the quantum gas [165].

A dramatic change in the collective behavior of the coupled BEC-cavity system is caused by – instead of driving the cavity field – directly illuminating the atoms with a far-detuned laser field, which propagates perpendicular to the cavity axis. This induces phase-coherent light scattering by the atoms into the cavity mode at a rate which is enhanced by the Purcell factor [166]. However, due to interference of scatterers, the state of the cavity field crucially depends on the atomic distribution within the resonator mode structure. As was originally proposed by H. Ritsch and P. Domokos [96], and later observed with laser cooled atoms in the group of V. Vuletic [72], this system features – above a certain driving intensity – spontaneous self-organization of the atoms in a checkerboard pattern accompanied by superradiant light scattering. In case of a quantum gas at zero temperature, this phenomenon constitutes a dynamic quantum phase transition from a superfluid phase into a supersolid-type phase, where translational symmetry is spontaneously broken. As we noticed recently, the underlying physics can be shown to be equivalent to the Dicke model which describes an ensemble of two-level atoms interacting with a single light mode. This fundamental model system in quantum optics was shown to exhibit a quantum phase

transition at a critical dipole coupling strength from a normal into a superradiant phase [167, 168]. In experiments currently under progress, we directly observed the formation of the self-organized phase within our BEC-cavity system, by monitoring the cavity light field and detecting a characteristic momentum distribution of the atomic ensemble. Besides its great interest in its own, this result paves the way to use off-resonant light scattering into a high-finesse cavity for a non-demolition detection method of different quantum many-body states and novel phases of ultracold gases [105, 19, 21].

A Physical constants

All physical constants used in this thesis have been published in [169] which can be accessed via `http://physics.nist.gov/constants`.
All data concerning the physical properties of ^{87}Rb have been taken from [92] and can be accessed via `http://steck.us/alkalidata/`.

Bibliography

[1] P. R. Berman (editor). *Cavity Quantum Electrodynamics.* Advances in Atomic, Molecular, and Optical Physics Suppl. 2 (Academic Press, San Diego, 1994).

[2] S. Haroche and J. M. Raimond. *Exploring the Quantum* (Oxford University Press, Oxford, 2006).

[3] M. Brune, F. Schmidt Kaler, A. Maali, J. Dreyer, E. Hagley, J. M. Raimond, and S. Haroche. 'Quantum Rabi oscillation: A direct test of field quantization in a cavity'. *Phys. Rev. Lett.* **76**(11), 1800–1803 (1996).

[4] K. M. Birnbaum, A. Boca, R. Miller, A. D. Boozer, T. E. Northup, and H. J. Kimble. 'Photon blockade in an optical cavity with one trapped atom'. *Nature* **436**(7047), 87–90 (2005).

[5] C. Guerlin, J. Bernu, S. Deleglise, C. Sayrin, S. Gleyzes, S. Kuhr, M. Brune, J.-M. Raimond, and S. Haroche. 'Progressive field-state collapse and quantum non-demolition photon counting'. *Nature* **448**(7156), 889–893 (2007).

[6] D. I. Schuster, A. A. Houck, J. A. Schreier, A. Wallraff, J. M. Gambetta, A. Blais, L. Frunzio, J. Majer, B. Johnson, M. H. Devoret, S. M. Girvin, and R. J. Schoelkopf. 'Resolving photon number states in a superconducting circuit'. *Nature* **445**(7127), 515–518 (2007).

[7] I. Schuster, A. Kubanek, A. Fuhrmanek, T. Puppe, P. W. H. Pinkse, K. Murr, and G. Rempe. 'Nonlinear spectroscopy of photons bound to one atom'. *Nat Phys* **4**(5), 382–385 (2008).

[8] 'Nature Insight on Ultracold Matter'. *Nature* **416**, 205 (2002).

[9] W. Ketterle, D. S. Durfee, and D. M. Stamper Kurn. 'Making, probing and understanding Bose-Einstein condensates'. In *Bose-Einstein Condensation in Atomic Gases*, edited by M. Inguscio, S. Stringari, and C. Wieman, volume CXL of *Proceedings of the International School of Physics Enrico Fermi*, pp. 67–176 (IOS Press, Amsterdam, 1999).

[10] M. R. Andrews, D. M. Kurn, H.-J. Miesner, D. S. Durfee, C. G. Townsend, S. Inouye, and W. Ketterle. 'Propagation of Sound in a Bose-Einstein Condensate'. *Phys. Rev. Lett.* **79**(4), 553–556 (1997). Erratum: Phys. Rev. Lett. 80, 2967 (1998).

[11] J. Stenger, S. Inouye, A. P. Chikkatur, D. M. Stamper Kurn, D. E. Pritchard, and W. Ketterle. 'Bragg Spectroscopy of a Bose-Einstein Condensate'. *Phys. Rev. Lett.* **82**(23), 4569–4573 (1999). Erratum: Phys. Rev. Lett. 84, 2283(E) (2000).

[12] D. M. Stamper Kurn, M. R. Andrews, A. P. Chikkatur, S. Inouye, H.-J. Miesner, J. Stenger, and W. Ketterle. 'Optical Confinement of a Bose-Einstein Condensate'. *Phys. Rev. Lett.* **80**(10), 2027–2030 (1998).

[13] M. Kozuma, L. Deng, E. W. Hagley, J. Wen, R. Lutwak, K. Helmerson, S. L. Rolston, and W. D. Phillips. 'Coherent Splitting of Bose-Einstein Condensed Atoms with Optically Induced Bragg Diffraction'. *Phys. Rev. Lett.* **82**(5), 871–875 (1999).

[14] Y. B. Ovchinnikov, J. H. Müller, M. R. Doery, E. J. D. Vredenbregt, K. Helmerson, S. L. Rolston, and W. D. Phillips. 'Diffraction of a Released Bose-Einstein Condensate by a Pulsed Standing Light Wave'. *Phys. Rev. Lett.* **83**(2), 284– (1999).

[15] J. Stenger, S. Inouye, D. Stamper Kurn, A. Chikkatur, D. Pritchard, and W. Ketterle. 'Bragg spectroscopy and superradiant Rayleigh scattering in a Bose-Einstein condensate'. *Appl. Phys. B* **69**(5 - 6), 347–352 (1999).

[16] B. P. Anderson and M. A. Kasevich. 'Macroscopic Quantum Interference from Atomic Tunnel Arrays'. *Science* **282**(5394), 1686–1689 (1998).

[17] M. Greiner, O. Mandel, T. Esslinger, T. W. Hänsch, and I. Bloch. 'Quantum phase transition from a superfluid to a Mott insulator in a gas of ultracold atoms'. *Nature* **415**(6867), 39–44 (2002).

[18] H. Zoubi and H. Ritsch. 'Exciton-polariton scattering as signature of defects in cold atom optical lattices'. *New Journal of Physics* (2), 023001 (2008).

[19] I. B. Mekhov and H. Ritsch. 'Quantum Nondemolition Measurements and State Preparation in Quantum Gases by Light Detection'. *Phys. Rev. Lett.* **102**(2), 020403–4 (2009).

[20] I. Mekhov and H. Ritsch. 'Quantum optics with quantum gases'. *Laser Physics* **19**(4), 610–615 (2009).

[21] L. Guo, S. Chen, B. Frigan, L. You, and Y. Zhang. 'Cavity-enhanced detection of magnetic order in lattice spin models'. *Phys. Rev. A* **79**(1), 013630–5 (2009).

[22] J. Larson, B. Damski, G. Morigi, and M. Lewenstein. 'Mott-Insulator States of Ultracold Atoms in Optical Resonators'. *Phys. Rev. Lett.* **100**(5), 050401–4 (2008).

[23] D. Nagy, G. Szirmai, and P. Domokos. 'Self-organization of a Bose-Einstein condensate in an optical cavity'. *The European Physical Journal D* **48**(1), 127–137 (2008).

[24] M. J. Bhaseen, M. Hohenadler, A. O. Silver, and B. D. Simons. 'Polaritons and Pairing Phenomena in Bose-Hubbard Mixtures'. *Phys. Rev. Lett.* **102**(13), 135301–4 (2009).

[25] J. Larson and M. Lewenstein. 'Dilute gas of ultracold two-level atoms inside a cavity: generalized Dicke model'. *New Journal of Physics* (6), 063027 (2009).

[26] S. Gupta, K. L. Moore, K. W. Murch, and D. M. Stamper Kurn. 'Cavity Nonlinear Optics at Low Photon Numbers from Collective Atomic Motion'. *Phys. Rev. Lett.* **99**(21), 213601 (2007).

[27] Y. Colombe, T. Steinmetz, G. Dubois, F. Linke, D. Hunger, and J. Reichel. 'Strong atom-field coupling for Bose-Einstein condensates in an optical cavity on a chip'. *Nature* **450**(7167), 272–276 (2007).

[28] M. Tavis and F. W. Cummings. 'Exact Solution for an N-Molecule Radiation-Field Hamiltonian'. *Phys. Rev.* **170**(2), 379–384 (1968).

[29] D. W. Vernooy and H. J. Kimble. 'Well-dressed states for wave-packet dynamics in cavity QED'. *Phys. Rev. A* **56**(5), 4287– (1997).

[30] A. C. Doherty, A. S. Parkins, S. M. Tan, and D. F. Walls. 'Motion of a two-level atom in an optical cavity'. *Phys. Rev. A* **56**(1), 833 (1997).

[31] P. Horak, S. M. Barnett, and H. Ritsch. 'Coherent dynamics of Bose-Einstein condensates in high-finesse optical cavities'. *Phys. Rev. A* **61**(3), 033609 (2000).

[32] T. Kippenberg, A. Tchebotareva, J. Kalkman, A. Polman, and K. Vahala. 'Purcell factor reduced scattering losses in optical microcavities'. In *Quantum Electronics Conference, 2005. EQEC '05. European*, pp. 358– (2005).

[33] T. Pellizzari, S. A. Gardiner, J. I. Cirac, and P. Zoller. 'Decoherence, Continuous Observation, and Quantum Computing: A Cavity QED Model'. *Phys. Rev. Lett.* **75**(21), 3788 (1995).

[34] L.-M. Duan, M. D. Lukin, J. I. Cirac, and P. Zoller. 'Long-distance quantum communication with atomic ensembles and linear optics'. *Nature* **414**(6862), 413–418 (2001).

[35] J. I. Cirac, P. Zoller, H. J. Kimble, and H. Mabuchi. 'Quantum State Transfer and Entanglement Distribution among Distant Nodes in a Quantum Network'. *Phys. Rev. Lett.* **78**(16), 3221–3224 (1997).

[36] S. J. van Enk, H. J. Kimble, and H. Mabuchi. 'Quantum Information Processing in Cavity-QED'. *Quantum Information Processing* **3**(1), 75–90 (2004).

[37] H. Mabuchi and A. C. Doherty. 'Cavity Quantum Electrodynamics: Coherence in Context'. *Science* **298**(5597), 1372–1377 (2002).

[38] H. Walther. 'Quantum phenomena of single atoms'. *Adv. Chem. Phys.* **122**, 167–197 (2002).

[39] J. M. Raimond, M. Brune, and S. Haroche. 'Colloquium: Manipulating quantum entanglement with atoms and photons in a cavity'. *Rev. Mod. Phys.* **73**(3), 565 (2001).

[40] H. J. Kimble. 'Strong interactions of single atoms and photons in cavity QED'. *Physica Scripta* **T76**, 127–137 (1998).

[41] G. Khitrova, H. M. Gibbs, M. Kira, S. W. Koch, and A. Scherer. 'Vacuum Rabi splitting in semiconductors'. *Nat Phys* **2**(2), 81–90 (2006).

[42] A. Wallraff, D. I. Schuster, A. Blais, L. Frunzio, R.-S. Huang, J. Majer, S. Kumar, S. M. Girvin, and R. J. Schoelkopf. 'Strong coupling of a single photon to a superconducting qubit using circuit quantum electrodynamics'. *Nature* **431**, 162–167 (2004).

[43] P. Maunz, T. Puppe, I. Schuster, N. Syassen, P. W. H. Pinkse, and G. Rempe. 'Cavity cooling of a single atom'. *Nature* **428**(6978), 50–52 (2004).

[44] A. D. Boozer, A. Boca, R. Miller, T. E. Northup, and H. J. Kimble. 'Cooling to the Ground State of Axial Motion for One Atom Strongly Coupled to an Optical Cavity'. *Phys. Rev. Lett.* **97**(8), 083602 (2006).

[45] K. W. Murch, K. L. Moore, S. Gupta, and D. M. Stamper-Kurn. 'Observation of quantum-measurement backaction with an ultracold atomic gas'. *Nature Physics* **4**, 561 (2008).

[46] A. Öttl, S. Ritter, M. Köhl, and T. Esslinger. 'Correlations and Counting Statistics of an Atom Laser'. *Phys. Rev. Lett.* **95**(9), 090404 (2005).

[47] S. Slama, S. Bux, G. Krenz, C. Zimmermann, and P. W. Courteille. 'Superradiant Rayleigh Scattering and Collective Atomic Recoil Lasing in a Ring Cavity'. *Phys. Rev. Lett.* **98**(5), 053603 (2007).

[48] P. F. Herskind, A. Dantan, J. P. Marler, M. Albert, and M. Drewsen. 'Realization of collective strong coupling with ion Coulomb crystals in an optical cavity'. *Nat Phys* **5**(7), 494–498 (2009).

[49] R. H. Dicke. 'Coherence in Spontaneous Radiation Processes'. *Phys. Rev.* **93**(1), 99–110 (1954).

[50] Sherson J., Julsgaard B., and Polzik E.S. 'Deterministic atom-light quantum interface'. *Adv. At. Mol. Opt. Phys.* **54**, 81–130 (2006).

[51] T. H. Maiman. 'Stimulated Optical Radiation in Ruby'. *Nature (London)* **187**(4736), 493–494 (1960).

[52] A. Ashkin. 'Acceleration and Trapping of Particles by Radiation Pressure'. *Phys. Rev. Lett.* **24**(4), 156– (1970).

[53] D. G. Grier. 'A revolution in optical manipulation'. *Nat Photon* **424**(6950), 810–816 (2003).

[54] T. Hänsch and A. Schawlow. 'Cooling of gases by laser radiation'. *Optics Communications* **13**(1), 68–69 (1975).

[55] S. Chu, J. E. Bjorkholm, A. Ashkin, and A. Cable. 'Experimental observation of optically trapped atoms'. *Phys. Rev. Lett.* **57**(3), 314–317 (1986).

[56] Rudolf Grimm, Matthias Weidemüller, and Yurii B. Ovchinnikov. 'Optical dipole traps for neutral atoms'. *Adv. At. Mol. Opt. Phys.* **Vol. 42**, 95–170 (2000).

[57] I. Bloch. 'Ultracold quantum gases in optical lattices'. *Nat Phys* **1**(1), 23–30 (2005).

[58] G. Birkl, M. Gatzke, I. H. Deutsch, S. L. Rolston, and W. D. Phillips. 'Bragg Scattering from Atoms in Optical Lattices'. *Phys. Rev. Lett.* **75**(15), 2823– (1995).

[59] M. Weidemüller, A. Görlitz, T. W. Hänsch, and A. Hemmerich. 'Local and global properties of light-bound atomic lattices investigated by Bragg diffraction'. *Phys. Rev. A* **58**(6), 4647– (1998).

[60] T. J. Kippenberg and K. J. Vahala. 'Cavity Opto-Mechanics'. *Opt. Express* **15**(25), 17172–17205 (2007).

[61] V. B. Braginsky and A. B. Manukin. *Measurement of weak forces in physics experiments* (University of Chicago Press, 1977).

[62] C. Hohberger, C. Hohberger, and K. Karrai. 'Self-oscillation of micromechanical resonators'. In *Nanotechnology, 2004. 4th IEEE Conference on*, edited by K. Karrai, pp. 419–421 (2004).

[63] A. Schliesser, P. Del'Haye, N. Nooshi, K. J. Vahala, and T. J. Kippenberg. 'Radiation Pressure Cooling of a Micromechanical Oscillator Using Dynamical Backaction'. *Phys. Rev. Lett.* **97**(24), 243905 (2006).

[64] O. Arcizet, P.-F. Cohadon, T. Briant, M. Pinard, and A. Heidmann. 'Radiation-pressure cooling and optomechanical instability of a micromirror'. *Nature* **444**(7115), 71–74 (2006).

[65] S. Gigan, H. R. Böhm, M. Paternostro, F. Blaser, G. Langer, J. B. Hertzberg, K. C. Schwab, D. Bäuerle, M. Aspelmeyer, and A. Zeilinger. 'Self-cooling of a micromirror by radiation pressure'. *Nature* **444**(7115), 67–70 (2006).

[66] T. Corbitt, Y. Chen, E. Innerhofer, H. Müller Ebhardt, D. Ottaway, H. Rehbein, D. Sigg, S. Whitcomb, C. Wipf, and N. Mavalvala. 'An

All-Optical Trap for a Gram-Scale Mirror'. *Phys. Rev. Lett.* **98**(15), 150802 (2007).

[67] J. D. Thompson, B. M. Zwickl, A. M. Jayich, F. Marquardt, S. M. Girvin, and J. G. E. Harris. 'Strong dispersive coupling of a high-finesse cavity to a micromechanical membrane'. *Nature* **452**(7183), 72–75 (2008).

[68] S. Groblacher, J. B. Hertzberg, M. R. Vanner, G. D. Cole, S. Gigan, K. C. Schwab, and M. Aspelmeyer. 'Demonstration of an ultracold micro-optomechanical oscillator in a cryogenic cavity'. *Nat Phys* **5**(7), 485–488 (2009).

[69] A. Schliesser, R. Rivière, O. Arcizet, and T. J. Kippenberg. 'Cooling and Measurement of a Micromechanical Oscillator Close to the Quantum Limit'. In *OSA Technical Digest (CD)*, pp. IFD1– (Optical Society of America, 2009).

[70] T. J. Kippenberg and K. J. Vahala. 'Cavity Optomechanics: Back-Action at the Mesoscale'. *Science* **321**(5893), 1172–1176 (2008).

[71] T. Botter, D. Brooks, S. Gupta, Z.-Y. Ma, K. Moore, K. Murch, T. Purdy, and D. Stamper Kurn. 'Quantum micro-mechanics with ultracold atoms'. *ArXiv e-prints* (2008). 0810.3841.

[72] A. T. Black, H. W. Chan, and V. Vuletić. 'Observation of Collective Friction Forces due to Spatial Self-Organization of Atoms: From Rayleigh to Bragg Scattering'. *Phys. Rev. Lett.* **91**(20), 203001 (2003).

[73] H. W. Chan, A. T. Black, and V. Vuletić. 'Observation of Collective-Emission-Induced Cooling of Atoms in an Optical Cavity'. *Phys. Rev. Lett.* **90**(6), 063003 (2003).

[74] B. Nagorny, Th. Elsässer, and A. Hemmerich. 'Collective Atomic Motion in an Optical Lattice Formed Inside a High Finesse Cavity'. *Phys. Rev. Lett.* **91**(15), 153003 (2003).

[75] P. W. H. Pinkse, T. Fischer, P. Maunz, and G. Rempe. 'Trapping an atom with single photons'. *Nature* **404**(6776), 365–368 (2000).

[76] C. J. Hood, T. W. Lynn, A. C. Doherty, A. S. Parkins, and H. J. Kimble. 'The Atom-Cavity Microscope: Single Atoms Bound in Orbit by Single Photons'. *Science* **287**(5457), 1447–1453 (2000).

[77] A. Öttl, S. Ritter, M. Köhl, and T. Esslinger. 'Hybrid apparatus for Bose-Einstein condensation and cavity quantum electrodynamics: Single atom detection in quantum degenerate gases'. *Rev. Sci. Instrum.* **77**, 063118 (2006).

[78] T. Bourdel, T. Donner, S. Ritter, A. Öttl, M. Köhl, and T. Esslinger. 'Cavity QED detection of interfering matter waves'. *Phys. Rev. A* **73**(4), 043602 (2006).

[79] S. Ritter, A. Öttl, T. Donner, T. Bourdel, M. Köhl, and T. Esslinger. 'Observing the Formation of Long-Range Order during Bose-Einstein Condensation'. *Phys. Rev. Lett.* **98**(9), 090402 (2007).

[80] T. Donner, S. Ritter, T. Bourdel, A. Öttl, M. Kohl, and T. Esslinger. 'Critical Behavior of a Trapped Interacting Bose Gas'. *Science* **315**(5818), 1556–1558 (2007).

[81] A. Öttl. 'Correlations and Counting Statistics of an Atom Laser'. Ph.D. thesis, ETH Zürich (2006).

[82] S. Ritter. 'Probing Coherence During Bose-Einstein Condensation'. Ph.D. thesis, ETH Zürich (2007).

[83] T. Donner. 'Critical Behavior of a Trapped Interacting Bose Gas'. Ph.D. thesis, ETH Zürich (2008).

[84] T. Stöferle. 'Exploring Atomic Quantum Gases in Optical Lattices'. Ph.D. thesis, ETH Zürich (2005).

[85] J. Fortágh, A. Grossmann, T. W. Hänsch, and C. Zimmermann. 'Fast loading of a magneto-optical trap from a pulsed thermal source'. *J. Appl. Phys.* **84**(12), 6499–6501 (1998).

[86] M. Greiner, I. Bloch, T. W. Hänsch, and T. Esslinger. 'Magnetic transport of trapped cold atoms over a large distance'. *Phys. Rev. A* **63**(3), 031401 (2001).

[87] T. Esslinger, I. Bloch, and T. W. Hänsch. 'Bose-Einstein condensation in a quadrupole-Ioffe-configuration trap'. *Phys. Rev. A* **58**(4), R2664–R2667 (1998).

[88] H. Kogelnik and T. Li. 'Laser beams and resonators'. *Appl. Opt.* **5**(10), 1550–1567 (1966).

[89] O. Svelto and D. C. Hanna. *Principles of Lasers* (Plenum Press, 1998), 4th edition.

[90] R. W. P. Drever, J. L. Hall, F. V. Kowalski, J. Hough, G. M. Ford, A. J. Munley, and H. Ward. 'Laser phase and frequency stabilization using an optical resonator'. *Appl. Phys. B* **31**(2), 97–105 (1983).

[91] H. Mabuchi, J. Ye, and H. Kimble. 'Full observation of single-atom dynamics in cavity QED'. *Appl. Phys. B* **68**(6), 1095–1108 (1999).

[92] D. A. Steck. arXiv: (2008). Revision 2.0.1, `http://steck.us/alkalidata`.

[93] S. Kuhr, W. Alt, D. Schrader, M. Muller, V. Gomer, and D. Meschede. 'Deterministic Delivery of a Single Atom'. *Science* **293**(5528), 278–280 (2001).

[94] J. A. Sauer, K. M. Fortier, M. S. Chang, C. D. Hamley, and M. S. Chapman. 'Cavity QED with optically transported atoms'. *Phys. Rev. A* **69**(5), 051804 (2004).

[95] R. Jördens. 'A Radio Frequency Source for the Preparation of Quantum States'. Master's thesis, ETH Zürich (2006).

[96] P. Domokos and H. Ritsch. 'Collective Cooling and Self-Organization of Atoms in a Cavity'. *Phys. Rev. Lett.* **89**(25), 253003 (2002).

[97] S. Nußmann, K. Murr, M. Hijlkema, B. Weber, A. Kuhn, and G. Rempe. 'Vacuum-stimulated cooling of single atoms in three dimensions'. *Nat. Phys.* **1**(2), 122–125 (2005).

[98] M. H. Anderson, J. R. Ensher, M. R. Matthews, C. E. Wieman, and E. A. Cornell. 'Observation of Bose-Einstein Condensation in a Dilute Atomic Vapor'. *Science* **269**, 198–201 (1995).

[99] M. Lewenstein, A. Kubasiak, J. Larson, C. Menotti, C. Morigi, K. Osterloh, and A. Sanpera. 'Travelling to exotic places with ultracold atoms'. In *Atomic Physics 20*, edited by C. Roos, H. Häffner, and R. Blatt, volume 869 of *XX International Conference on Atomic Physics; ICAP 2006*, pp. 201–211 (American Institute of Physics, 2006).

[100] F. Brennecke, T. Donner, S. Ritter, T. Bourdel, M. Köhl, and T. Esslinger. 'Cavity QED with a Bose-Einstein condensate'. *Nature* **450**(7167), 268–271 (2007).

[101] E. Jaynes and F. Cummings. 'Comparison of quantum and semiclassical radiation theories with application to the beam maser'. *Proc. IEEE* **51**(1), 89–109 (1963).

[102] S. Leslie, N. Shenvi, K. R. Brown, D. M. Stamper Kurn, and K. B. Whaley. 'Transmission spectrum of an optical cavity containing N atoms'. *Phys. Rev. A* **69**(4), 043805 (2004).

[103] M. G. Raizen, R. J. Thompson, R. J. Brecha, H. J. Kimble, and H. J. Carmichael. 'Normal-mode splitting and linewidth averaging for two-state atoms in an optical cavity'. *Phys. Rev. Lett.* **63**(3), 240–243 (1989).

[104] A. K. Tuchman, R. Long, G. Vrijsen, J. Boudet, J. Lee, and M. A. Kasevich. 'Normal-mode splitting with large collective cooperativity'. *Phys. Rev. A* **74**(5), 053821–4 (2006).

[105] I. B. Mekhov, C. Maschler, and H. Ritsch. 'Probing quantum phases of ultracold atoms in optical lattices by transmission spectra in cavity quantum electrodynamics'. *Nat. Phys.* **3**, 319–323 (2007).

[106] B. W. Shore and P. L. Knight. 'The Jaynes-Cummings Model'. *J. Mod. Optics* **40**(7), 1195–1238 (1993).

[107] J. M. Fink, R. Bianchetti, M. Baur, M. Goppl, L. Steffen, S. Filipp, P. J. Leek, A. Blais, and A. Wallraff. 'Dressed Collective Qubit States and the Tavis-Cummings Model in Circuit QED'. *Phys. Rev. Lett.* **103**(8), 083601–4 (2009).

[108] J. M. Fink, M. Goppl, M. Baur, R. Bianchetti, P. J. Leek, A. Blais, and A. Wallraff. 'Climbing the Jaynes-Cummings ladder and observing its nonlinearity in a cavity QED system'. *Nature* **454**(7202), 315–318 (2008).

[109] G. Rempe, H. Walther, and N. Klein. 'Observation of quantum collapse and revival in a one-atom maser'. *Phys. Rev. Lett.* **58**(4), 353–356 (1987).

[110] M. G. Moore, O. Zobay, and P. Meystre. 'Quantum optics of a Bose-Einstein condensate coupled to a quantized light field'. *Phys. Rev. A* **60**(2), 1491–1506 (1999).

[111] L. Pitaevskii and S. Stringari. *Bose-Einstein Condensation* (Oxford University Press, Oxford, 2003).

[112] H. J. Carmichael. *An Open Systems Approach to Quantum Optics.* Lecture Notes in Physics, New Series M (Springer, Berlin, 1993).

[113] R. J. Thompson, Q. A. Turchette, O. Carnal, and H. J. Kimble. 'Nonlinear spectroscopy in the strong-coupling regime of cavity QED'. *Phys. Rev. A* **57**(4), 3084–3104 (1998).

[114] K. M. Birnbaum, A. S. Parkins, and H. J. Kimble. 'Cavity QED with multiple hyperfine levels'. *Phys. Rev. A* **74**(6), 063802 (2006).

[115] D. Meiser and P. Meystre. 'Superstrong coupling regime of cavity quantum electrodynamics'. *Phys. Rev. A* **74**(6), 065801 (2006).

[116] C. J. Pethick and H. Smith. *Bose-Einstein Condensation in Dilute Gases* (Cambridge University Press, 2002).

[117] I. B. Mekhov, C. Maschler, and H. Ritsch. 'Cavity-Enhanced Light Scattering in Optical Lattices to Probe Atomic Quantum Statistics'. *Phys. Rev. Lett.* **98**(10), 100402–4 (2007).

[118] G. Hechenblaikner, M. Gangl, P. Horak, and H. Ritsch. 'Cooling an atom in a weakly driven high-Q cavity'. *Phys. Rev. A* **58**(4), 3030 (1998).

[119] A. J. Daley, P. O. Fedichev, and P. Zoller. 'Single-atom cooling by superfluid immersion: A nondestructive method for qubits'. *Phys. Rev. A* **69**(2), 022306 (2004).

[120] F. Brennecke, S. Ritter, T. Donner, and T. Esslinger. 'Cavity Optomechanics with a Bose-Einstein Condensate'. *Science* **322**(5899), 235–238 (2008).

[121] M. Lewenstein, A. Sanpera, V. Ahufinger, B. Damski, A. Sen, and U. Sen. 'Ultracold atomic gases in optical lattices: mimicking condensed matter physics and beyond'. *Advances in Physics* **56**(2), 243–379 (2007).

[122] V. B. Braginsky, Y. I. Vorontsov, and K. S. Thorne. 'Quantum Nondemolition Measurements'. *Science* **209**(4456), 547–557 (1980).

[123] O. Arcizet, P.-F. Cohadon, T. Briant, M. Pinard, A. Heidmann, J.-M. Mackowski, C. Michel, L. Pinard, O. Francais, and L. Rousseau. 'High-Sensitivity Optical Monitoring of a Micromechanical Resonator with a Quantum-Limited Optomechanical Sensor'. *Phys. Rev. Lett.* **97**(13), 133601 (2006).

[124] V. B. Braginsky. 'Development of quantum measurement methods (Methodological notes on part of Einstein's scientific legacy)'. *Physics-Uspekhi* **48**(6), 595–600 (2005).

[125] D. Kleckner and D. Bouwmeester. 'Sub-kelvin optical cooling of a micromechanical resonator'. *Nature* **444**(7115), 75–78 (2006).

[126] T. J. Kippenberg, H. Rokhsari, T. Carmon, A. Scherer, and K. J. Vahala. 'Analysis of Radiation-Pressure Induced Mechanical Oscillation of an Optical Microcavity'. *Phys. Rev. Lett.* **95**(3), 033901 (2005).

[127] A. Naik, O. Buu, M. D. LaHaye, A. D. Armour, A. A. Clerk, M. P. Blencowe, and K. C. Schwab. 'Cooling a nanomechanical resonator with quantum back-action'. *Nature* **443**(7108), 193–196 (2006).

[128] J. D. Teufel, J. W. Harlow, C. A. Regal, and K. W. Lehnert. 'Dynamical Backaction of Microwave Fields on a Nanomechanical Oscillator'. *Phys. Rev. Lett.* **101**(19), 197203–4 (2008).

[129] A. Dorsel, J. D. McCullen, P. Meystre, E. Vignes, and H. Walther. 'Optical Bistability and Mirror Confinement Induced by Radiation Pressure'. *Phys. Rev. Lett.* **51**(17), 1550 (1983).

[130] B. S. Sheard, M. B. Gray, C. M. Mow Lowry, D. E. McClelland, and S. E. Whitcomb. 'Observation and characterization of an optical spring'. *Phys. Rev. A* **69**(5), 051801– (2004).

[131] F. Marquardt, J. P. Chen, A. A. Clerk, and S. M. Girvin. 'Quantum Theory of Cavity-Assisted Sideband Cooling of Mechanical Motion'. *Phys. Rev. Lett.* **99**(9), 09390 (2007).

[132] C. Höhberger Metzger and K. Karrai. 'Cavity cooling of a microlever'. *Nature* **432**(7020), 1002–1005 (2004).

[133] S. Mancini, V. I. Man'ko, and P. Tombesi. 'Ponderomotive control of quantum macroscopic coherence'. *Phys. Rev. A* **55**(4), 3042 (1997).

[134] W. Marshall, C. Simon, R. Penrose, and D. Bouwmeester. 'Towards Quantum Superpositions of a Mirror'. *Phys. Rev. Lett.* **91**(13), 130401 (2003).

[135] Peter Domokos and Helmut Ritsch. 'Mechanical effects of light in optical resonators'. *J. Opt. Soc. Am. B* **20**(5), 1098–1130 (2003).

[136] A. C. Doherty, A. S. Parkins, S. M. Tan, and D. F. Walls. 'Motional states of atoms in cavity QED'. *Phys. Rev. A* **57**(6), 4804 (1998).

[137] C. Maschler, I. B. Mekhov, and H. Ritsch. 'Ultracold atoms in optical lattices generated by quantized light fields'. *The European Physical Journal D* **46**(3), 545–560 (2008).

[138] M. Ludwig, B. Kubala, and F. Marquardt. 'The optomechanical instability in the quantum regime' (2008). (available at http://arxiv.org/abs/0803.3714).

[139] N. Bogoliubov. 'On the theory of superfluidity'. *J. Phys. (USSR)* **11**, 23 (1947).

[140] G. K. Campbell, A. E. Leanhardt, J. Mun, M. Boyd, E. W. Streed, W. Ketterle, and D. E. Pritchard. 'Photon Recoil Momentum in Dispersive Media'. *Phys. Rev. Lett.* **94**(17), 170403–4 (2005).

[141] J. Schneider and A. Schenzle. 'Investigations of a two-mode atom-laser model'. *Phys. Rev. A* **61**(5), 053611 (2000).

[142] E. Abraham and S. D. Smith. 'Optical bistability and related devices'. *Reports on Progress in Physics* **45**(8), 815–885 (1982).

[143] R. W. Boyd. *Nonlinear Optics* (Academic Press, Boston, 2008).

[144] L. A. Lugiato. 'Theory of optical bistability'. In *Progress in optics. Volume 21. Amsterdam, North-Holland Physics Publishing*, pp. 69–216 (1984).

[145] R. Bonifacio and L. A. Lugiato. 'Optical bistability and cooperative effects in resonance fluorescence'. *Phys. Rev. A* **18**(3), 1129– (1978).

[146] G. Rempe, R. J. Thompson, R. J. Brecha, W. D. Lee, and H. J. Kimble. 'Optical bistability and photon statistics in cavity quantum electrodynamics'. *Phys. Rev. Lett.* **67**(13), 1727–1730 (1991).

[147] J. Gripp, S. L. Mielke, L. A. Orozco, and H. J. Carmichael. 'Anharmonicity of the vacuum Rabi peaks in a many-atom system'. *Phys. Rev. A* **54**(5), R3746– (1996).

[148] S. Ritter, F. Brennecke, C. Guerlin, K. Baumann, T. Donner, and T. Esslinger. 'Dynamical Coupling between a Bose-Einstein Condensate and a Cavity Optical Lattice'. *Appl. Phys. B* **95**, 213 (2009).

[149] C. Fabre, M. Pinard, S. Bourzeix, A. Heidmann, E. Giacobino, and S. Reynaud. 'Quantum-noise reduction using a cavity with a movable mirror'. *Phys. Rev. A* **49**(2), 1337– (1994).

[150] C. Maschler and H. Ritsch. 'Cold Atom Dynamics in a Quantum Optical Lattice Potential'. *Phys. Rev. Lett.* **95**(26), 260401 (2005).

[151] S. Mancini and P. Tombesi. 'Quantum noise reduction by radiation pressure'. *Phys. Rev. A* **49**(5), 4055 (1994).

[152] D. Diakonov, L. M. Jensen, C. J. Pethick, and H. Smith. 'Loop structure of the lowest Bloch band for a Bose-Einstein condensate'. *Phys. Rev. A* **66**(1), 013604– (2002).

[153] B. Wu and Q. Niu. 'Nonlinear Landau-Zener tunneling'. *Phys. Rev. A* **61**(2), 023402– (2000).

[154] F. L. Moore, J. C. Robinson, C. F. Bharucha, B. Sundaram, and M. G. Raizen. 'Atom Optics Realization of the Quantum delta -Kicked Rotor'. *Phys. Rev. Lett.* **75**(25), 4598– (1995).

[155] P. Horak and H. Ritsch. 'Dissipative dynamics of Bose condensates in optical cavities'. *Phys. Rev. A* **63**(2), 023603 (2001).

[156] K. Murch. 'Cavity Quantum Optomechanics with Ultracold Atoms'. Ph.D. thesis, University of California, Berkeley (2008).

[157] O. Morsch and M. Oberthaler. 'Dynamics of Bose-Einstein condensates in optical lattices'. *Rev. Mod. Phys.* **78**(1), 179–37 (2006).

[158] F. Bloch. 'Über die Quantenmechanik der Elektronen in Kristallgittern'. *Z. Phys.* **52**, 555 (1928).

[159] M. D. Lukin, M. Fleischhauer, R. Cote, L. M. Duan, D. Jaksch, J. I. Cirac, and P. Zoller. 'Dipole Blockade and Quantum Information Processing in Mesoscopic Atomic Ensembles'. *Phys. Rev. Lett.* **87**(3), 037901 (2001).

[160] A. Imamoglu. 'Cavity QED Based on Collective Magnetic Dipole Coupling: Spin Ensembles as Hybrid Two-Level Systems'. *Phys. Rev. Lett.* **102**(8), 083602–4 (2009).

[161] J. Verdu, H. Zoubi, C. Koller, J. Majer, H. Ritsch, and J. Schmiedmayer. 'Strong Magnetic Coupling of an Ultracold Gas to a Superconducting Waveguide Cavity'. *Phys. Rev. Lett.* **103**(4), 043603–4 (2009).

[162] T. F. Gallagher. *Rydberg Atoms* (Cambridge Univ. Press, Cambridge, 1984).

[163] T. Vogt, M. Viteau, A. Chotia, J. Zhao, D. Comparat, and P. Pillet. 'Electric-Field Induced Dipole Blockade with Rydberg Atoms'. *Phys. Rev. Lett.* **99**(7), 073002–4 (2007).

[164] P. Horak and H. Ritsch. 'Manipulating a Bose-Einstein condensate with a single photon'. *Eur. Phys. J. D* **13**, 279–287 (2001).

[165] K. Hammerer, M. Wallquist, C. Genes, M. Ludwig, F. Marquardt, P. Treutlein, P. Zoller, J. Ye, and H. J. Kimble. 'Strong Coupling of a Mechanical Oscillator and a Single Atom'. *Phys. Rev. Lett.* **103**(6), 063005–4 (2009).

[166] E. M. Purcell. 'Spontaneous Emission Probabilities at Radio Frequencies'. *Phys. Rev.* **69**, 674 (1946).

[167] K. Hepp and E. H. Lieb. 'On the superradiant phase transition for molecules in a quantized radiation field: the Dicke maser model'. *Annals of Physics* **76**(2), 360–404 (1973).

[168] F. Dimer, B. Estienne, A. S. Parkins, and H. J. Carmichael. 'Proposed realization of the Dicke-model quantum phase transition in an optical cavity QED system'. *Phys. Rev. A* **75**(1), 013804–14 (2007).

[169] P. J. Mohr and B. N. Taylor. 'CODATA recommended values of the fundamental physical constants: 2002'. *Rev. Mod. Phys.* **77**(1), 1–107 (2005).

List of publications

1. **Criticality and Correlations in Cold Atomic Gases**
   M. Köhl, T. Donner, S. Ritter, T. Bourdel, A. Öttl, F. Brennecke, and T. Esslinger
   Advances in Solid State Physics 47, 79 (2008).

2. **Cavity QED with a Bose-Einstein condensate**
   F. Brennecke, T. Donner, S. Ritter, T. Bourdel, M. Köhl, and T. Esslinger
   Nature 450, 268 (2007).

3. **Cavity Optomechanics with a Bose-Einstein condensate**
   F. Brennecke*, S. Ritter*, T. Donner, and T. Esslinger
   Science 322, 235 (2008).

4. **Dynamical coupling between a Bose-Einstein condensate and a cavity optical lattice**
   S. Ritter, F. Brennecke, K. Baumann, T. Donner, C. Guerlin, and T. Esslinger.
   Appl. Phys. B 95, 213 (2009).

Credits

Die vergangenen dreieinhalb Jahre, die ich in Zürich verbringen durfte, gehören mit zu den schönsten in meinem Leben. Obschon der Beginn dieser Zeit von so manchem Zweifel begleitet war, so wurde mir im Laufe des Doktorats mehr als deutlich warum mein Gefühl diesen Weg gewählt hatte. Dies habe ich vor allem den vielen Menschen zu verdanken, welche mich in diese Zeit begleitet und unterstützt haben.

So hatte ich das Glück in einer sehr lebendigen Arbeitsgruppe mitarbeiten zu dürfen, in der nicht nur die Forschung im Vordergrund steht sondern auch das Miteinander und Füreinander eine wichtige Rolle spielen. Die Zeit als Doktorand erlaubte es mir, aus dem Gebiet der theoretischen Physik "auszubrechen" und in die für mich damals unbekannte Welt des physikalischen Experiments einzutauchen. Die geduldige Begleitung und vielseitige Unterstützung die mir dabei die ganze Arbeitsgruppe entgegengebracht hat, waren ganz entscheidend für das Gelingen dieser Zeit. Dass Zürich mir eine zweite Heimat wurde, habe ich vor allem Deborah und unserem gemeinsamen Sohn Wanja zu verdanken, deren Nähe jeden Tag von neuem ein Geschenk ist. So gibt es also jede Menge Dank auszusprechen:

- mein besonderer Dank gilt Tilman Esslinger für die Ermöglichung und Betreuung dieser Arbeit, sowie die äusserst menschliche und erfahrene Art und Weise die Arbeitsgruppe zu leiten und zusammenzuhalten. Danke für die lebendige Atmosphäre, die vielseitige Unterstützung und die vielen Diskussionen über Physik!

- Toni Öttl, Stephan Ritter und Michael Köhl – der ersten Generation des Cavity-Experimentes – gebührt mein tiefer Dank für einen vielseitigen und fast immer funktionierenden experimentellen Aufbau, der noch heute unzählige verborgene Details enthält, die nur darauf warten zum Einsatz zu kommen. Vielen Dank für die schöne gemeinsame Zeit und die vielen anregenden Gespräche.

- Tobias Donner und Thomas Bourdel – der zweiten Generation des Experiments – gilt mein Dank für die unzähligen gemeinsamen Stunden

in Labor und Büro, ihren Beistand bei grundlegenden experimentellen und physikalischen Fragen und eine wunderbare Zusammenarbeit.

- ein besonderer Dank geht an Kristian Baumann und Christine Guerlin für ihre Begeisterung und ihren unermüdlichen Einsatz die "Hohlraum-Forschung" voranzutreiben. Danke für die fröhliche gemeinsame Zeit und die lebendige Stimmung im Team.

- Henning Moritz danke ich für die intensive Begleitung vieler Angelegenheiten innerhalb der Arbeitsgruppe, die unermüdlichen Bemühungen sein langjährig angesammeltes Wissen an uns weiterzugeben, sowie die vielen hilfreichen Tipps zu optischen, elektronischen und physikalischen Fragen.

- den "alten Gitterhasen" Ken Günter, Niels Strohmaier und Robert Jördens für eine stimmungsvolle und ausgelassene Atmosphäre. Ein besonderer Dank geht an Robert für den unermüdlichen Beistand in Sachen Elektronik, Computer und physikalische Fragen aller Art, sowie das rege Interesse an der Arbeit und den Gedanken anderer.

- der dritten Gitterphysiker-Generation Daniel Greif und Leticia Tarruell für die lebendige Atmosphäre.

- dem gesamten "Lithium-Team" Bruno Zimmermann, Torben Müller und Jakob Meineke für die Organisation so vieler Dinge innerhalb der Gruppe, und die Einblicke in das Entstehen eines faszinierenden Experiments. An Jakob geht ein herzlicher Dank für so manches lange Gespräch über das Leben, Wissenschaft und die Welt.

- Den neuen Mitarbeitern Silvan Leinss und Thomas Uehlinger für gute Stimmung in der Arbeitsgruppe.

- Für anregende wissenschaftliche Gespräche möchte ich mich bedanken bei Iacopo Carusotto, Helmut Ritsch, Peter Domokos, Dan Stamper-Kurn, Atac Imamoglu, Gianni Blatter und Matthias Troyer, und vielen anderen.

- Ein herzlicher Dank geht an Alexander Frank, unserem Fachmann in Sachen Elektronik, der uns unermüdlich mit elektronischen Geräten versorgt und damit zum Gelingen unserer Experimente entscheidend beiträgt. Danke für die stete Bereitschaft für Rat und Tat und die gute Stimmung in D16.

- Ein grosser Dank gebührt Veronica Bürgisser für die sorgfältige und unermüdliche Büroarbeit, sowie die Hilfsbereitschaft und Anteilnahme in so vielen Bereichen.

- Mein ganz herzlicher Dank gilt Rebecca, Linda und Beat für die vielen Stunden welche sie in den letzten Monaten mit Wanja verbracht haben, und damit das Entstehen dieser Arbeit ganz entscheidend mit ermöglicht haben.

- Für die Nähe und die grosse Unterstützung während des vergangenen halben Jahres möchte ich meinem Bruder Friedemann von Herzen danken.

- Meinen Eltern gilt ein besonderer Dank: für die langjährige Unterstützung und all das, was sie mir auf den Weg mitgegeben haben.

- unserem gemeinsamen Sohn Wanja für das Lächeln das er uns jeden Morgen schenkt, und die unzähligen Stunden die er mich von der Arbeit abhielt, um mir zu zeigen wie schön das Leben ist.

- Mein tiefer Dank gilt Deborah – für ihre Liebe, ihre Ausdauer und Lebensfreude, sowie ihre unermessliche Unterstützung während der letzten drei Jahre.

Zürich, den 30. September 2009